The Hong Kong Polytechnic University

Department of Building Services Engineering

Numerical and Experimental Analysis of Heat Transfer and Airflow in Double Skin Facades with Integrated Amorphous Silicon PV Cells

Han Jun

A thesis submitted in partial fulfillment of the requirements for the Degree of Doctor of Philosophy

December 2009

CERTIFICATE OF ORIGINALITY

I hereby declare that this thesis is my own work and that, to the best of my knowledge and belief, it reproduces no material previously published or written, nor material that has been accepted for the award of any other degree or diploma, except where due acknowledgement has been made in the text.

_____ (Signed)

Han Jun (Name of student)

Department of Building Services Engineering

The Hong Kong Polytechnic University

Hong Kong SAR, China

December 2009

ABSTRACT

Abstract of thesis entitled : Numerical and Experimental Analysis of Heat Transfer and Airflow in Double Skin Facades with Integrated a-Si PV Cells

Submitted by : Han Jun

For the degree of : Doctor of Philosophy
at The Hong Kong Polytechnic University in December, 2009.

A double skin façade (DSF) is a strategy utilized for improving building performance through using an inner and outer wall on a building with a cavity created between two walls. There is an increasing growing tendency for architects and engineers to use double skin façade in the building construction. If photovoltaic modules or solar cells are integrated with a DSF, this façade becomes a building-integrated photovoltaic (BIPV) façade.

This thesis presents a numerical and experimental analysis of heat transfer and airflow in DSF system with integration of a-Si PV cells at the Hong Kong Polytechnic University, which generates both electricity and providing day lighting. A 2D numerical model is developed to explore the thermal behaviour and fluid dynamics in the air cavity of the DSF system for both open and closed inlet and outlet operational modes. The combined radiation and convection heat transfer in the air cavity are analyzed in detail in this thesis.

Steady natural convective airflow in a novel type glazing system with integrated semi-transparent photovoltaic (PV) cells has been analyzed numerically using a stream function vorticity formulation. Based on the resulting numerical predictions, the effects of Rayleigh numbers on airflow patterns and local heat transfer coefficients on vertical glazing surfaces are investigated for Rayleigh numbers in the range of $10^3 \leq Ra \leq 2 \times 10^5$. Good agreement for the Nusselt numbers was observed between numerical simulation results in this thesis and those of earlier experimental and theoretical results available from the literature.

In addition, the effect of air gap thickness in the cavity on the heat transfer through the cavity is evaluated. The effect of the thickness of the air layer between two glass panes on the heat flux through the PV window is investigated for different temperature differences ($T_{out} - T_{in}$). In Hong Kong, the outdoor design temperatures for A/C systems are 32°C for summer and 10°C for winter. The indoor air temperature in a typical office in Hong Kong is supposed to be maintained, for energy savings, at 25°C in summer and 22°C in winter. The effect of the thickness of the air layer in relation to two temperature differences, i.e. 12°C and 7°C has been considered. It is found that heat transfer through the window can be considerably reduced by optimizing the thickness of the air layer. The overall heat transfer is decreasing slightly when the thickness of the air layer is up to 60 mm. Therefore, the optimum thickness of the air layer could be chosen as 60 mm – 80 mm when energy saving due to less energy transport through the window is considered.

Various turbulence models (RNG $\kappa-\varepsilon$ model, Standard $\kappa-\varepsilon$ model, Realizable $\kappa-\varepsilon$ model) were employed and velocity and temperature profiles predicted were compared and discussed in this thesis. A test rig was developed and calibrated for this study. An experimental study was carried out in the lab of the Department of the Building Services Engineering, and predicted results were then compared with experimental data to evaluate the numerical simulation accuracy. Experimental measurements taken in the full scale indoor test facility are in good agreement with predicted results. The experimental results indicated that the inside air temperature for PV DSF system is quite lower than temperature in conventional façade with internal curtain for shading purposes. It is found that the temperature in the PV façade system is more stable. The temperature variation in conventional façade system with internal curtain is larger. There are 4 temperature peak have been observed during the measurement. The maximum temperature for conventional facade is close to 34^{o}C at 13:10 PM, 29^{o}C for PV facade. This indicated that the effectiveness of the solar screening through the use of the naturally ventilation of air beneath the PV module. The temperature deviation between the two systems becomes smaller late in the afternoon.

The results show that heat transfer and airflow in the cavity is a complex problem, which could influence the thermal performance of the PV DSF system. The results also show this novel glazing system type developed in the current thesis could not only generate electricity but also achieve potential energy savings by reducing the

air conditioning cooling load when applied in subtropical climatic conditions and simultaneously provide visual comfort for occupants in the indoor environment.

Keywords: Double skin façade (DSF); Double sided PV façade (DSPV); a-Si PV cells; Thin-film solar cell; Building integrated photovoltaics (BIPV); Airflow and heat transfer; Computational fluid dynamics; Numerical prediction; Experimental study; Laminar convective heat transfer; Turbulence modelling; Thermal and energy performance; Low-e coating; Heat gain.

PUBLICATIONS LIST

Journal papers

- J. Han, L. Lu, H. Yang, Numerical evaluation of the mixed convective heat transfer in a double pane window integrated with see-through a-Si PV cells with low-e coatings. ***Applied Energy*** (In Press)
- J. Han, L. Lu, H. Yang, Thermal behavior of a novel type see-through glazing system with integrated PV cells. ***Building and Environment*** 2009, 44 (10): 2129-2136.
- J. Han, L. Lu, H. Yang, Investigation on the thermal performance of different lightweight roofing structures and its effect on space cooling load. ***Applied Thermal Engineering*** 2009, 29 (11-12): 2491-2499.
- L. Lu, J. Han, H. Yang, Investigating the effect of indoor water canal on the cooling load estimation and condensation issues of Venetian Macao. ***Building Services Engineering Research & Technology*** 2008, 29(3): 249-259.
- H. Yang, J. Han, L. Sun, Recent Research and development of BIPV in Hong Kong ***Advanced Materials Industry*** 2008, 9: 25-31.
- L. Lu, J. Han, H. Yang, Analysis of moisture transfer and vapor condensation in porous building roof for large space air-conditioning in hot humid areas. ***Journal of HVAC***, (In Press)
- J. Ji, J. Han, T. T. Chow, H. Yi, J. Lu, W. He, W. Sun, Effect of fluid flow and packing factor on energy performance of a wall-mounted hybrid photovoltaic/water-heating collector system. ***Energy and Buildings*** 2006, 38 (12):1380-1387.

- J. Ji, J. Han, T. T. Chow, C. Han, J. Lu, W. He, Effect of flow channel dimensions on the performance of a box-frame photovoltaic/thermal collector ***Proceedings of the Institution of Mechanical Engineers, Part A: Journal of Power and Energy*** 2006, 220 (7): 681-688.
- J. Ji, J. Han, T. Zhou, W. He, G. Pei, J. Lu, Numerical study on the electric and thermal performance of hybrid PV/T collector wall ***Taiyangneng Xuebao/Acta Energiae Solaris Sinica*** 2006, 27 (11): 1089-1096.
- J. Han, L. Lu, H. Yang, Numerical and experimental study of natural air convection in a double pane glazing cavity with thin-film solar cells. Completed for submission

Conference papers

- J. Han, L. Lu, H. Yang, Numerical analysis on the thermal performance of a lightweight aluminum stand-seaming roofing structure with experimental validation. First International Conference on Building Energy and Environment, Proceeding Vol 1-3 Pages: 397-404 2008.
- J. Han, L. Lu, H. Yang, A two-dimensional numerical study for natural convection in the cavity of a double glazed window with integrated semi-transparent PV. The First International Conference on Applied Energy (ICAE09).

ACKNOWLEDGEMENTS

I would like to offer my sincere gratitude to my chief-supervisor, Prof. Hongxing Yang for his expert guidance, continuous encouragement and constant support during my three years of post graduate study for my PhD. His expertise in renewable energy research and his wisdom opened my eyes and decreased my ignorance. I cherish the opportunity of studying under him during this period.

Thanks are also due to my co-supervisor Dr. Lin Lu of the Department of Building Services Engineering for her academic guidance and kind assistance over the past three years. Her constructive suggestions regarding my papers and thesis manuscripts were very much appreciated. Without her kind assistance, the completion of this thesis would have been more difficult.

I am grateful to Professor Robert F. Boehm, Professor Yi-tong Chan, and Dr. J. H. Nie at the University of Nevada, Las Vegas (UNLV) for sharing with me their expertise. Their encouragement and guidance to me during my studying at UNLV is appreciated and it is a memorable experience.

Thanks are also due to my colleagues in the Renewable Energy Research Group and technicians in the Building Services Department, for their assistance in laboratory

work. I am also grateful to Ms Elaine Anson and Dr. Stephen Evans for their guidance on my English writing.

I also appreciate The Hong Kong Polytechnic University for providing me with a studentship. Without this financial support, it would not have been possible to complete my PhD study in Hong Kong. The financial support from the Research Grants Council (RGC), and Innovation and Technology Found (ITF) of the Hong Kong SAR government for the project is also acknowledged.

Finally, I wish to dedicate this thesis to my parents, Han Yuan-Ming and Lin Shu-Qiong and to thank them for their love, patience and support.

TABLE OF CONTENTS

LIST OF FIGURES

LIST OF TABLES

NOMENCLATURE

Symbols	Description
A	Aspect ratio (-)
C	Specific heat (kJ/kgK)
D	Thickness or depth (m)
$F_{i,j}$	View factor between segment i to j (-)
g	Gravitational acceleration (m/s^2)
H	Height of the cavity (m)
h	Heat transfer coefficient (W/m^2K)
k	Thermal conductivity (W/mK)
I	Solar radition intensity (W/m^2), electrcity current (amp)
L	Length of the cavity or thickness (m)
n	Number of iteration and exponent in Eqn 2.15
N	Number of cavity (-)
Nu	Nusselt number (-)
p	Static pressure (N/m^2)
Pr	Prandtl number (-)
Q_r	Dimensionless net radiation heat flux (-)
Ra	Rayleigh number (-)
r	Thermal resistivity (mK/W)
S	Solar intensity available at distance x (W/m^2)
T	Temperature (K)
t	Time (s)
x, y	Coordinates
X,Y	Non-dimensional coordinates
U	U-value (W/m^2K)
u	Velocity component in x-direction (m/s)

V	Voltage (volt)
v	Velocity component in y-direction (m/s)

Greek symbols

α	Thermal diffusivity (m^2/s), absorptance
β	Thermal expansion coefficient (1/K)
ρ	Density (kg/m^3)
ψ	Stream function (m^2/s)
λ	Thermal diffusivity of glass (m^2/s)
ς	Constant,10^{-4}
Φ	General non-dimensional variable (-)
ϕ	Inclination angle (deg)
ε	Emittance (-)
τ	Transmittance (-)
Ψ	Non-dimensional stream function (-)
Ω	Non-dimensional vorticity (-)
Θ	Non-dimensional temperature (-)
ν	Kinematic viscosity (m^2/s)
ω	Vorticity (1/s)

Subscripts

a	Air, air gap
C	Cold surface
c	Infill air convection heat transfer
cell	Solar cell
e	Ambient
eff	Effective
fg	Front glass
g	Glass pane
l	Laminar flow
m	Mean

o, out	Outdoor
oc	Open circuit
PV	Photovoltaic cells
r	Radiation heat transfer
s	Air space
sc	Short circuit
t	Multiple glazed unit, turbulent flow
H	Hot surface
i, in	Indoor

CHAPTER 1 INTRODUCTION

1.1 Double skin façade

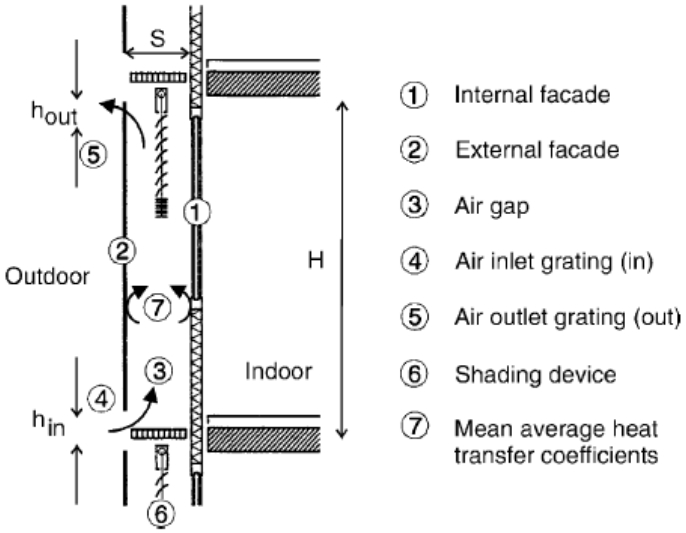

Figure 1.1 Schematic diagram of a double skin façade by Faist (1996)

Double skin façade (DSF) technology is a strategy utilized for improving building performance by using an inner and outer wall on a building with a cavity created between two walls. According to the Belgian Building Research Institute (BBRI), the definition of DSF is that it is a façade covering one or several storeys constructed with multiple glazed skins. In general, the structure of a DSF consists of three main parts: (1) building envelope, (2) two bounding surfaces and (3) air cavity created by two bounding surfaces. The schematic diagram of a DSF system is shown in Figure 1.1.The skins can be air tight or ventilated as shown in Figure 1.2. On the other hand, the air cavity ventilation strategy may vary with time.

Devices and systems are generally integrated in order to improve the indoor climate with active or passive techniques. Most of the time, such systems are managed in semi automatic way via control systems.

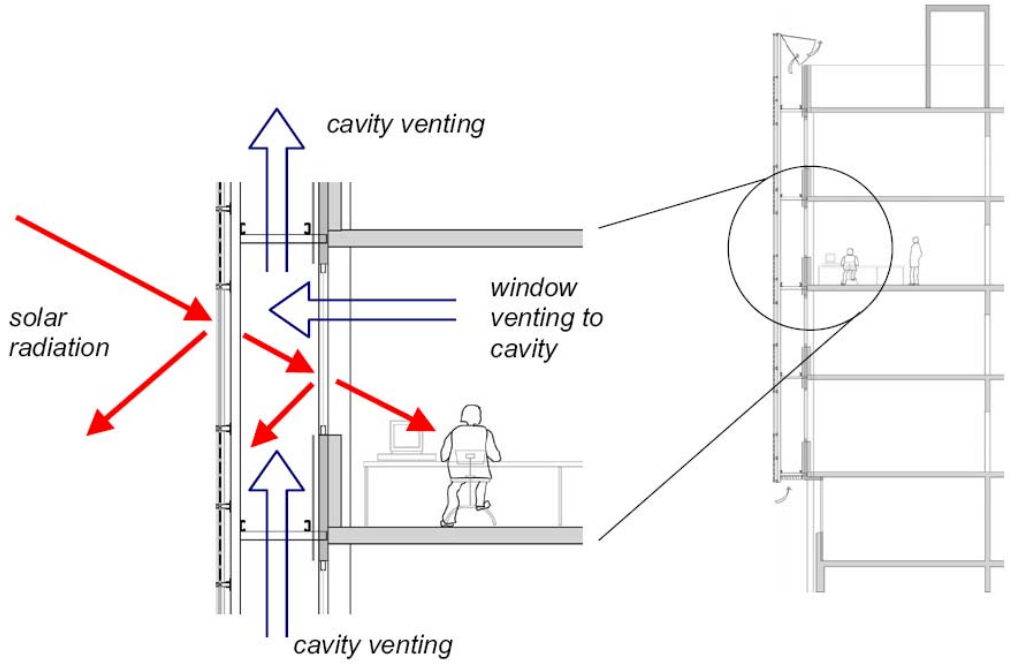

Figure 1.2 Solar radiation through an office building and air movement in the DSF cavity

There is an increasing growing tendency for architects and engineers to use double skin façades in the building construction. The driving potentials for using this kind of technologies are as follows:

- The increasing effort in reducing the heat gain through buildings' external envelopes, so as to reduce corresponding cooling load of air-conditioning (A/C) system;

- The need for acoustics control, especially for building located in a metropolitan city, for example in Hong Kong;
- The need for improvement of aesthetical architectural appearance;
- The need for improvement of indoor air quality (IAQ) for thermal comfort of the indoor occupants, particularly in office buildings in the occupancy period;
- The potential applications of the natural day lighting utilization. Visual contact between indoor occupants and outdoor environment may not be sacrificed when transparent clear glass façade is utilized.

1.1.1 Advantages and disadvantages of DSF design concept

Buildings with DSF, also named double-envelope facades or glass double facades, are complex from a building physics point of view. This kind of façade design has both advantages and drawbacks. The advantages have been eagerly accepted by architects and engineers when they intend to employ such kind of advanced technology in their design. One of the main advantages of the DSF systems is that they are capable of providing natural or combined mechanical ventilation. From the benefit of natural ventilation, limiting the period of time in which the mechanical ventilation is used reduces the energy consumption of the building and the possibility of occurrence of the 'sick building sysdrome' (when HVAC systems are present), as indicated by Silva (2008) and Saelens (2002). On the other hand the second façade has the capability of reduce the influence coming from outdoor wind load and noise. Another benefit from the DSF system, as

described by Lee et al. (2002), is that DSF façade allow any possible renovations of historical buildings desired to be protected.

Overheating during the summer period and condensation issues in the severe winter period are the problems a designer of a DSF commonly face. The problem could be even worse, especially when the peak outdoor ambient temperatures coincide with higher solar radiation. Many researchers suggested that this kind of risk of overheating in summer could be minimized when proper measures or strategies are fully considered and employed during the design stage. Another disadvantage is higher manufacturing costs compared with a conventional single façade. Other maintenance and operational costs are added. These costs may include cleaning, inspection or other services. Architects and engineers may need to convince clients to use these advanced facades systems despite increased cost to jump the cost barrier.

1.2 Development of DSF

DSF buildings were first built in the US and Europe in the 1970s during the first energy crisis as an attempt to improve building performance. Poirazis (2004) mentioned that a mechanically ventilated multiple skin façade in the construction of the Industrial Museum in Brussels was first introduced by Jobard. With frequently use of the new materials such as cast iron, steel reinforced concrete in the modern commercial buildings, load-bearing function of the former facades were becoming less important. Transparent glass curtain walls were commonly

used by architects to cater for the desire for natural day lighting, and visual contact between indoor occupants and outdoor views at that time.

The energy crises in 1973 and 1979 evoked the recognition of public and policy makers as well as designers of buildings the importance of improving energy efficiency in the building sector as buildings consume a large portion of the total energy use. With the increase in the usage of glass in buildings, many disadvantages of using the large-area glass façade become apparent. For example, higher air-conditioning (A/C) system costs from such buildings have been identified. These include heat transfer through window glazing of the building external wall as one of the major thermal loads in the building envelope heat gain. In addition to the higher levels of A/C cooling load that result in these kinds of buildings, other problems, such as overheating during the summer period and considerations from the acoustics issues also resulted.

One way to solve such problems mentioned above is to employ more advanced glazing technologies, including the use of double glazed windows or facades instead of using single glazed façades. One of the most important features is that a double glazed window or façade is thermally insulated by air cavity created between two opposite walls. The air cavity could be ventilated or non-ventilated, i.e. closed cavity.

During the last 30 years, research and development in DSF technology achieved a relatively high technological standard. The recent resurgence of efficient building design has renewed interest in this concept. Since Leadership in Energy and Environmental Design (LEED) green building certification awards points for reduction in energy consumption vs. a base case, this strategy has been used to optimize energy performance of buildings.

A south oriented outdoor test stand was designed and built on top of a unit of the new Mechanical Engineering Faculty Building of the Technical University Munich in Garching as shown in Figure 1.3.

Figure 1.3 Outdoor test facility for double skin façade system from Zollner (2002)

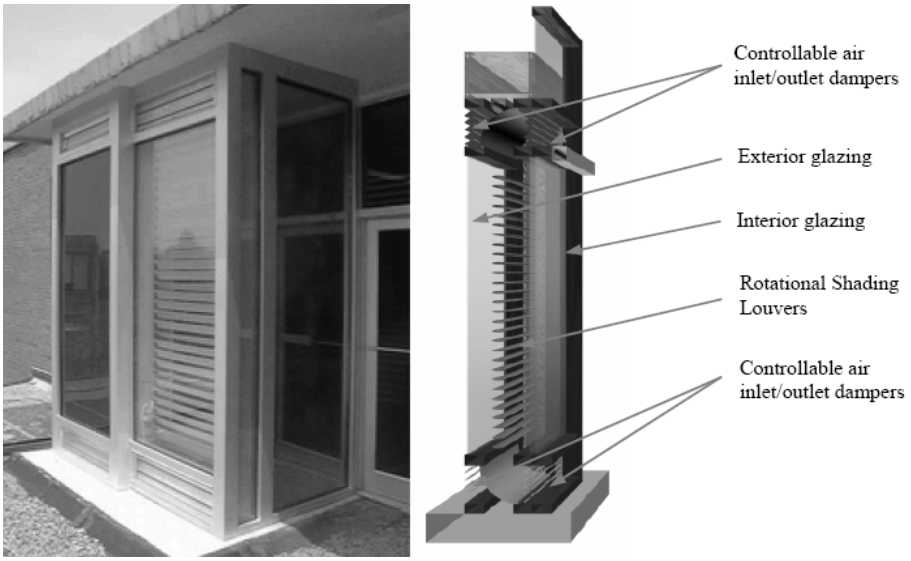

Figure 1.4 Smart façade system installed at The Georgia Institute of Technology from Park (2003)

A smart façade system has been introduced by Park (2003) at the Georgia Institute of Technology, as shown in Figure 1.4. The demo unit consists of a double pane exterior glazing, single pane interior glazing, an automatic rotating louver, and electrical controlled ventilation inlet/outlet dampers. A motorized venetian blind system and ventilation damper are controlled by a smart controller for both benefits of large windows with reduced energy demands for heating and cooling and maintain thermal and visual comfort to a optimal level.

1.3 DSF using photovoltaic glass

Photovoltaic glass is a special glass with integrated photovoltaic solar cells, to convert solar energy into electricity. This means that the power for an entire

building can be produced within the building components such as roof and façade. Solar cells are embedded between two glass panes and a special resin is filled between the panes and space between solar cells, securely wrapping the solar cells on all sides. Each individual cell has two electrical connections, which are linked to other cells in the module, to form a system which generates a direct electrical current. With the incorporation of photovoltaic glass, as well as other systems and components, it is possible to utilize the power generation from photovoltaic cells to reduce building electricity consumption from utilities and cost. This most promising renewable energy technology incorporates a sustainable feature into the construction of the building envelope.

There are various options for the selection of cells, for example, polycrystalline Silicon (p-Si) PV cell, and amorphous Silicon (a-Si) PV cell. Figure 1.5 shows the structure of a semi-transparent PV module laminated with p-Si PV cells. These cells are spaced so that some portion of light could pass through the glass, which facilitate natural daylight in the building. Several layers are incorporated together to create the PV module including glass, Ethylen Vinyl Acetate (EVA) sheet using as encapsulation material, PV cells, glass, air gap with spacer and glass as described by Park (2009). For thermal insulation purposes, an additional glass sheet is usually placed behind the PV module and an air gap between them is created for thermal resistance.

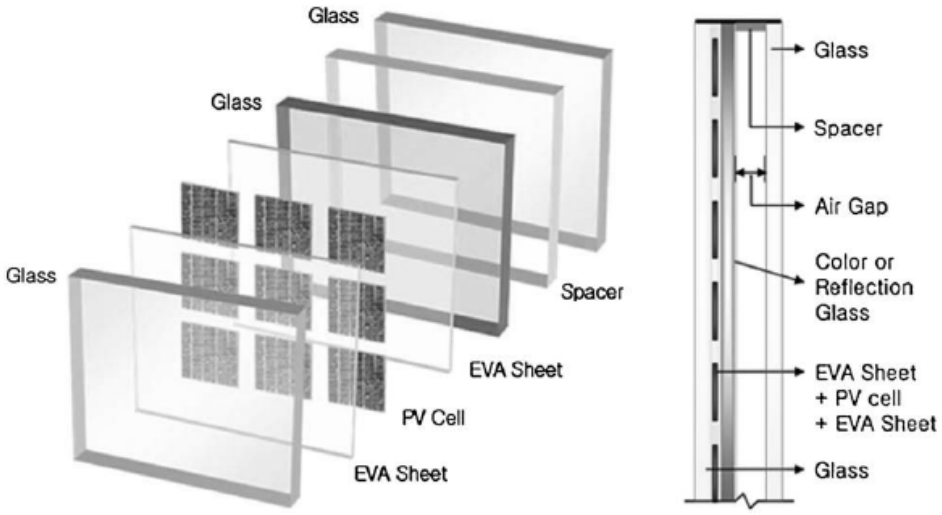

Figure 1.5 The structure of a photovoltaic glass by Park (2009)

1.3.1 Ventilated photovoltaic (PV) façade

Ventilated PV façade function as a multi-purpose façade system is a relative new concept in the renewable energy applications. It has the potential of maximizing PV power output due to the reduced operational temperature of the solar cell due to the ventilated air stream behind the PV panel, thus improve the PV electrical conversion efficiency. The air flow in the channel created by two parallel vertical plates is driven by buoyancy force, an external pressure difference due to wind effects, or by combined effect. In addition to produce electricity from the PV modules, other advantages or benefits from the weather buffer zone created between the inside and outside of the building could be offered as well. Cool air stream in the channel during the summer season and warm air stream during the winter season could be circulated for ventilation of air. Cooling load and heating

load for A/C system are consequently reduced and better thermal comfort of the indoor occupants is also achieved.

1.3.2 Non-ventilated PV window and curtain wall

Compared with ventilated PV window (Chow et al. 2007), non-ventilated PV window eliminate the need for cleaning requirement in the air cavity and provide well sound insulation. The problems, however, exist in the over heating of the closed air cavity during severe summer weather conditions. Attention thus must be paid on solving the problem so as to meet general or even the toughest building codes. Many appropriate measures are commonly adopted, for example, the air cavity is integrated with duct system of the central A/C system. It is a good approach but further investigation on application in various weather conditions is needed. In general, PV windows have the same characteristics as conventional double pane windows, so architects, developers, and builders do not need make big design efforts and building changes to develop PV embedded buildings. This approach is truly sustaining and low maintenance.

1.4 Objectives of the research

Use of semi-transparent PV modules is an increasing trend for BIPV applications. Few previous investigations, however, consider the characteristics of airflow and heat transfer in the glazing cavity formed between exterior and internal gazing

using semi-transparent PV modules. It is necessary to study the energy performance of the current system.

The main objective of the research is to development of a DSF system integrated with semi-transparent PV cells, and to assess its thermal and energy performance by theoretical model and experimental investigations.

The objectives of the research are as follows:

1) To develop a mathematical model to explore the thermal performance of the double skin façade with integrated amorphous silicon (a-Si) thin-film photovoltaic (TFPV) cells.
2) To obtain experimental information on a real test-rig under controlled conditions to gain insight into the complex behavior of the PV DSF system. The measurements shall serve for model verification purposes.
3) To use a two-dimensional steady state computational fluid dynamics (CFD) model to study the fluid flow in the air cavity of double facades with integrated PV panels. The convective heat transfer coefficient necessary for predicting the total heat flow through the DSF shall be calculated in detail.
4) To combine a building energy simulation program with the CFD model for further evaluation of the annual heat gain of the PV DSF system and power generation from the TFPV cells.

1.5 Organization of the thesis

This thesis consists of 8 chapters. The current chapter is an introductory chapter which introduces background information related to the topic, and outlines the content of this thesis. The objectives of the thesis are established in this chapter and justified with reference to relevant studies in the area.

Chapter 2 reviews the past work in the existing literature relevant to the current research. A literature review of the definition and classification of the double skin façade system and its energy as well as thermal performance are given in this chapter.

Chapter 3 presents the experiment study of the double skin photovoltaic façade system which is developed in the Solar Simulation Lab of The Hong Kong Polytechnic University. Experimental methodology and instruments used in the experiment are extensively described. Various operational modes were conduced and the experimental results are discussed.

Chapter 4 presents the numerical investigation of an open cavity for ventilated double skin photovoltaic façade. The air flow in the channel of the window will be simulated by consideration of both laminar and turbulent flow. Various turbulent modules will be employed and the results from them will be discussed. The heat transfer and air flow characteristics in the channel will be evaluated by numerical simulation. Various factors affecting the air flow and heat transmission will be

identified and examined. Predicted results from the numerical simulation are analyzed in detail.

Chapter 5 presents the theoretical study on the heat transfer and air flow characteristics in the closed cavity for non-ventilation double skin photovoltaic window. The motivation for development a validated mathematical model is the requirement of the precise predictions of the thermal performance of a PV DSF system. The numerical model and method for solution of it are discussed.

In Chapter 6, the predicted results from the numerical methods are validated with experimental results available in the existing literature and collected data from experimental measurements of a well developed test rig in the Solar Simulation Lab and through an outdoor test.

In Chapter 7, various factors affecting the performance of the double skin photovoltaic façade system has been indentified and analyzed in detail. In the last chapter, conclusions are drawn and recommendations for future research are proposed.

CHAPTER 2: LITERATURE REVIEW

2.1 Introduction

Thermal modeling of the energy performance and thermal behavior of air cavity in a double skin façade system is a complicated task as many parameters may affect the performance of the façade and ultimately affect the total building energy performance. Among these critical parameters commonly investigated and noted by other researchers in the existing literature are air flow rate in the cavity, cavity width, solar heat gain coefficients (SHGC), shading coefficients, and day lighting parameter.

Over several years, there have been considerable efforts directed toward the development of advanced facade systems, and many of those efforts were focused on air flow simulations in the cavity, temperature and velocity distribution along the cavity as well as day lighting utilization analysis. For the simulation of the air flow in the cavity, different turbulence models were used. For the heat transfer in the cavity, various assumptions were made. Many works consider the effect of the heat transfer by radiation in the cavity, while others consider the convection heat transfer solely. On the other hand, life cycle cost analysis of DSF system is also performed by different researchers to evaluate the feasibility for application of DSF under various climate conditions. Different investigations and methodologies employed to model the thermal and energy performance of the cavity of the DSF

with its integrated building as well as study on ventilated photovoltaic facade are extensively reviewed in this section.

2.2 Double skin façade technology

2.2.1 Experimental investigation of the thermal performance

It is crucial to determine the air flow rate and velocity distribution in the cavity as they will affect the temperature of air in the cavity, and thus affect the thermal performance of the total façade system as well as the building energy use. Airflow through both naturally or mechanically ventilated envelopes has been experimentally analyzed in the existing literature. Most common measurement techniques for calculating the air flow rates both in naturally and mechanically ventilated active envelopes are described by Saelens and Hens (2001, 2004, 2008). They describe three measuring methods to determine the airflow in ducts and cavities: 1) measuring the pressure difference across an orifice, nozzle or venture tube; 2) measuring the air velocity using anemometers; 3) measuring the air flow directly using tracer gas techniques. In the study, a method was proposed to determine the airflow through the cavity by means of the pressure difference over the louver ventilation grid. As indicated by Saelens, for mechanically ventilated cavities, an excellent way to determine the airflow rate is by measuring the pressure difference across an orifice placed in the exhaust duct. This method, however, is less suitable for naturally ventilated cavities. Saelens (2001) noted that the driving forces are usually small and because of the high flow resistance of the orifice, the flow in the cavity would be too much affected. Moreover, finding a

suitable place for the orifices would be difficult as no exhaust duct is available.

2.2.2 Experimental investigation of laminar and turbulent flow in the channel

Laminar natural convective heat transfer in parallel-plate vertical channel was studied in many experimental investigations by various researchers. The first comprehensive experimental work was conducted by Elenbaas (1942). His work has served as a benchmark for most subsequent studies. A large number of studies on experimental measurements of laminar convective heat transfer in the vertical parallel plates were reported during the past few years. The effect of inter plate spacing on natural convection heat transfer characteristics of a vertical channel heated on one side was explored experimentally and numerically by Sparrow and Azevedo (1985). Fedorov and Viskanta (1997) conducted a comprehensive literature survey of mixed convection between vertical parallel plates.

Moshfegh and Sandberg (1998) used tracer gas with a so called constant flow technique to measure the flow rate in the channel. At the bottom of the channel, gas is introduced with a known volume flow rate. The volume concentration is recorded at the exit. The concentration is read with an infrared gas analyzer giving the volume concentration in parts per million (ppm). An experimental study on natural convective heat transfer in an open channel was carried out by Fossa (2008). The effect of the geometrical configuration of heat sources on the heat transfer behaviour was evaluated for a series of vertical heaters. Physical

mechanisms influencing the thermal behaviour of a double-skin photovoltaic façade was investigated in their work. The research result is useful in controlling the energy transfer from ambient to the PV surfaces and vise versa. PV module conversion efficiency is increased due to lower operation temperature. The experimental results show that the proper selection of the separation distance or air gap depth and heating configuration can noticeably decrease the surface temperatures and hence enhance the conversion efficiency of PV modules.

Turbulent flow and natural convection in vertical channels have been intensively investigated by various researchers. The first experimental study on turbulent free convection heat transfer in an asymmetrically heated vertical channel was conducted by Miyamoto *et al.* (1986). The channel was created by two vertical parallel plates. Other studies on turbulent natural convection along plates include Vliet and Liu (1969), Tsuji and Nakano (1988) and Ozisik (1987).

Although experimental values are very reliable when performed in a controlled environment, there are several major drawbacks to this approach. It is expensive and time consuming. Numerical approaches, for example Computational Fluid Dynamics (CFD), are commonly used during the building design stage and this approach will be discussed in the following section.

2.2.3 Existing mathematical model for theoretical investigations

Previous researchers have shown substantial and growing interests in the DSF design focusing mostly in areas of the thermal performance (energy use, reduction of heating and cooling demand during winter and summer seasons, reduction of peak heating or cooling loads), solar optical performance (use of solar control), acoustic performance (acoustic control in buildings located in noise polluted areas) and day lighting performance (use of natural daylight other than artificial daylight) of the glass façade system and air flow simulation in the cavity. It is important to accurately predict all these performances of the façade system by employing an appropriate mathematical model in order to design a cost effective and appropriate system that satisfies all users during the occupancy period of the building constructed with double skin facades.

Various researchers have developed theoretical models to study DSF systems and modified systems with integration of photovoltaic solar cells since a large number of design or geometrical parameters can influence the entire system's function and other physical properties of the air cavity. Defining a mathematical model to simplify the real model seems to be the most reliable and economic approach. The total performance of the DSF system will also affect the performance of the building. The accuracy of calculations of the façade performance during the design stage will produce more precise predictions. In order to calculate the temperatures at different heights in the cavity, air flow simulation of the double skin façade cavity should be conducted.

Different flow models (i.e. laminar flow and turbulent flow models) were used to simulate the air dynamics and heat transfer in the air cavity. Long-wave radiation calculation in the cavity was considered, while some researchers simulate the system without consideration of radiation effect. According to Liao and Athienitis (2005) and other researchers, the heat exchange by radiation in the air cavity of building integrated photovoltaic (BIPV) system is important.

The modeling and simulation of the DSF cavity is a complicated task, since different elements interact with each other influencing the function of the cavity. Due to highly nonlinear nature of DSF systems, an analytical approach to investigate on airflow and thermal behavior of DSF systems becomes impracticable. Only a few simple analytical studies exist in the previous research due to highly nonlinear nature of the systems itself leading to the impracticability of any analytical approach as indicated by Park (2003). Previous simple analytical studies, for example, are these studies by Brandle (1982), Rippati (1984), Mueller (1984), Wright (1986), Barakat (1987), Hayashi (1989), Robbins (1993), Cho (1995), Luecke (1995), Onur (1996), Haddad (1998, 1999), Oosthuizen (1999), van Passen (2000), Saelens (2002).

Holmes (1994), Inoue et al. (1985), Sarlens and Tack (1997) have developed analytical solutions to the airflow in the cavity. Holmes (1994) provides an analytical solution for a single ventilated cavity by employing an exponential vertical temperature gradient. Inoue et al. (1985) introduce ventilation on either

side of the shading and assumed a linear vertical temperature gradient is existed in the air cavity. Saelens and Tack (1997) provide analytical expressions for an airflow window including a shading device with ventilation on either side of the cavity.

There is a growing research interesting in studying heat transfer and fluid flow in air gaps behind photovoltaic panels. Like air motion mechanism in a solar chimney and conventional DSF, air flow in the air gap behind PV panel is driven by buoyancy forces and wind effects. The PV panel is heated by the incident solar radiation and from the PV panel heat is transferred to the air gap by convection and radiation heat transfer as indicated by Moshfegh and Sandberg (1998). Brinkworth et al. (1999) derived a simplified method for prediction of the air flow rate in naturally ventilated PV cladding for buildings. The method is based on a one-dimensional 'loop analysis' in which the buoyancy forces are balanced by pressure drops due to friction in duct. The methods also consider the effect of the wind force effects at the entrance and exit of the PV ventilation gap. The mass flow rate and temperature rise can be directly predicted through solution of a simple cubic equation. Tonui and Tripanagnostopoulos (2008) presented air cooling of a commercial PV module configured as PV/T air solar collector by natural flow. Modification techniques to enhance heat transfer to the air in the channels were studied. The considered methods consist of thin metal sheet suspended at the middle or fins attached to the back wall of the air-channel to improve heat extraction from the module. Ibrahim et al. (1988) provide a

simplified loop analysis for a naturally ventilated channel heated from one side by PV elements. Moshfeg and Sandbergy (1996) employed a 2D finite element model in a CFD study with idealized boundary conditions to investigate the convective heat transfer in a vertical air channel behind the PV module. Analytical expressions for the mass flow rate, velocity, temperature rise and location of neutral height in air gap behind solar cells located on vertical facades were derived by the same authors. Mootz and Bezian (1996) presented a 2D laminar flow model.

Many mathematical models in the literature involve the modeling of the ventilated PV façade by evaluation of heat transfer through radiation, convection, conduction and electrical power generation from the solar cells. Among these models, the simplest approach is to use the single zone model and each element is represented by a node and connected together using the thermal network as was done by Liao (2005). The heat transfer through the elements is described using the U factor. Saelens (2002) pointed out that a simple U factor lacks the complexity to accurately model this type of façade.

For modeling heat conduction through glass pane, various mathematical models are available in the literature to consider the effect of the solar radiation absorbed by the glass. Both transient and steady state analysis of the heat transfer by conduction in the solid part (i.e. glass panels) exist. The mathematical model of 2D transient energy equation for the glass sheet is used by Ismail (1998, 2009), as

follows:

$$\frac{\partial T}{\partial \mathrm{t}} = \frac{k}{\rho c}\left[\frac{\partial^2 T}{\partial x^2} + \frac{\partial^2 T}{\partial y^2}\right] - \frac{1}{\rho c}\frac{\partial I_q}{\partial y} \tag{2.1}$$

The term $\partial I_q / \partial y$ is the solar radiation absorbed in the glass per unit volume and can be written in terms of the radiation attenuation across the glass sheet characterized by its extinction coefficient as

$$dI_q = -\beta I_q dy \tag{2.2}$$

Fung (2006) used the following energy balance equation for the front-glass of a BIPV system:

$$\frac{\partial T_{fg}(x,t)}{\partial t} = \lambda \frac{\partial^2 T_{fg}(x,t)}{\partial x^2} + \frac{\lambda}{k_g}\frac{dS_{fg}}{dx} \tag{2.3}$$

$T_{fg}(x,t)$ is the inside node temperature of the front-glass at distance x and time t, λ_g and k_g are the thermal diffusivity and thermal conductance of the glass respectively; the term dS_{fg}/dx corresponds to the heat generated in the glass due to the solar radiation.

Chow et al. (2007) use the following mathematical equations to model the solid part, i.e. the glass panes. Solar radiation absorbed by glass is considered as boundary conditions, and this treatment is different from previous mathematical modeling of the glass. No lateral heat transfer across the horizontal width of the window assembly was assumed, the energy balance per unit length of the outer glass pane gives

$$D_{g,o}\rho_g C_g \frac{\partial T_{g,o}}{\partial t} = G\alpha_{eff,o} + U_{cg}(T_c - T_{g,o})(1-\tau_c) + h_{g,a}(T_a - T_{g,o})\tau_c + h_{r,g}(T_{g,i} - T_{g,o})\tau_c$$

$$+ (h_{r,ge} + h_{ge})(T_e - T_{g,o}) + D_{g,o}k_g \frac{\partial^2 T_{g,o}}{\partial x^2} \quad (2.4)$$

where $D_{g,o}, \rho_g$, C_g and k_g are, respectively, the thickness, density, specific heat capacity, and heat conductivity of outer glass, $T_{g,o}$, T_a, T_c and T_e, respectively, the temperatures of outer glass, air at ventilating gap, solar cell and ambient, G the incident solar irradiance, U_{cg} the effective heat transfer coefficient between outer glass and solar cells, $\alpha_{eff,o}$ the effective absorptance of outer glass $h_{r,ge}$ and h_{ge}, respectively, the radiative and convective heat transfer coefficients between outer glass and ambient, $h_{g,a}$ the convective heat transfer coefficient between out glass and air in ventilating gap, and τ_c is the solar cell transmittance.

2.2.4 Convection heat transfer coefficients

Natural convective heat transfer inside enclosures has long been a very interesting and important research area as it has a lot of engineering applications. It impacts the flow patterns and heat transfer processes in solar collectors, building façade, and double glazed windows. Coefficients of heat transfer by convection in an air cavity were calculated by using empirical expressions of Nusselt number as a function of Rayleigh number in many existing literatures. Cavity height H is usually taking as reference length in the calculation process. Hsieh and Yang

(1997) conducted experiment studies for various heated water rectangular enclosure with aspect ratios H/W = 20 (ratio of height to width) at high Rayleigh numbers. The following correlations were deduced, for aspect ratio $A_H = 20$.

For laminar flow regime:

$$Nu = 0.224 Ra^{0.257} \Pr^{0.056} \qquad 1.54 \times 10^8 \le Ra \le 1.58 \times 10^9 \tag{2.5}$$

For turbulent flow regime:

$$Nu = 0.059 Ra^{0.315} \Pr^{0.056} \qquad 1.58 \times 10^8 \le Ra \le 1.48 \times 10^{10} \tag{2.6}$$

Seki (1989) also proposed following similar correlations, for laminar flow:

$$10^7 < Ra < 10^9 \quad 6 < A_H < 30 \tag{2.7}$$

For turbulent flow:

$$Nu = 0.096 Ra^{0.3} \Pr^{0.051} \qquad 10^{10} < Ra < 10^{11} \quad 6 < A_H < 30 \tag{2.8}$$

In the above calculations, the Rayleigh numbers are calculated based on an overall temperature difference between two hot and cold wall of the cavity. The convective heat transfer coefficient is then deduced by following expression:

$$Nu = \frac{hH}{k} \tag{2.9}$$

The correlations between the average Nusselt numbers with other parameters, proposed by Yin et al. (1978), are listed below:

$$Nu = 0.23 A^{-0.131} Ra_L^{0.269} \quad \text{for} \quad 10^3 \le Ra_L \le 5 \times 10^6 \quad \text{and} \quad 4.9 \le A \le 79.7 \tag{2.10}$$

The correlations from Elsherbiny et al. (1982) are listed below:

$$Nu_1 = 0.0605 \times Ra_L^{1/3} \tag{2.11}$$

$$Nu_2 = \left[1 + \left\{ \frac{0.104 Ra_L^{0.293}}{1 + (6310 / Ra_L)^{1.36}} \right\}^3 \right]^{1/3} \tag{2.12}$$

$$Nu_3 = 0.242\left(\frac{Ra_L}{A}\right)^{0.272} \tag{2.13}$$

$$Nu = \max(Nu_1, Nu_2, Nu_3) \tag{2.14}$$

for $5 \le A \le 110$, $A = 20 : Ra_L < 2\times10^6$,

$A = 40 : Ra_L < 2\times10^5, A = 80 : Ra_L < 3\times10^4$

Balocco, (2003) recommended a correlation valid for a vertical wall at uniform temperature and wide vertical isothermal volume (W>>L). According to Holman (1991) and Warren (1998), the Nusselt number can be obtained from the following equations:

$$Nu = [(Nu_l)^n + (Nu_t)^n]^{1/n} \tag{2.15}$$

$$Nu_l = \frac{2}{In(1 + 2/C_l \times Ra^{1/3})} \tag{2.16}$$

$$Nu_t = \frac{C_t \times Ra^{1/3}}{1 + 1.4\times10^9\ \mathrm{Pr}/Ra} \tag{2.17}$$

where the coefficients C_l (for laminar flow)and C_t(for turbulent flow) can be determined as follows:

$$C_l = \frac{0.671}{[1 + (0.492/\mathrm{Pr}^{9/16})]^{4/9}} \tag{2.18}$$

$$C_t = 0.16[\frac{\mathrm{Pr}^{0.22}}{1 + 0.61\mathrm{Pr}^{0.81}}]^{0.42} \tag{2.19}$$

A composite expression for the average Nusselt number for natural convection was proposed by Mittelman et al. (2009) for natural convective heat transfer behind the PV module with a back mounted channel.

$$\overline{Nu} = \left[\frac{6.25}{Ra^{"} Sin\phi} + \frac{1.64}{(Ra^{"} Sin\phi)^{2/5}} \right]^{-1/2} \quad (2.20)$$

The above equation is not sufficient to predict cooling rates as it neglects radiative heat transfer. The radiative cooling rate in case of black vertical wall was predicted by Moutsogolu and Wang (1989). Combined convective and radiative heat transfer was proposed by Brinkworth (2002), and Brinkworth and Sandberg (2006).

2.3 Computational fluid dynamics modeling

The recent increase of computational resources and availability of commercial Computational Fluid Dynamics (CFD) software have made realization of numerical solution to the problem of heat transfer by convection in buildings and building components with little calculation difficulty. Computational fluid dynamics is a numerical approach that is informative while also saving time and money. A very complex thermo fluid phenomenon under the outdoor environmental conditions exists in the DSF system. Such a phenomenon involves heat transfer by conduction, convection, and radiation with laminar, transient, and turbulent flow regimes. It has been noted that detailed computational fluid dynamics simulation of the fluid flow inside the air cavity is needed to solve this problem. Computational fluid dynamics techniques and models have the advantages of lower cost, high speed, flexibility to sensitivity analysis, ability to simulate realistic conditions and ability to simulate ideal conditions at which experimental studies are hard to conduct. However, only a few simplified cases

exist in the literature.

2.3.1 Coupling of computational fluid dynamics and building energy simulation

In order to gain an accurate prediction of total building energy use and indoor environment, it is crucial to integrate computational fluid dynamics (CFD) and building energy simulation (BES) programs together. Thermal coupling strategies between the façade and the whole building must be adequately simulated. More complementary information could be provided by both programs. Building energy simulation as a power tool could be used to evaluate thermal performance of any building component i.e. windows, roofs or walls and their effects on the total energy consumptions of buildings and building heating or cooling load as well as interior surface temperatures of building envelops. During the evaluation process, determination of air temperature distributions and heat transfer by convection in the indoor environment could be performed by CFD. Zhai and Chen (2005) compared the functions of building energy simulation and computational fluid dynamics programs in their work. It indicates that BES program is capable of considering weather and solar impact, enclosure thermal behaviors, HVAC system capacity and energy consumption, while the CFD program is able to determine thermal comfort including air temperature, air velocity, air humidity, and airflow turbulence and indoor air quality, for example contaminant concentrations and air distribution. Detailed coupling strategies and methods were also described in their

work.

The literature contains many reports of work concerning the integration of energy simulation and computational fluid dynamics programs. The principles, strategies and method for building energy simulation and CFD coupling were discussed by Zhai and Chen (2002, 2003). Crawley et al. (2000) used this concept by incorporating a CFD program into an energy simulation program i.e. EnergyPluse.

2.4 Building integrated photovoltaic (BIPV) system

Incorporating PV cells into building envelope or other building components is often termed Building Integrated Photovoltaic (BIPV). Compared with a stand alone system, BIPV system is more cost effective as no additional supporting structure or frames work are needed.

Building integrated photovoltaics (BIPV) has long been credited as one of the most important applications for PV in developed countries and has been well-developed all over the world among the other types of PV applications. PV modules, especially semi-transparent a-Si solar cells, can be incorporated in a glass-glass construction for providing shading solutions with lower maintenance cost compared with conventional double skin façade without integration of PV, as shown in Figure 2.1.

Figure 2.1 Example of a semi-transparent PV façade

2.4.1 Ventilated photovoltaic façades

PV panels may experience undesirably high temperatures due to part of the absorbed solar radiation that is not converted into electricity. This heat input can increase the cells temperatures thus decreasing the conversion efficiency of solar cells. Open channels beneath PV modules are commonly used to extract the additional heat. The air gap on the back of the PV modules provides natural cooling for the PV cell and reduces its operational temperature. Natural cooling using free convection is a simple method with lower cost to remove heat from the back of the PV modules and to keep the electrical efficiency at an acceptable level. By maintaining reasonable temperature on the PV cells, their efficiency could be enhanced dramatically and their working life extended through a reduction of thermal cycles and stresses. The output electrical generation is, therefore, increased.

Natural ventilation is induced by buoyancy forces due to a temperature difference between the inlets and outlets of the building envelope. There are so many similar structures functioning like this, for example, wind towers, Trombe walls and solar chimneys. Ventilated building integrated PV façade systems involve complicated air flow and natural convective heat transfer phenomena. It has long been noted and interested by various researchers and described in the literature. There is a growing interest in studying heat and fluid flow in air gaps behind PV panels in order to maximize the utilization of the solar energy from the PV system. These previous works include Brinkworth et al. (1997, 2000, 2005, 2006), Mittelman et al. (2009), Tonui and Tripanagnostopoulos (2005) as well as Ibrahim et al. (2006).

Brinkworth et al. (1997) indicated that providing a ventilated air gap behind a PV panel is an effective way to reduce the increase in PV module temperature, which otherwise lead to a decrease in electrical output. The results showed that reduction in temperature of up to 20 K can be obtained by heat transfer to an air flow induced by buoyancy in a duct behind the PV component, with a significant increase in the electrical output and reduction of heat gain into the building. A PV roof installation was developed, and measured data from the full scale test rig was used to evaluate model predictions through a CFD simulation tool. Important design parameters, for example, the depth of the cooling duct were identified and its effect on the thermal and electrical performance of the system was evaluated. As observed by Martin (2003) the greater the depth behind the modules, the greater the cooling due to natural convection. Natural ventilation effects of an air

gap on PV module's power output and heat transfer across a PV wall and PV-roof have been investigated by Yang et al. (2000). A scale analysis and numerical study of PV modules with a back mounted air channel that provides heat transfer rates over a practical range of operating conditions and channel geometries was conducted by Mittelman et al. (2009). The passive air cooling rate of an open channel beneath PV panels was predicted. The results illustrate the effect of the Rayleigh number and channel aspect ratio on the channel Nusselt number for combined convection and radiation heat transfer.

Moshfegh and Sandberg (1998) explored the heat transfer and air flow characteristics of buoyancy driven air flow behind PV panel. In order to enhance heat transfer in the cavity, Tonui and Tripanagnostopoulos (2005) proposed a system with a Thin Flat Metallic Sheet (TFMS) inserted in the middle of the air channel as a baffle sheet, as shown in Figure 2.2. Heat extraction from the PV panel above the air gap was enhanced. Shading, on the other hand, to the roof to reduce heat conduction to the interior of the building is also provided. The reference system, as showing in the left of the Figure 2.2, it has a simple air duct that is attached at the back of the PV module. The modified system, TFMS has a similar air duct but insert a thin sheet of aluminum plate. It functions like a parallel double pass air channel with increased heat extraction surface. By using the air channel, the temperature of PV module could be reduced so that cell efficiency is improved. The controlled warm air in the channel, on the other hand, could be utilized for winter preheating or summer cooling. Mei and Infield (2003) modeled

the PV facades system by using the TRNSYS simulation program. There are total three major components in the building simulation model. There are the PV façade (PV panel, air gap and inner double glazing); the solar air collectors; and a TRNSYS single zone building model plus additional controller models. The main features of the entire model were outlined and the thermal impact of the ventilated PV façade was assessed. It was found that twelve percent of heating energy could be saved using the pre-heated ventilation of the air for the buildings located in Barcelona in winter.

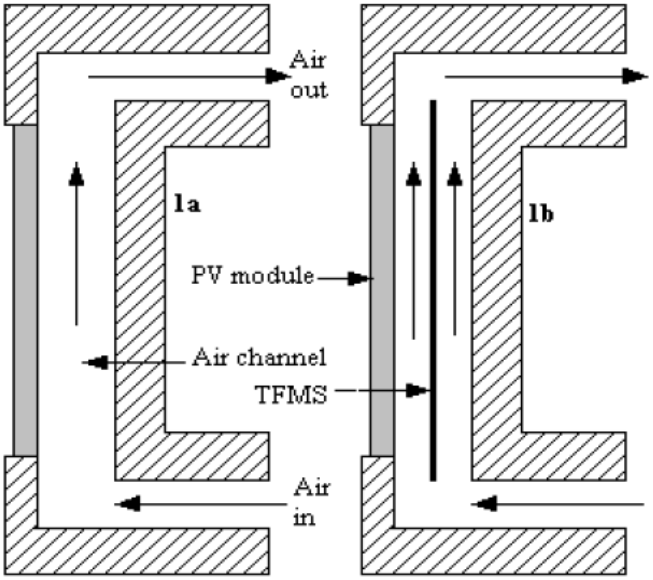

Figure 2.2 Cross section of the PV/T air system, reference system is showing on the left (1a) and modified system showing on the right (1b)

Directly using of the warmed air from the PV façade for building heating is an effective way to use the extra thermal energy from PV-solar heating system during winter season. In summer, the warmed air exhausted from the channel behind the

PV panel can be collected to provide thermal energy driving the solar adsorption cooling system for building cooling according to Mei et al. (2006). The authors have recently completed an EU project which concerned the ventilated PV-solar air heating system combining with a desiccant cooling machine constructed and installed in the Mataro Library, near Barcelona. The cooling performance of the solar powered desiccant cooling system was evaluated by the detailed modeling of the complete cooling process. It is shown that air of 70^{o}C generated from their solar air heating system can be efficiently utilized to regenerate the sorption wheel in the desiccant cooling machine. The average COP of the cooling system through the summer season is approximate 0.518 and solar fraction 75% can be achieved.

Importance of thermal stratification in the air cavity behind the photovoltaic module in performance prediction or simulation of a ventilated photovoltaic façade, as shown in Figure 2.3, was identified by Leal et al. (2003) and Yun et al. (2007). The results indicated that considering the thermal stratification and air movement is crucial. Three vertical zones were created in the air gap behind the PV module. The effect of vertical thermal stratification, and buoyancy and wind forces were considered. Research showed that it is useful in describing thermal stratification within the building to divide a zone into multiple zones.

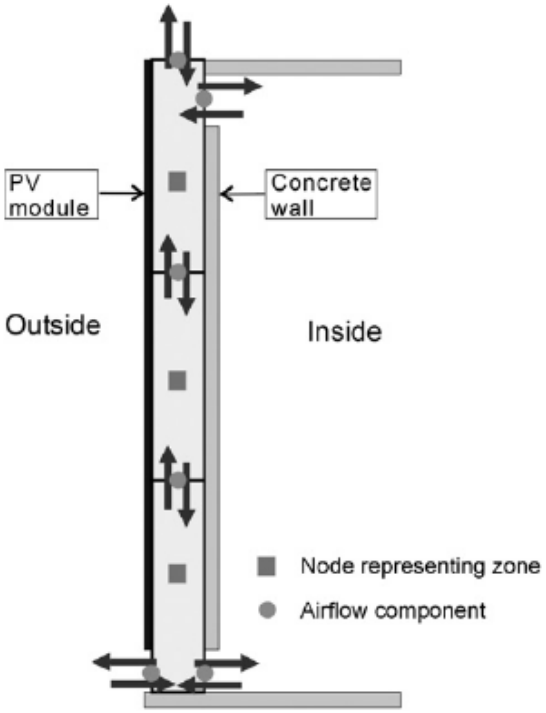

Figure 2.3 Schematic diagram of ventilated PV façade by Yun et al. (2007)

2.4.2 Electrical power generation from BIPV system

Building integrated photovoltaic technology offers both architects and engineers the option to develop innovative and aesthetically pleasing designs. Electrical power generation from the BIPV system can supply some of building's energy demand rather than dependent being entirely on grid utility. In Europe, a recent marketing survey shows that almost seventy percent of sample of polled architects are intending to install PV elements in the design of new developed buildings or on existing buildings during refurbishment. Since 1990 various projects were relative to using photovoltaic for innovative design and benefit of the green energy

power generation. For example, a total 1689 kWh of electricity with an average annual solar irradiation 596 kWh/m^2 can be generated from a PV project in Berlin Kreuzberg, Germany as indicated by Liao (2005).

According to Pearsall (1996), the goal of Europe is to reach 2000 MW_p capacity with PV electricity generation in 2010, among which 900MW_p will be contributed by PV roof systems and 400MW_p by photovoltaic wall systems. Not only will the program save conventional energy use, but it will also offset the 'peak' electricity generation from coal and oil and the emissions from diesel and propane generators. Currently environmental protection is a very important determinant for using photovoltaics in buildings.

2.4.3 The effect of the BIPV on building cooling load

Previous research indicated that it is possible to reduce the cooling load in office buildings as well as other buildings in hot arid and hot humid areas if a double skin facade is employed. Research has also shown that double skin façade with incorporated photovoltaics is capable of reducing the total solar heat gain, and thus can contribute to reduce the entire building cooling load. The reductions on cooling loads in rooms range from 19% to 40% depending on the glazing thermal and visual performance characteristics of the exterior glazing of the double skin façade according to Hamza (2005). Yang et al. (1999) proposed simplified methods to calculate the cooling load component of a PV façade. The heat transfer

across a photovoltaic wall (PV wall) was investigated to determine the cooling load component contributed by building-integrated PV walls. A new definition of equivalent hourly average outdoor temperature is given for simplifying the calculation procedures of the cooling load component. It is indicated that the cooling load component can be obtained conveniently by using the average outdoor temperature and recommended film coefficients of the special building claddings. The photovoltaic integration in building walls reduces the corresponding cooling load components by 33%-50%.

Chow et al. (2009) investigated the energy performance of "see-through" PV glazing as applied to a typical open-plan office environment of Hong Kong. Theoretical models developed through the ESP-r simulation platform were validated with measurements from an experimental test rig. It is found that their natural-ventilated PV double-glazing technology could cut down the air-conditioning power consumption by 28%, as compared to the conventional single absorptive glazing system.

2.5 Photovoltaic solar cell and its efficiency

According to Wikipedia (the free encyclopedia), a solar cell is a device that converts the energy of sunlight directly into electricity by the photovoltaic effect. Sometimes the term solar cell is reserved for devices intended specifically to capture energy from sunlight, while the term photovoltaic cell is used when the

light source is unspecified. Assemblies of cells are used to make solar panels, solar modules, or photovoltaic arrays. Photovoltaics is the field of technology and research related to the application of solar cells in producing electricity for practical use. The energy generated this way is an example of solar energy (also called solar power).

Commercially available PV modules are rated based on the American Society for Testing Materials (ASTM) standard reporting conditions (SRC). The SRC are: solar radiation $G_T = 1000\,\mathrm{W/m^2}$, cell temperature $T_{cell} = 25^oC$, and AM = 1.5. That is to say, a typical 75 Watt PV module has 75 Watt label ratings at SRC according to King (1997). Figure 2.4 shows the characteristic curve of a PV module measured in the Solar Simulation Lab of the Department of Building Services Engineering, Hong Kong Polytechnic University.

Figure 2.4 illustrates a typical current (*I*) - voltage (*V*) curve of amorphous silicon cell. The curve shows the relationships between the current and voltage generated by amorphous silicon cell. In the curve the important parameters such as, short circuit current I_{SC}, open circuit voltage V_{OC} and maximum power point $P_{\max}$ are also indicated in the curve. The series resistance R_s, in normal situations, can be neglected in the short-circuit condition. The short circuit current I_{sc} is equal to the light-generated current I_L, which is proportional to the solar irradiance on the cell surface. Therefore I_{sc} is also proportional to the irradiance, i.e. $I_{sc} \propto S$, which is described by Fung, (2006).

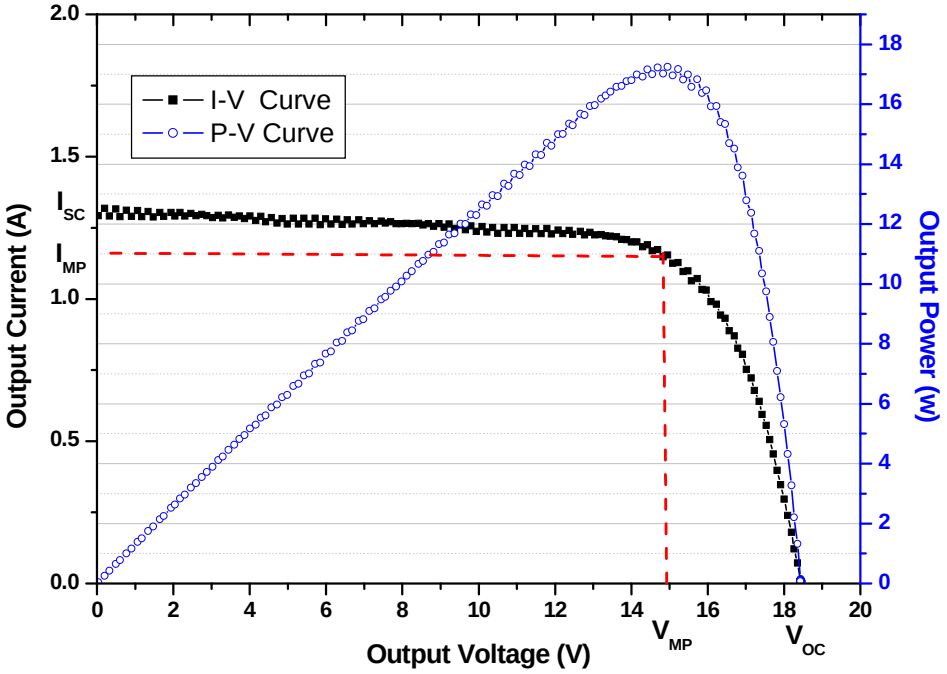

Figure 2.4 I-V characteristic curve of PV module

According to Markvart, (2000) the dependence of temperature of solar cell current is much smaller than that of solar cell voltage. A constant short circuit current, therefore, can be assumed with change in module temperature for the purpose of module modeling. The diode current and resistance terms, at an average irradiance level, are negligible. The correlations between open circuit voltage V_{oc} and the solar irradiance S can be expressed as follows,

$$V_{oc} \propto \ln \left(\frac{K \cdot S}{I_o}\right) \tag{2. 21}$$

According to Lasnier and Ang (1990), the open circuit voltage will decrease linearly with increasing cell temperature as the saturated current increases

exponentially with the cell temperature.

$$V_{oc} \propto \frac{1}{T_{cell}} \tag{2.22}$$

2.6 Summary

A literature review is presented in this chapter. The literature review focuses on definition and classification of DSF system, modeling of heat transfer and air flow in the air channel of DSF systems, experimental investigation for the natural convective heat transfer in vertical parallel plates, which create the air channel as well as various methods to evaluate the energy performance of ventilated PV façade.

The literature review indicates that several studies have been conducted theoretically and experimentally on natural convective heat transfer and air flow in the air cavity or channel of DSF system. Research on energy performance of double skin photovoltaic façade is also increasing in the past literature.

However, so far, no research has been conducted on the natural convective heat transfer in windows or facades integrated with semi-transparent PV cells, in order to assess the local and average heat transfer coefficients. Determining the local and average heat transfer coefficients is important for estimating the amount of cooling load reduction and conversion efficiency improvement of the BIPV facade. To contribute further information on this issue, heat transfer through windows

with semi-transparent PV is investigated in this study. The various parameters affecting the local heat transfer coefficients on vertical glazing surfaces are also evaluated and based on simulation results, the optimum thermal thickness of the air layer is provided.

CHAPTER 3: EXPERIMENTAL INVESTIGATION OF THE VENTILATED PV DSF

3.1 Introduction

A series of well recorded experiments were carried out in order to examine the validity of the simulation models used in this study. The experimental study was carried out in the Solar Simulation Lab of The Department of Buildings Services Engineering, The Hong Kong Polytechnic University. An experiment rig has been set up in the lab. The measured data from the test rig were employed to verify the corresponding simulation models.

In this chapter, the detailed descriptions of the experimental test rig and its major components are presented. That is followed by describing the experimental methodology.

3.2 Experiment set-up

This study aimed to investigate the effect of ventilated PV glazing system on the heat transmission through building envelope for finding possible heat control strategies. An indoor experimental testing facility in Hong Kong Polytechnic University was set up during the testing period for the above mentioned purposes. This test rig allows change solar radiation levels and makes comparison easy to

conduct among different operational conditions with same solar irradiation level. This maybe difficult to conduct under outdoor testing conditions as weather conditions, i. e. solar radiation and ambient air temperature change from time to time. In the previous literature, researchers attempted to find similar weather conditions among all test data collected for their comparison purposes, which may introduce some errors in the comparison.

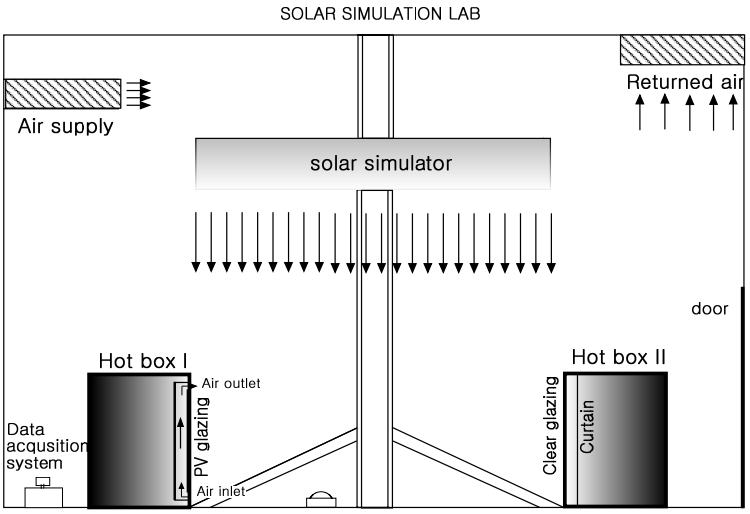

Figure 3.1 Schematic of the locations of two hot boxes for thermal performance comparison

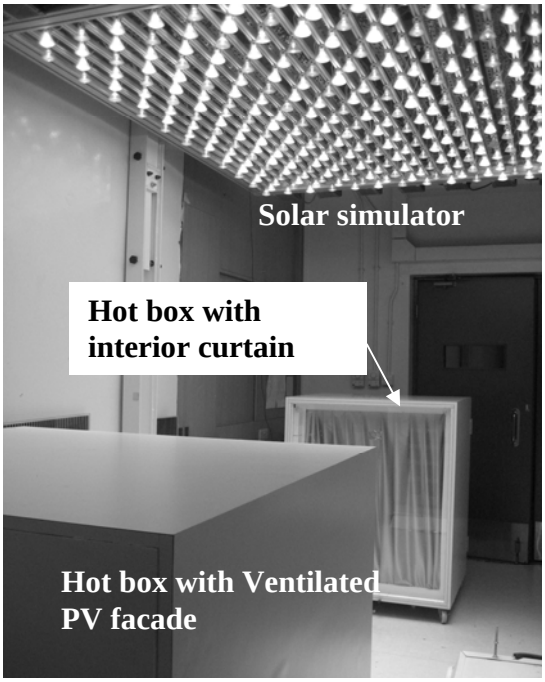

Figure 3.2 Photo of the test rig in the Solar Simulation Lab

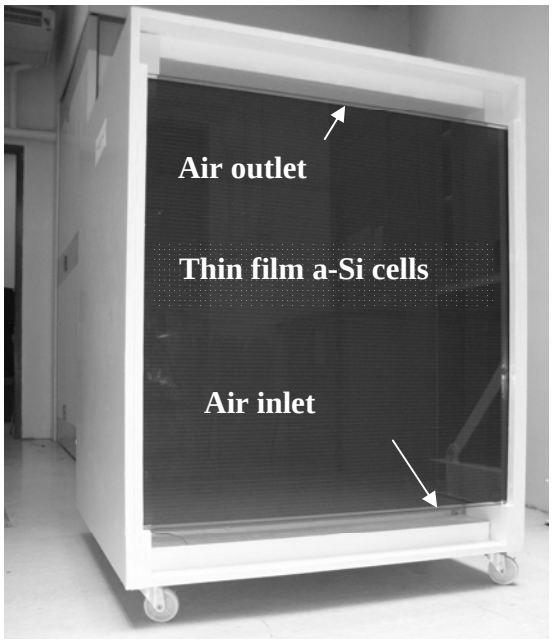

Figure 3.3 Photo of the hot box with double skin photovoltaic façade integrated in the front surface of the box

Figure 3.1 shows a schematic of the view of the experimental apparatus. The interior wall surfaces of the two hot boxes are well insulated by polyurethane (PU) insulation layer. The photo of the test rig is shown in Figure 3.2. The experimental rig included two well insulated hot boxes and a solar simulator which provides simulated light to the module surface. The front side of the hot box was mounted with a PV module as shown in Figure 3.3. The PV module is under the exposure of the solar simulator. Heat transfer by convection and radiation occurs on the surface of the PV module. Heat absorbed by the PV module increases its temperature and part of the heat transmitted through the module.

The exterior and interior temperature of the hot box, the ambient temperature, the air flow rate, the inlet and outlet temperature of air in the ventilation channel behind the PV module were logged at constant time interval through Midi Date Logger – GL800 as shown in Figure 3.4. The GL800 data logger accepts voltage, temperature, humidity, pulse and logic signals. The sensors are connected via rear mounted screw terminals. With its channel-to-channel isolation, wiring errors or overloaded channels will not affect neighboring channels. Its built-in 12.0MB non-volatile memory retains data even if the power supply is interrupted. The included software provides real-time waveform monitoring, data upload and data export to spreadsheets as described on the website of the products.

The solar radiation incident on the vertical façade is an important data in the experiment. A pyranometer (MS-802, EKO), as shown in Figure 3.5, was used to

measure the solar heat flux per unit area of the module during the measurement. MS-802 from EKO Instrument Co. Ltd was employed in the experiments. The pyranometer is sensitive to specific wavelength ranging from 300 to 2800 nm. It is suitable for measuring solar radiation generated by a solar simulator. During the measurements, the pyranometer was put next to the PV modules in order to measure the actual solar irradiance falling on the module. The sensitivity of the pyranometer is 6.86 mV/kW/m^2. The detailed specification of MS-802 is listed in Table 3.1. The measured solar radiation is in unit of W/m^2. It the global irradiance includes the direct, diffuse and reflected solar radiation.

Figure 3.4 The photo of the GL 800 Midi Logger
cited from http://www.microdaq.com/graphtec/gl800_midi_logger.

Figure 3.5 The photo of the pyranometer

Table 3.1 Specification of the pyranometer MS-802

Specifications	MS-802
Response time 95%	8 (sec)
Directional response (at 1000 W/m^2)	± 10 W/m^2
Sensitivity	6.86 mV/kW/m^2
Non-linearity	± 0.2 (at 1000 W/m^2)
Operating temperature	- 20^{o}C — + 60^{o}C
Temperature response (for 50^{o}C band)	<± 1%
Wavelength range (more than 50% of transmittance)	305 to 2800 nm

One of the most important instruments in the experiment is the solar simulator. It contains 363 (11 × 33) halogen diachronic lamps empowered by 12 VDC. The solar simulator is mounted on a steel supporting framework as shown in Figure 3.1. The height of it is adjustable for operation under various test conditions; see for example, in cater for different inclination angles.

The thin film solar cells are used for this application in order to explore the thermal performance of the hot box integrated with semi-transparent solar cells. The cost for thin film amorphous silicon cells is lower compared with polycrystalline silicon cells. The successful doping of amorphous silicon created tremendous interest in this material. The technical data for this PV module and the dimensions of the hot box are listed in Table 3.1

Table 3.2 Basic parameters of components in the test rig

Components	Specification
PV glazing	
Panel dimensions (H × W × D)	0.95 m × 0.98 m × 0.012m
Solar cell type	Amorphous silicon
PV area	0.466 m^2
PV efficiency	6%
Max power voltage(V)	69 V
Max power current (A)	0.28 A
Open circuit voltage (V)	89 V
Short circuit current (A)	0.38 A
Clear float glass	
Dimensions (H × W × D)	1.18 m × 0.98 m × 0.005 m
Effective transmittance	0.86
Air channel behind PV	
Thickness of the air layer	16 cm
Dimensions of the air inlet opening (H × W)	0.1 m × 0.98 m
Dimensions of the air outlet opening (H × W)	0.1 m × 0.98 m
Height of the air channel	1 m
Dimensions of the hot-box (H ×W × D)	1.22 m × 0.82 m × 0.99 m

3.3 Solar radiation on the vertical surfaces measurement

A series of thermocouples were used to examine the thermal performance of the hot box integrated with double skin photovoltaic façade and the one without PV façade but integrated with conventional interior curtain. Nine thermocouples were inserted in the air channel along the channel height and nine thermocouples were mounted on the surfaces of the PV module. The air temperatures in two hot boxes were also measured by two thermocouples.

Solar radiation falling on the surface of the PV module and clear glass from the Solar Simulator is measured and recorded. Figure 3.6 presents the solar radiation distribution on the surface. It is found that the solar radiation intensity can be approximated as unity for an area with same distance from the bottom of the PV module, and only small non-unity areas are found in the measured data. This may cause from uncertainty in the measurement. Previous research, Fung (2004) and Cheng (2007) assume that the solar radiant flux can be regarded as uniform as the number of halogen lamps is large and diffuse angle of the product is wide.

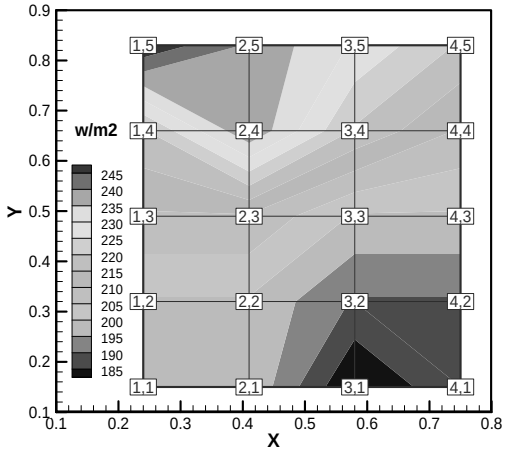

a)

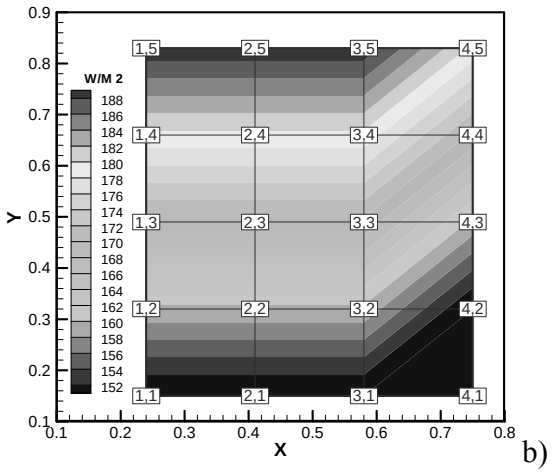

b)

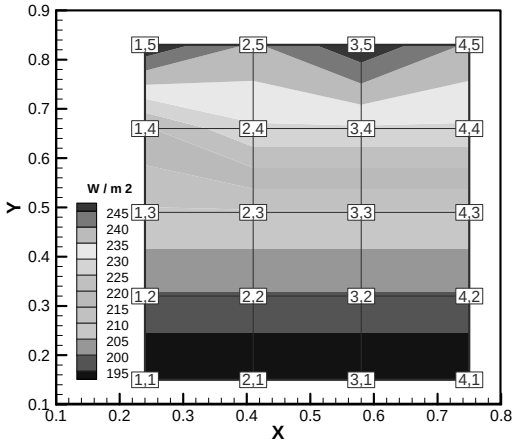

c)

Figure 3.6 Distribution of the solar radiation intensity on the surface of the PV module for three different solar radiation levels

3.4 Comparison of the surfaces temperatures for ventilated and non-ventilated PV façades

Acknowledgment of detailed temperature distribution of PV façade is useful in the double skin photovoltaic façade design. In this section, the comparison of the surface temperature distribution for ventilated and non-ventilated PV façade was examined. Figure 3.7 shows the temperature distribution of PV module for ventilated (upper) and non-ventilated (lower) conditions. Well-proportioned

temperature distribution may benefit better operation of PV module and help to extend its average life-span by eliminating thermal stress as that may destroy solar cells.

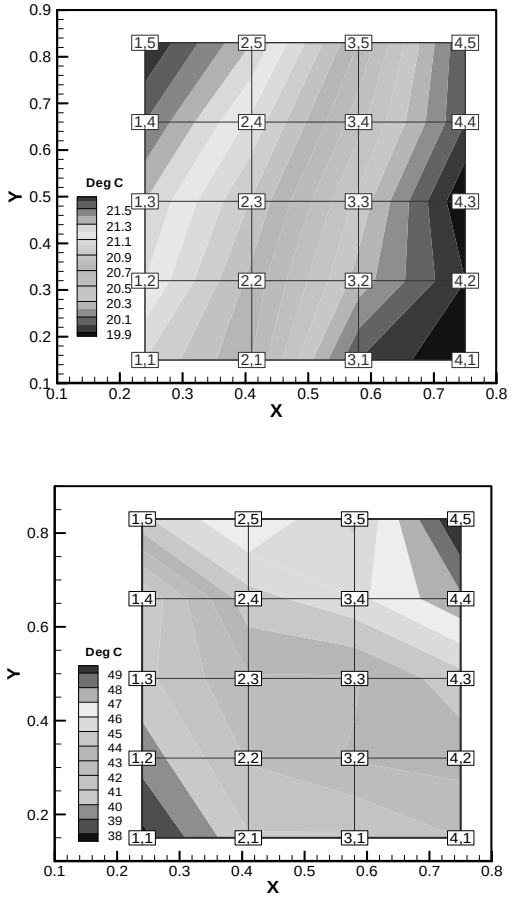

Figure 3.7 Temperature distribution of the PV module for ventilated (upper) and non-ventilated (lower) conditions

3.5 Comparison of the thermal performance of two hot box with and without PV

In this section, the performance of the double skin photovoltaic façade in variety

of operational modes was examined. There are three operational modes conducted during the experiment. Operational mode I refers to the PV module working under the closed cavity of the façade; Operational mode II refers to PV module working under the open cavity of the façade with forced ventilation and Operational mode III refers to PV module working under the open cavity of the façade with natural ventilation as illustrated in Table 3.3.

Table 3.3 Operational modes for DSPV system

Operating Mode	I	II	III
Feature	Closed cavity	Open cavity forced ventilation	Open cavity free convection

Figure 3.8 shows the temperature profiles of air in two hot boxes with and without PV. The data was collected from May 24, 2009 to May 26, 2009. The double skin photovoltaic façade was working under two operational modes, i.e. Operational mode I for closed cavity and Operational mode II for open cavity with forced ventilation. It is found that air temperature in the hot box with PV façade is lower than that without PV façade under the two operational modes. Compared with conventional façade using clear glass, PV façade is useful in controlling the heat transmission through the façade. This is the possible reason for why the air temperature in the hot box with PV façade is lower than that with conventional façade. The maximum air temperature difference between two hot boxes could reach 12^{o}C as shown in the figure. For difference of the two operational modes of

the façade with PV, it is found that air in the hot box under Operational mode II is lower than that for Operational mode I. The measured data indicated that maximum air temperature in the hot box with PV façade under Operational mode I is about 36°C, while it is only about 29°C for Operational mode II. This is partly due to forced ventilated enhanced the convective heat transfer. More heat is extracted to the air in the air channel behind the PV module. This is desirable for PV module operation as thermal regulation of the PV module is realized by the forced ventilation behind the module.

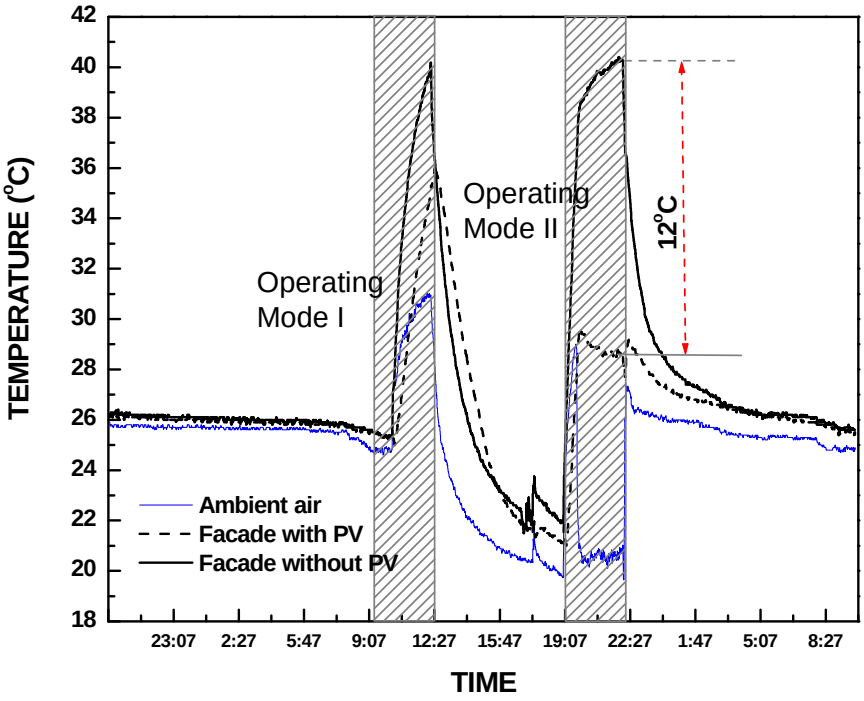

Figure 3.8 Comparison of the air temperature for two operational modes

Figure 3.9 shows the temperature profile of air in the two hot boxes with and without PV façade under Operational mode III, i.e. free natural ventilation for the PV façade is presented. The difference between this and previous conditions is that an interior curtain is employed in the conventional façade for shading purposes. Results indicated that natural ventilation for the PV façade is a convenient way to control the heat transmission of the PV module under moderate weather conditions. The maximum air temperature in the hot box with PV façade under natural ventilations condition is approximately 50°C, while it is only 40°C under forced ventilation conditions for the PV façade.

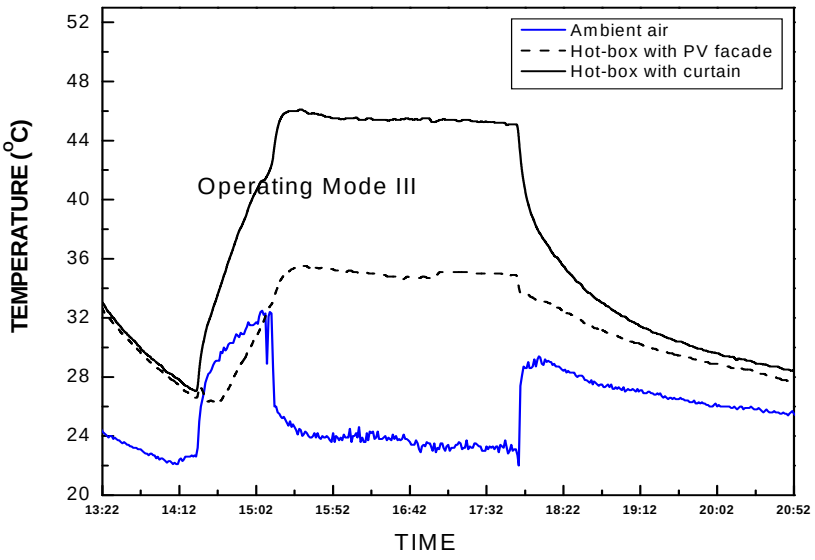

Figure 3.9 Comparison of the air temperatures in hot box with and without PV façade. Mode III for natural ventilation (data collected on 05/26/2009)

Figure 3.10 shows interior surface temperature variations for ventilated PV façade and conventional façade with internal curtain. The measured data indicate that interior surface has lower temperature than that of the conventional clear glass façade with internal curtain. This is mainly because lower heat transfer mission occurred in the PV façade glazing cavity. Data were collected in the laboratory of Hong Kong Polytechnic University for three days. The maximum temperature difference for the first day is reached at 8^{o}C, 11^{o}C for the second day, 10^{o}C for the last day. This may indicate that lower indoor temperature could be achieved in a building with a PV double skin façade in summer. Thus comfortable indoor environment could be created for occupants during the summer season.

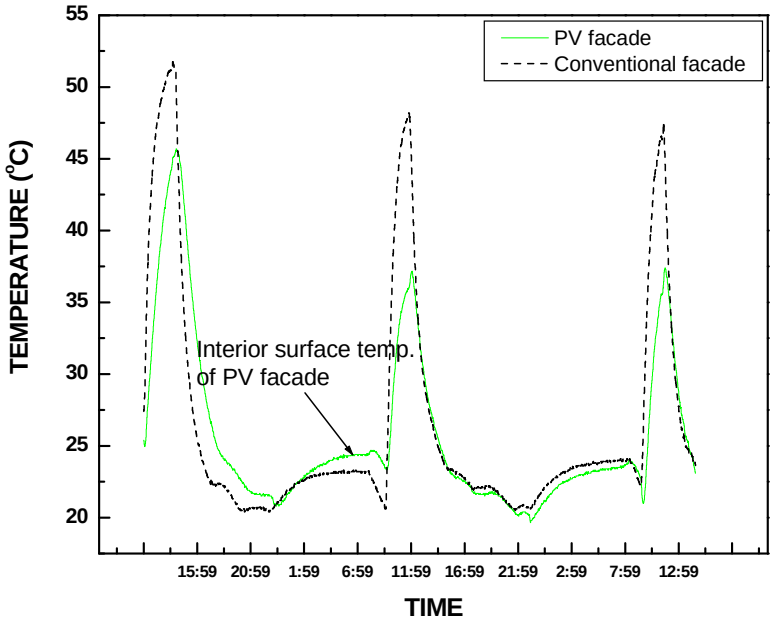

Figure 3.10 Interior surface temperature variations for ventilated PV façade and conventional façade with internal curtain

3.6 Outdoor measurement

Previous section describes the experiment conducted at indoor facilities using artificial radiation sources. In this section, an outdoor measurement has been conducted at the campus of The Hong Kong Polytechnic University in order to explore the thermal performance of the double sided PV (DSPV) façade or named as PV DSF system when working under the real subtropical whether conditions. The outer glazing of the DSPV façade consists of semi-transparent PV glass panel with a-Si solar cells, and the inner glazing is a clear glass panel. Figure 3.11 shows the outdoor test facility for DSPV façade and the conventional façade with internal curtain. Both two hot-boxes are south oriented to obtain maximum solar radiation. Various surface temperatures of the two hot-boxes and air temperatures in the air channel of the DSPV system are monitored by means of T type thermocouples.

Figure 3.11 Outdoor test facility for DSPV façade and the conventional façade with internal curtain

The experiment under natural ventilation is conducted at high-noon. Figure 3.12 shows the temperature variation inside the DSPV façade and the conventional façade system. The experimental results indicated that the inside air temperature for DSPV façade is quite lower than temperature in conventional façade with internal curtain for shading purposes. It is found that the temperature in the DSPV façade system is more stable. The temperature variation in conventional façade system with internal curtain is larger. There are 4 temperature peak have been observed during the measurement. The maximum temperature for conventional facade is close to 34^{o}C at 13:10 PM, 29^{o}C for DSPV facade. This indicated that the effectiveness of the solar screening through the use of the naturally ventilation of air beneath the PV module. The temperature deviation between the two systems becomes smaller late in the afternoon.

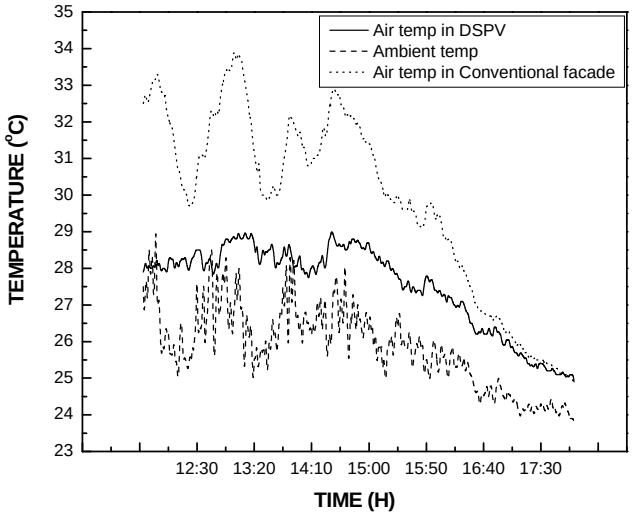

Figure 3.12 Comparison of air temperatures inside DSPV façade and conventional façade system

3.7 Summary

In this section, a number of experiments including outdoor and indoor measurements were carried out in order to examine the validity of the simulation models and the thermal performances of the double skin photovoltaic façade and conventional façade with clear glass. The laboratory measurements using developed test rig and existing equipment in the Solar Simulation Lab of The Department of Building Services Engineering, Hong Kong Polytechnic University were performed. The detailed methodology of the experiment and the equipment used were described. Comparison among a variety of operational modes for double skin photovoltaic façade, i.e. Operational mode I for closed cavity, Operational mode II for forced ventilation and Operational mode III for natural ventilation were carried out and results were analyzed in detail. Results indicated that natural ventilation for the PV façade is convenient way to control the heat transmission of the PV module under moderate weather conditions. It is found that air temperature in the hot box with PV façade is lower than that without PV façade under two operational modes. Compared with the conventional façade using clear glass, the PV façade is useful in controlling the heat transmission through the façade.

CHAPTER 4: MODELING OF CONVECTIVE HEAT TRANSFER IN THE OPEN AIR CAVITY OF VENTILATED PV DSF SYSTEM

4.1 Introduction

Traditionally, windows play an important role in controlling heat transmission in indoor space during the summer period and external ambient heat loss during the winter period. In order to decrease solar transmission through windows, shading and blinds in the air cavities of the double glazed window are, therefore, often employed. In addition to the use blinds in the cavities of double-glazed windows for shade and thermal control, photovoltaic or solar cells could be integrated with the glass to absorb solar radiation. This novel glazing system type could not only generate electricity but also achieve potential energy savings by reducing the air conditioning cooling load when applied in subtropical climatic conditions and simultaneously provide visual comfort in the indoor environment. The innovative natural-ventilated PV double-glazing technology could significantly cut down the air-conditioning power consumption when all design parameters are fully considered in the design stage.

Figure 4.1 (a) and Figure 4.2 (b) show the schematic of ventilated double panes PV window for summer ventilated in hot climate and winter heating in cold

weather conditions. In this chapter, the air flow in the channel of the window will be simulated by consideration of both laminar and turbulent flow. Various turbulent models will be employed and the results from them will be discussed. The heat transfer and air flow characteristics in the channel will be evaluated by numerical simulation. Various factors affecting the air flow and heat transmission will be identified and examined. Predicted results from the numerical simulation will be analyzed in detail.

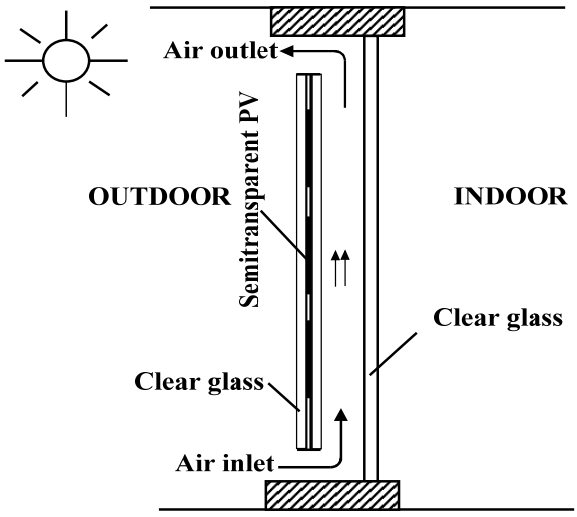

Figure 4.1 (a) Schematic of ventilated double-paned PV window with the PV on outside for summer ventilation in hot climates

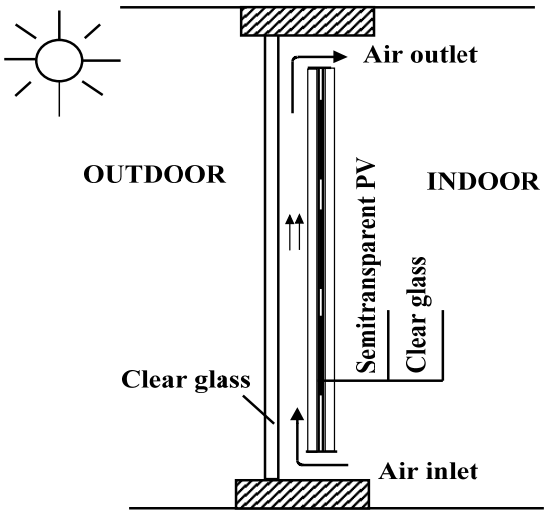

Figure 4.2 (b) Schematic of ventilated double-paned PV window with the PV on the inside for winter heating in cold climates

4.2 Computational fluid dynamics analysis of the air flow pattern in the cavity

4.2.1 Problem statements

The physical problem is buoyancy force induced natural convective heat transfer in air cavity created by two parallel vertical walls. See Figure 4.3. one surface of the wall is created by semi-transparent photovoltaic glass panel. The problem, at this stage, is considered to be steady state and two dimensional (2D). The top and bottom walls are well insulated, whereas the left wall is maintained at a lower temperature (T_c) and the right wall is maintained at a higher temperature (T_h), with $T_h > T_c$. Two air vents are located on the bottom and top of the photovoltaic panel for cool air inlet and warmer air outflow, respectively. It is assumed that the

influence of the temperature on density is confined only to the body force term of the momentum equation and that all other fluid properties are independent of temperature and pressure by adopting the similar assumptions by Shi (2004). The flow fields are considered to be steady and fluid is assumed incompressible.

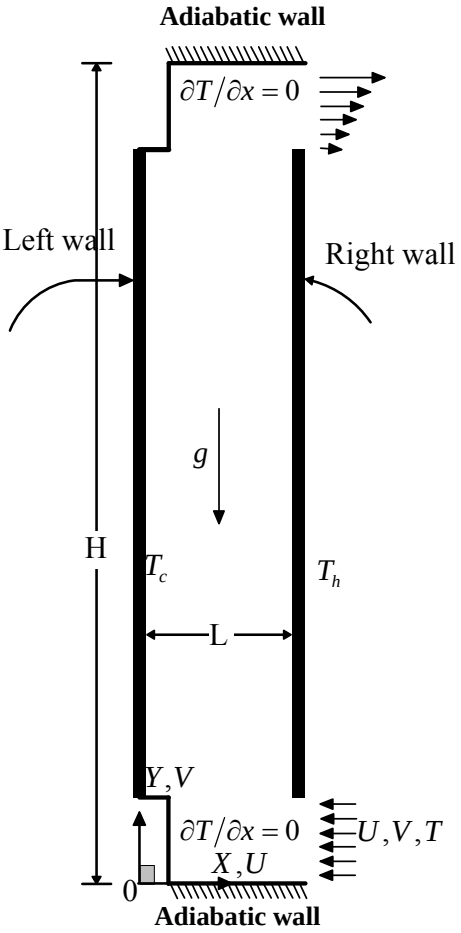

Figure 4.3 Schematic of the problem for natural convective heat transfer in an air cavity created by two vertical walls. Two openings for airflow are located on top and bottom.

4.2.2 Governing equations

In many practical engineering problems, the flows in the glazing cavity are turbulent, and it is a highly complex phenomenon. Fully developed turbulent flow is featured by entangled eddies of different sizes. Theoretically, it is possible to directly apply the conservation equations to the entire flow field considered. It is, however, unreasonably difficult to do it practically. Therefore, it is important to describe turbulent motion in terms of average quantities in order to create a usable numerical model of a turbulent flow field. The time averaged Navier Stokes equations of motion for steady, 2D flow in a vertical channel that is created by two parallel walls can be written according to Fedorov and Viskanta, (1997). Assume that fluid is incompressible flow and Boussinesq approximation is considered. Following the study by Anwar (2008), the mathematical model is described in the following section. The continuity equation for conservation of mass is described as follows:

$$\frac{\partial(\rho \bar{u})}{\partial x} + \frac{\partial(\rho \bar{v})}{\partial y} = 0 \tag{4.1}$$

The equations for conservation of momentum in *x*, *y* directions are as follows:

$$\frac{\partial}{\partial x}(\rho \bar{u}\bar{u}) + \frac{\partial}{\partial y}(\rho \bar{u}\bar{v}) = -\frac{\partial p}{\partial x} + \frac{\partial}{\partial x}\left[(\mu + \mu_t)\frac{\partial \bar{u}}{\partial x}\right] + \frac{\partial}{\partial y}\left[(\mu + \mu_t)\frac{\partial \bar{u}}{\partial y}\right] - \frac{2}{3}\rho\frac{\partial k}{\partial x} \tag{4.2}$$

$$\frac{\partial}{\partial x}(\rho \bar{u}\bar{v}) + \frac{\partial}{\partial y}(\rho \bar{v}\bar{v}) = -\frac{\partial p}{\partial y} + \frac{\partial}{\partial x}\left[(\mu + \mu_t)\frac{\partial \bar{v}}{\partial x}\right] + \frac{\partial}{\partial y}\left[(\mu + \mu_t)\frac{\partial \bar{v}}{\partial y}\right] - \frac{2}{3}\rho\frac{\partial k}{\partial y} + (\rho - \rho_o)g \tag{4.3}$$

The equation for conservation of energy is described as follows:

$$\frac{\partial}{\partial x}(\rho \bar{u} T) + \frac{\partial}{\partial y}(\rho \bar{v} T) = \frac{\partial}{\partial x}\left[\left(\frac{\kappa}{C_P} + \frac{\mu_t}{\mathrm{Pr}_t}\right)\frac{\partial T}{\partial x}\right] + \frac{\partial}{\partial y}\left[\left(\frac{\kappa}{C_P} + \frac{\mu_t}{\mathrm{Pr}_t}\right)\frac{\partial T}{\partial y}\right] \tag{4.4}$$

In above equations, μ_t is the turbulent dynamic viscosity that is to be calculated from the kinetic energy of the turbulence, k, and the turbulent kinetic energy dissipation rate, ε.Various turbulence correlations were employed in order to constitute a closed set of equations and then solve them reasonably.

Specific boundary conditions are needed to solve the partial difference equations (PDE) noted above. The boundary conditions are as follows:

- Boundary condition at the inlet and outlet

$$P_i = P_a \ , \ T_i = T_a \qquad \text{at} \quad y = 0 \tag{4.5}$$

$$P_o = P_a , \ P_o = P_a \qquad \text{at} \quad y = H \tag{4.6}$$

- Boundary condition at the walls

No slip boundary conditions on the wall are considered except at the inlet and outlet.

$$\bar{u}_i = 0, \text{ for } 0 \le y \le H \ , \ x = 0 \ \text{ and } \ x = L \tag{4.7}$$

Turbulence kinetic energy at the walls,

$$k = 0, \text{ for } 0 \le y \le H \ , \ x = 0 \ \text{ and } \ x = L \tag{4.8}$$

$$T = T_l, \text{ for } 0 \le y \le H \ , \ x = 0 \tag{4.9}$$

$$T = T_h, \text{ for } 0 \le y \le H, \quad x = L \tag{4.10}$$

$$\frac{\partial T}{\partial x} = 0, \text{ for } \quad y = 0 \text{ and } \quad y = H \tag{4.11}$$

4.2.3 Computational procedure

The present investigation deals with numerical predictions of air flow and temperature distribution in a two-dimensional air cavity, which is isothermally heated from one side and cooled on the other side. The Navier-Stokes equations and energy equation are solved numerically by iterative finite difference technique. The governing equations are substituted by a set of difference equations, used to all grid points in the calculation domain being considered.

4.2.3.1 Discretization approaches

A finite-difference numerical solution technique based on integration over the control volume is used to solve the model equations with appropriate boundary conditions. The SIMPLER algorithm is employed to solve the model equations in primitive variables and this is discussed by Patankar (1980) in detail. A network of grid points is first established throughout the domain of interest, when a finite-difference technique is to be used to solve a partial differential equation and associated boundary and possibly initial conditions. Figure 4.4 shows how the approximation of replacing the continuous calculation domain by a set of discrete

points P could be accomplished in the two-dimensional (2D) region.

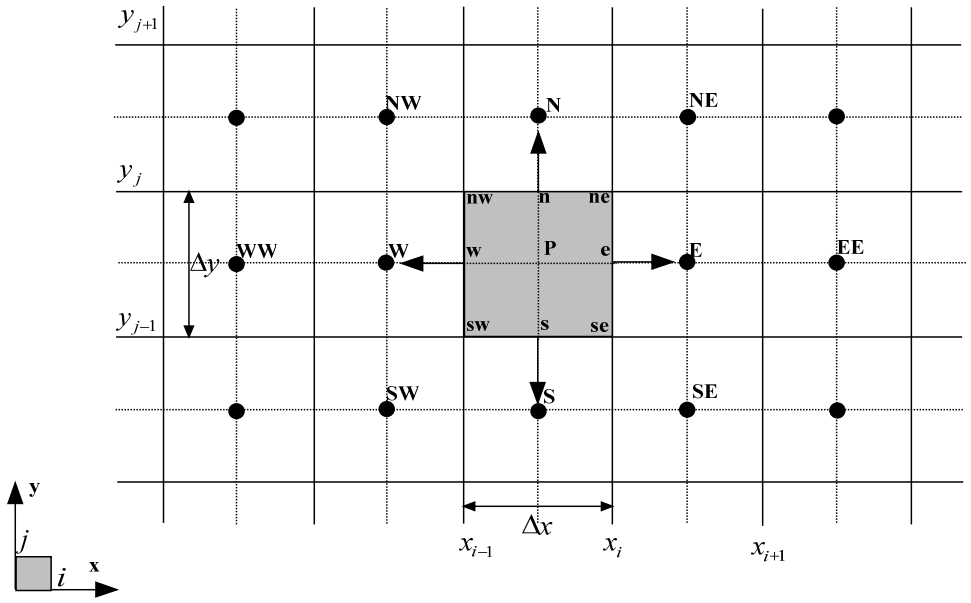

Figure 4.4 Typical example of a control volume for 2D computation

4.2.3.2 Grid generation

In order to resolve the turbulent boundary layer that is very thin compared to the height of the flow field, more control volumes near the two vertical walls are desirable and a finer grid is needed when creating the mesh of the computational domain. Another reason for using condensed grid near the wall is because the velocity is changing greatly in the boundary layer of the vertical walls. The flow at the center region of the cavity is not influenced as that occurs near the wall boundary and temperature tends to stay stable, some coarse grids, therefore, could be employed in the study and satisfy the grid density requirements for accurate solutions. Figure 4.5 shows example of the grid size distribution. A non-uniform

grid arrangement is employed for numerical investigation of natural convective heat transfer and fluid flow in air cavity created by two parallel vertical plates.

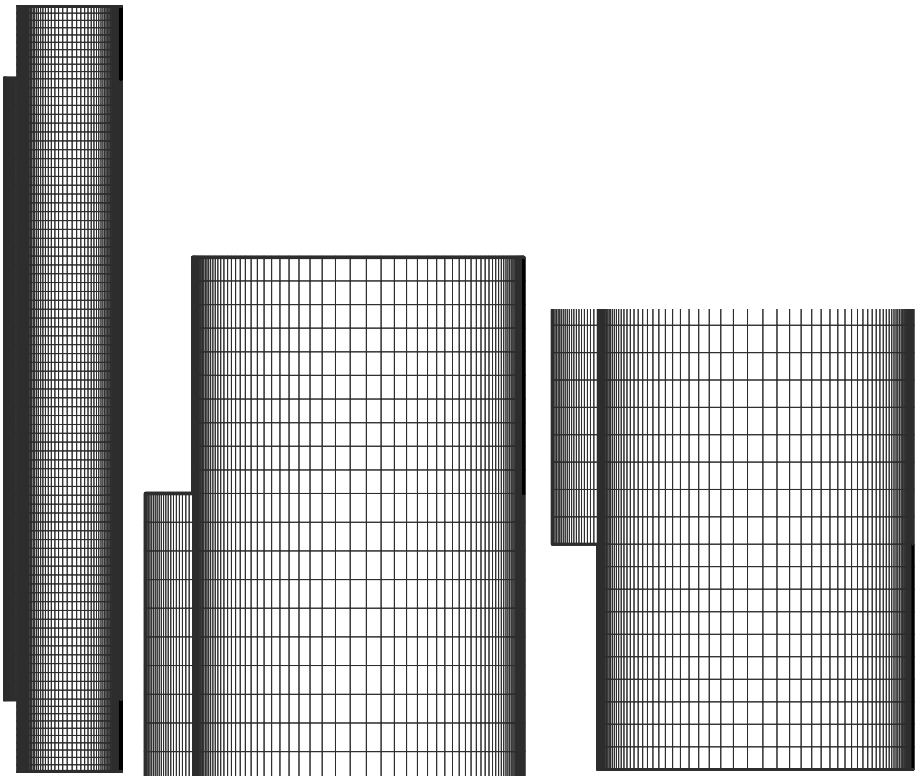

Figure 4.5 Example of grid size distribution for the channel wall shows the boundary layer flow regions at both vertical walls. Partial enlarged drawings for upper left and lower right of entire grid is shown on the middle and right of the figure.

4.2.3.3 Solution of resulting equations

4.2.3.3.1 Iterative methods

A lot of iterative methods are commonly used to solve system of equations. These iterative methods include: Jacobi method, Gauss-Seidel method, Successive

Over-Relaxation (SOR), or LSOR, Alternative Direction Implicit (ADI) method, Conjugate Gradient methods, Biconjungate Gradients and CGSTAB, Multigrid Methods. In this study, the successive over-relaxation method has been used for the solution of the resulting algebra equations.

4.2.3.3.2 Convergence criteria

Solution of the discretized equations tends to the exact solution of the differential equation as the grid spacing tends to zero. A converged solution was obtained by iterating in time until variations in the primitive variables between subsequent time-step were very small. Determining when a numerical simulation is fully converged is important in getting accurate and reliable results. It was found that the convergence criteria less than 10^{-4} for all equations and 10^{-6} for the energy equation could rapid the speed of obtaining a converged solution.

4.2.3.3.3 Grid independent study

In order to determine the proper grid size for this study and assess the numerical accuracy of the results obtained by this mesh design, a grid independence study was performed by using various grid sizes for inlet air velocity of 0.5 m/s and Rayleigh number in the range of 10^6 to 10^7 in the air channel. Five different grid densities were used for the grid independent study. One physical case was investigated for various grid sizes: the air flow enters the air cavity with intake temperature 23^{o}C and air velocity of 0.5 m/s.

Grid independence of the results was established by employing various grid size meshes, ranging in size from 90 × 26 to 90 × 110. Figure 4.6 shows temperatures at mid-height of the y/h = 0.5 with various grid sizes, 90 × 26 (coarse mesh), 90 × 100 (medium mesh), 90 × 110 (fine mesh). The velocity profiles at the mid-height of the cavity are predicted on various meshes size and predicted results are compared and illustrated in Figure 4.7. Figure 4.8 shows the velocity profiles along height of the cavity at x/L = 0.5 with various grid sizes. As can be seen from the figure, the difference is very small. The medium mesh was employed in order to save computational time and obtain reasonable numerical solutions.

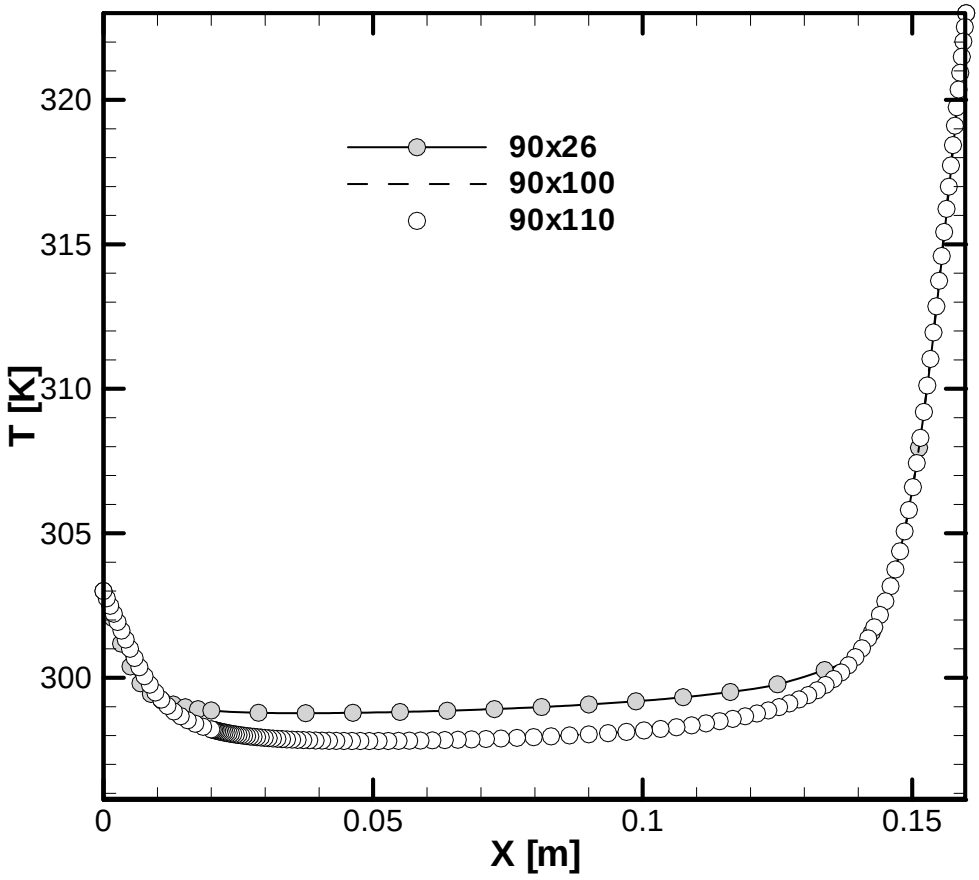

Figure 4.6 Temperature profiles at mid-height of the cavity y/h = 0.5 with various grid sizes

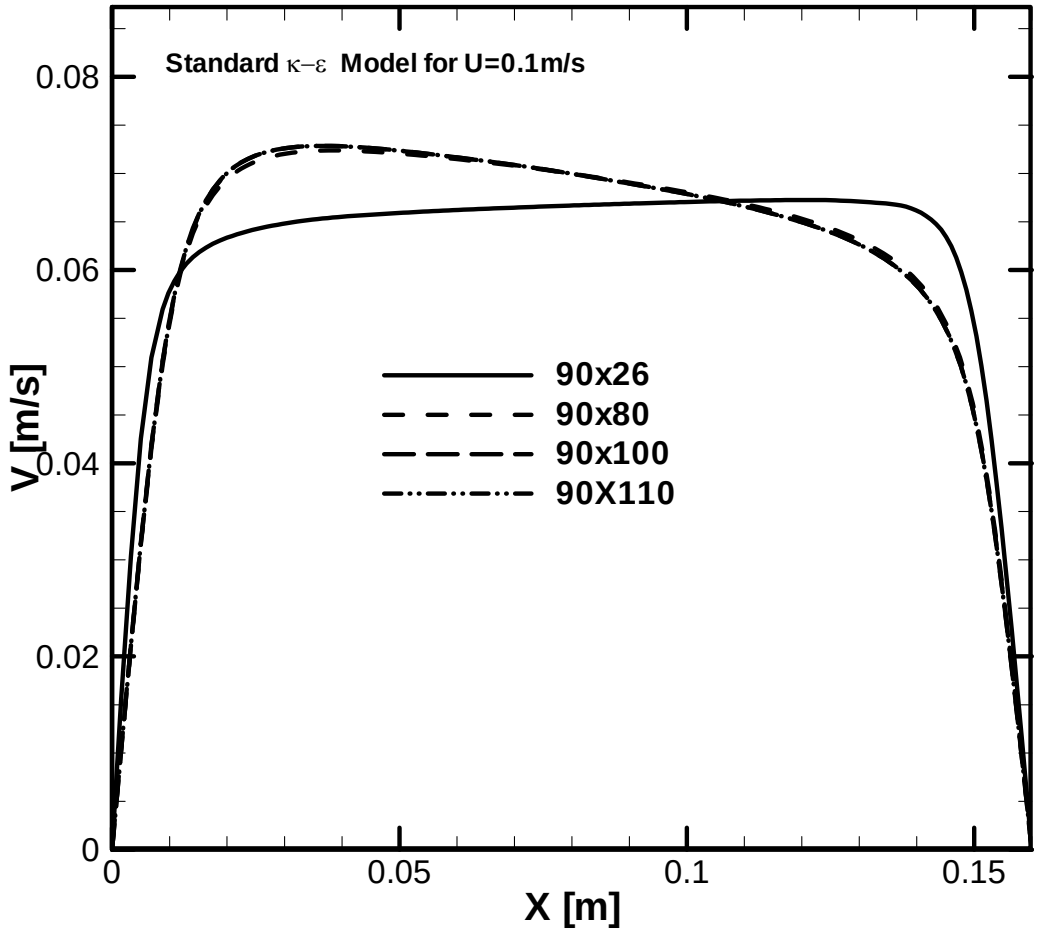

Figure 4.7 Velocity profiles at mid-height of the cavity y/h = 0.5 with various grid sizes

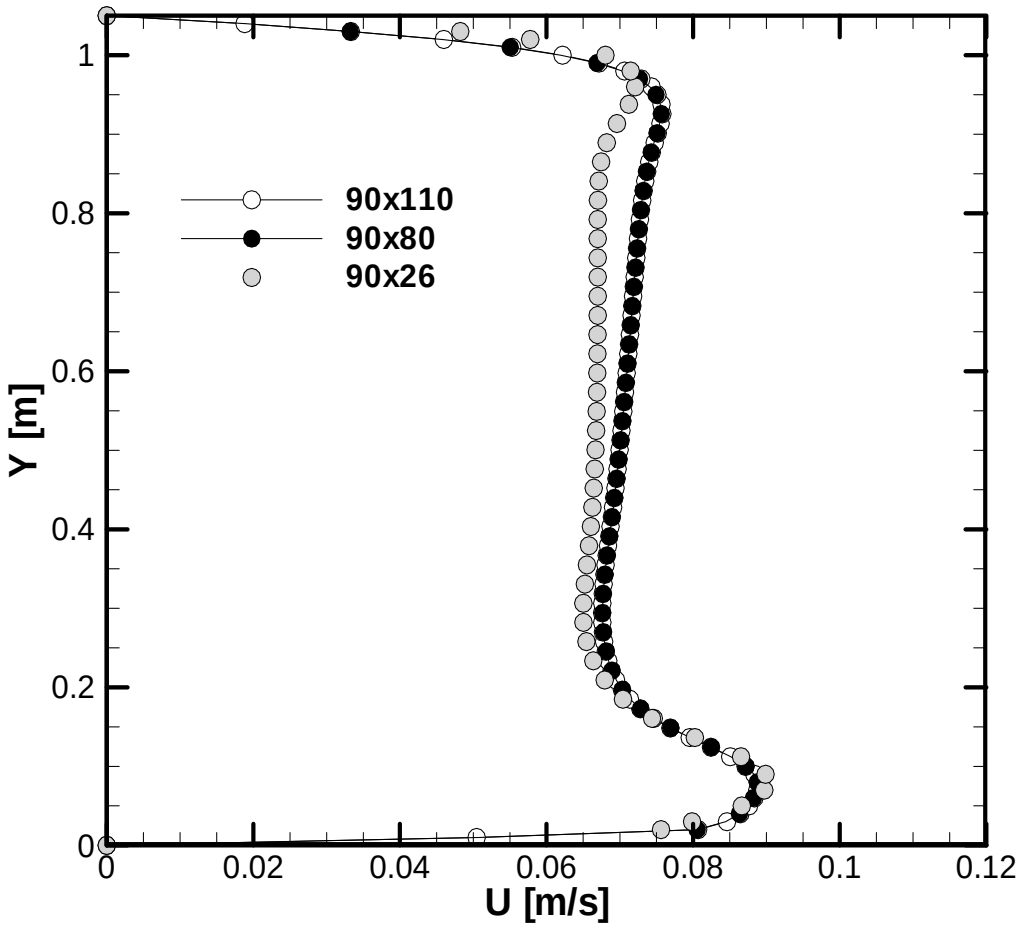

Figure 4.8 Velocity profiles along the height of the cavity at x/L = 0.5 with various grid sizes

4.3 Results and analysis

Heat transfer by natural convection from vertical plates with uniform wall temperature of heat flux has long been the interesting of many researchers. A large number of studies exist in the literature, and many of them consider laminar flow in an air channel. The present study considers the turbulent natural convection in the air channel behind the PV model. Various turbulent models were employed in the investigation, and the predicted results were compared in order to find suitable turbulence models.

Figure 4.9 shows the comparison of the velocity distribution at mid-height of the air cavity for both laminar and turbulent flow. It was found that the difference from RNG $\kappa-\varepsilon$ turbulence model and Stand $\kappa-\varepsilon$ turbulence model is larger at the regions near two vertical walls, and the difference in the middle of the cavity is small. Figure 4.10 presents the velocity profiles at mid-height of the cavity y/h = 0.5 with various turbulence models. It can be found that Realizable $\kappa-\varepsilon$ turbulence model and Stand $\kappa-\varepsilon$ turbulence model have similar velocity profiles. The predicted result from RNG $\kappa-\varepsilon$ turbulence model has larger difference from other two turbulence models. Figure 4.11 presents the temperature profiles at mid-height of the cavity y/h = 0.5 with various turbulence models. It indicated that all the turbulence models present similar results, and the deviation among them is quite small.

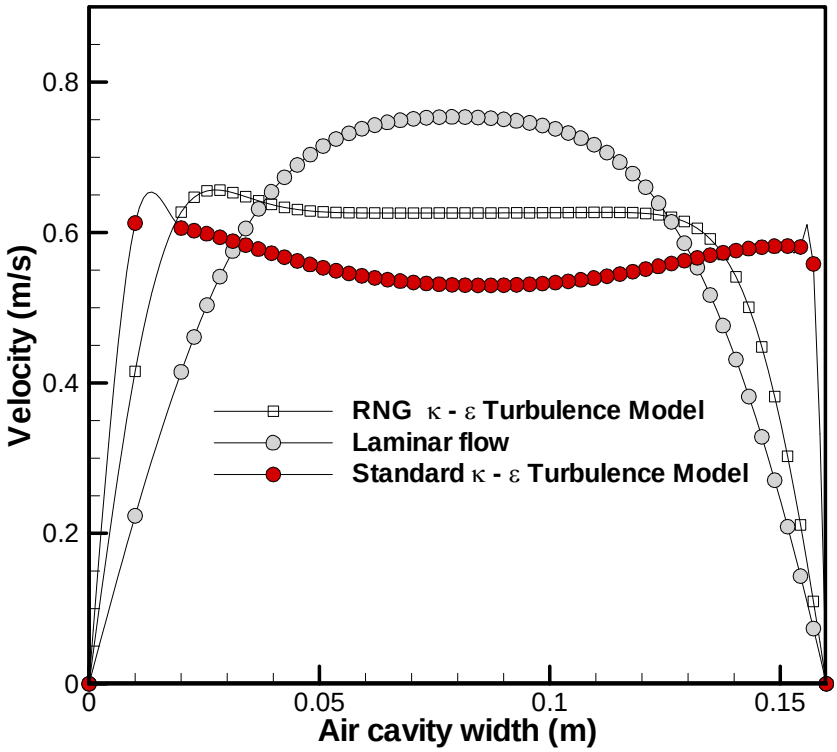

Figure 4.9 Comparison of the velocity distribution at mid-height of the air cavity

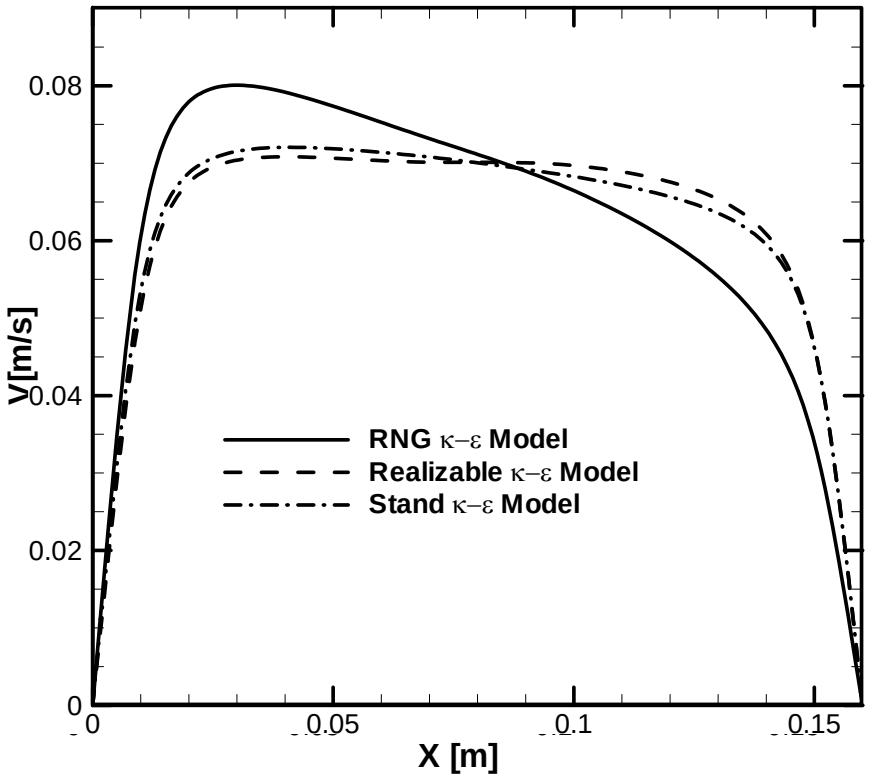

Figure 4.10 Velocity profiles at mid-height of the cavity y/h = 0.5 with various turbulence models

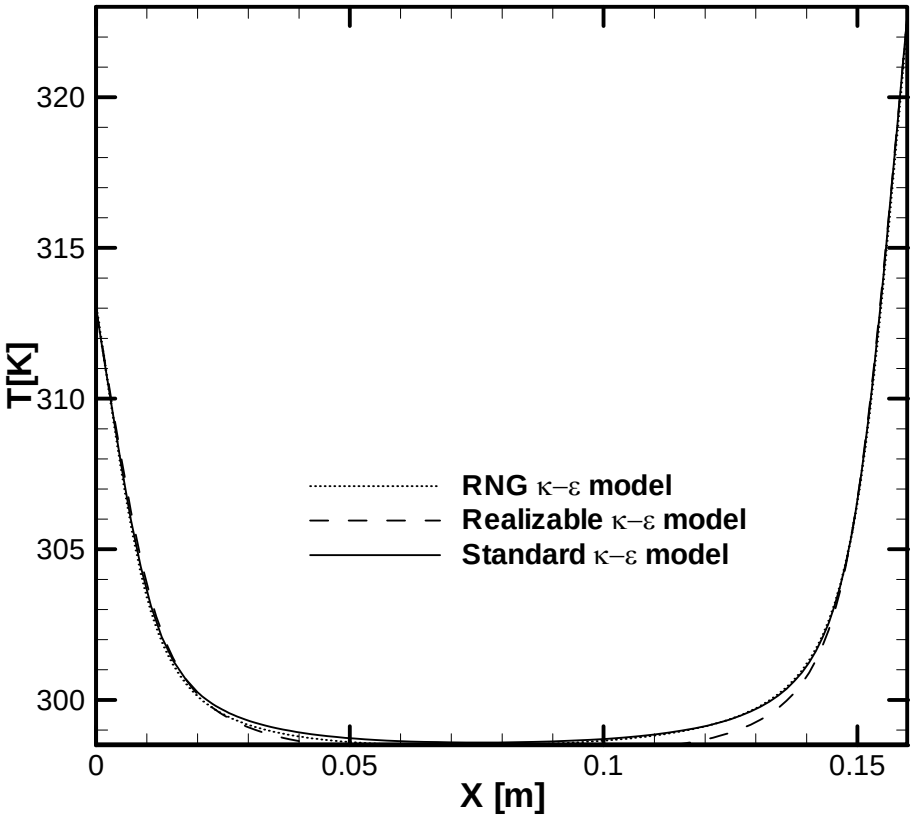

Figure 4.11 Temperature profiles at mid-height of the cavity y/h = 0.5 with various turbulence models

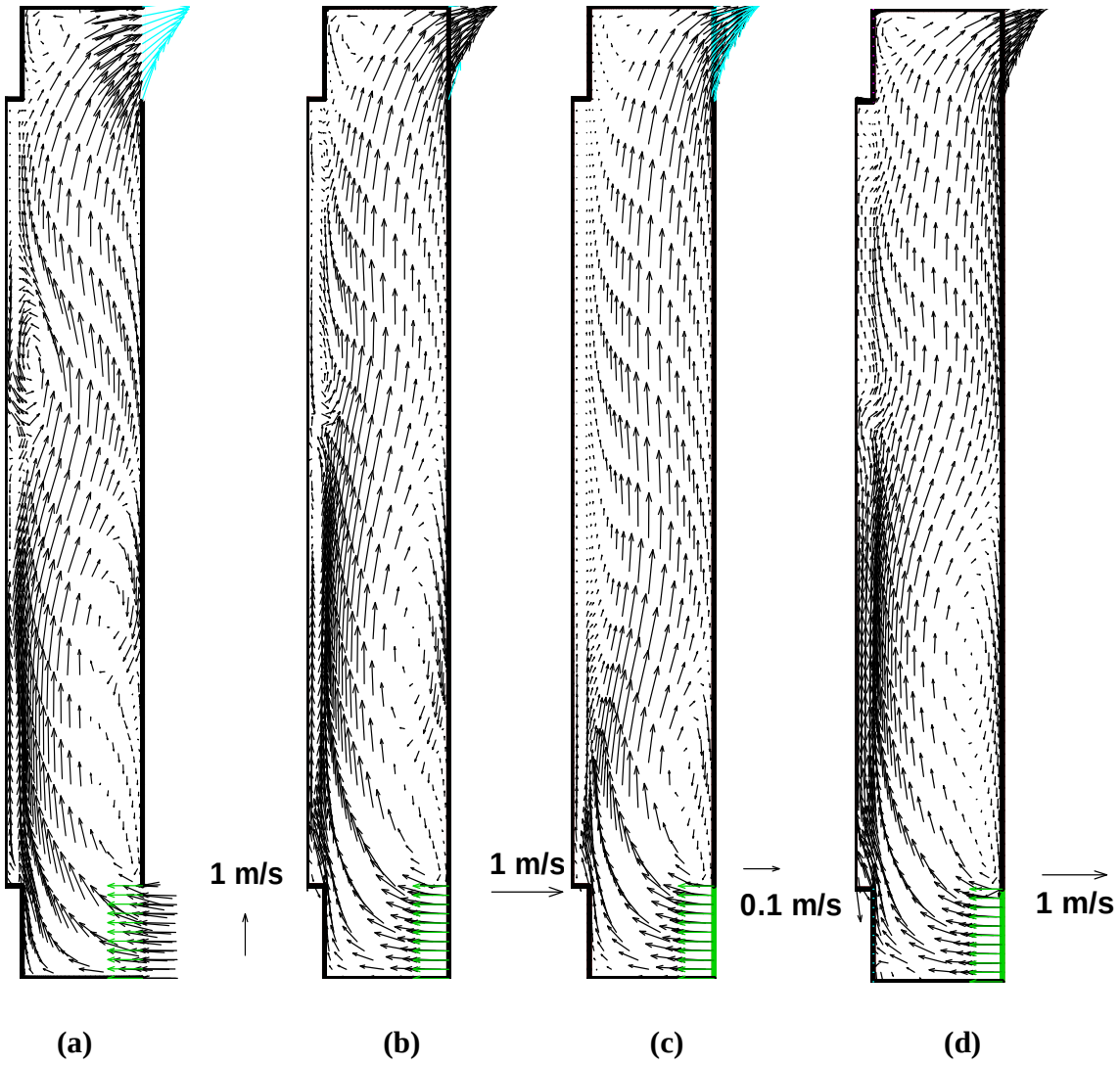

Figure 4.12 Effect of various inlet velocities on the flow structure for velocities at 0.9, 0.5, 0.1 m/s for laminar flow (a, b, c) and turbulent flow (d)

a)Vin = 0.9m/s, b) Vin = 0.5 m/s, c) Vin = 0.1m/s, d)Vin = 0.1 m/s

Previous reports in literature have indicated that the inlet condition is of vital importance in the simulation of the flow in the double skin façade system. In the previous modeling, the ambient temperature is often used as the inlet temperature. Liao et al. (2005) indicated that the inlet modeling is important to the whole BIPV system energy analysis. Inlet numerical modeling coupled with many other physics, see large turbulence, inflow and backflow, due to many factors affected. Figure 4.12 shows the effect of various inlet velocities on the flow structure for the velocities at 0.9, 0.5, 0.1m/s for laminar flow and 0.1m/s for turbulent flow.

4.4 Summary

This chapter presents the thermal performance and air flow analysis of a double sided PV (DSPV) façade using thin film PV panel as external skin. Undesirably high temperature experienced by photovoltaic panel will decrease the conversion efficiency of PV cells and overheating in closed glazing cavity in summer may cause thermal discomfort of indoor occupants. Thermal regulation of the temperature rise by fitting a naturally ventilated open channel back the PV panel is a potentially cost effective way to maintain maximum solar to electricity conversion and reduce heat gain of the building external envelope. In this chapter, natural convection flow in the 2D tall glazing cavity heated from the vertical side was investigated numerically. The flow in the façade cavity was considered either laminar or turbulent. Different inlet conditions for laminar flow were evaluated and various $k-\varepsilon$ turbulence models (RNG $k-\varepsilon$ model, Realizable $k-\varepsilon$ model, Stand $k-\varepsilon$ model) were compared.

The heat transfer and air flow characteristics in the channel were evaluated by numerical simulation. Various factors affecting the air flow and heat transmission were identified and examined. Predicted results from the numerical simulation were analyzed in detail.

CHAPTER 5: MODELING OF CONVECTIVE HEAT TRANSFER IN THE CLOSED AIR CAVITY OF NON-VENTILATED PV DSF SYSTEM

5.1 Introduction

Advanced glazing systems have been substantially applied in both high-rise office buildings and commercial buildings in Hong Kong, over the past few years. The application of a double-skin facade can achieve energy savings through the reduction of air conditioning (A/C) energy. Natural lighting utilization and sound insulation can also be enhanced. A quiet and healthy working environment could thus be provided in a metropolitan city like Hong Kong. A new application of the glazing system is to integrate building facades with semi-transparent photovoltaic (PV) cells. These solar cells can not only generate electricity, but also provide shade. The void between the two glass panes could serve as a thermal insulation layer and reduce the amount of energy consumed by the air-conditioning system in the building due to low conductivity of the air in the cavity. When the glazing is integrated with photovoltaic cells, an additional function of the building envelope is also created. This kind of solar energy applications is called building-integrated photovoltaics (BIPV). In this application, the windows are integrated with semi-transparent PV cells, which generate electricity as an energy source, thus

contributing a dual function to the building envelope. Additional structural installation and maintenance cost could, therefore, be substantially reduced.

5.2 Computational fluid dynamics analysis of the air flow pattern in the closed cavity

5.2.1 Problem statements

Incorporating energy efficiency or sustainable features in building construction design in urban areas could eventually help to reduce the reliance on fossil fuel resources which, in turn, could contribute to the reduction of the effect of global warming. A PV module integrated in a building facade could generate electricity and substantially reduce the amount of carbon dioxide emissions from power stations. Figure 5.1 shows the building facade in which the glazing is integrated with an amorphous PV module. In this application, solar cells provide dual functions, i.e. they provide the building with both shading and electricity.

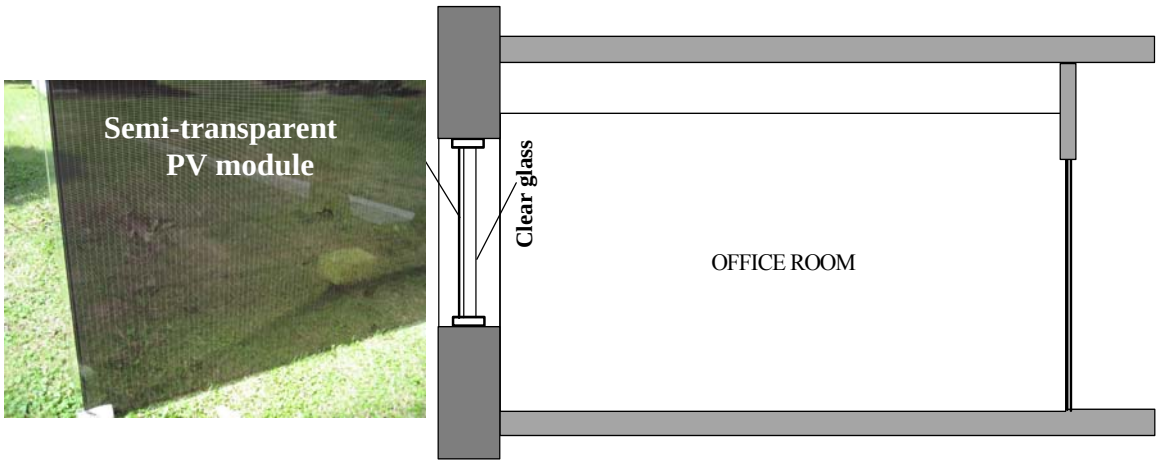

Figure 5.1 Glazing with integrated semi-transparent PV module for potential application in an office room

The current window system composes of two layers of highly transparent glass sheets, and a serious of opaque solar cells that are encapsulated in between the two glass sheets as depicted in Figure 5.2 (a). This advanced glazing system can produce electricity, and at the same time, daylight can penetrate through the thin film PV module as shown in Figure 5.2 (b).

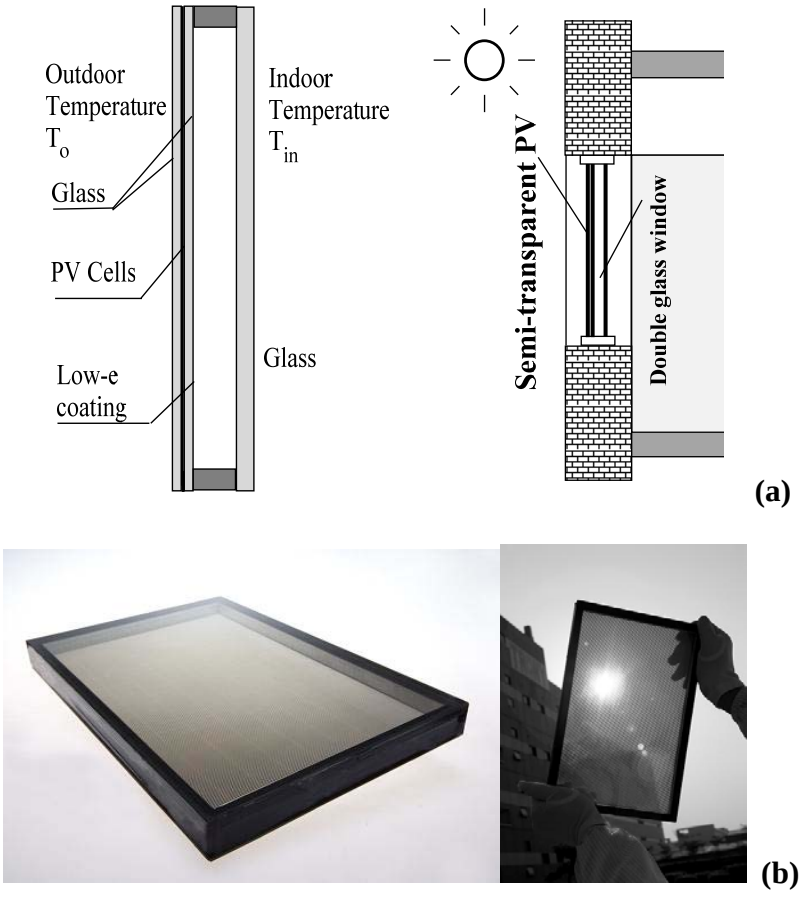

Figure 5.2 Schematic diagram of double pane window integrated with PV glass with low-e coating (a), photo of the a-Si thin film PV module from Trony, Shenzhen, China (b)

5.2.2 Governing equations

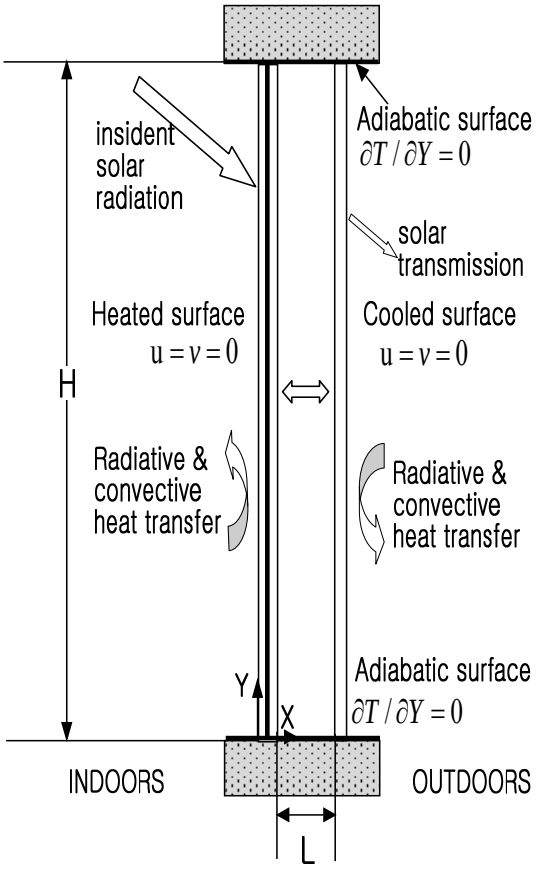

Figure 5.3 The schematic diagram of the air cavity studied

The problem to be treated here is of natural convective flows in the cavity of a double glazed window integrated with semi-transparent PV cells. It is a two-dimensional laminar incompressible flow except for the buoyancy effects where the Bousinesq approximation is applied. The governing equations for the fluid flow and heat transfer are as follows:

$$\frac{\partial u}{\partial x}+\frac{\partial v}{\partial y}=0 \tag{5.1}$$

$$u\frac{\partial u}{\partial x}+v\frac{\partial u}{\partial y}=-\frac{1}{\rho}\frac{\partial p}{\partial x}+\nu(\frac{\partial^2 u}{\partial x^2}+\frac{\partial^2 u}{\partial y^2}) \tag{5.2}$$

$$u\frac{\partial v}{\partial x}+v\frac{\partial v}{\partial y}=-\frac{1}{\rho}\frac{\partial p}{\partial y}+\nu(\frac{\partial^2 v}{\partial x^2}+\frac{\partial^2 v}{\partial y^2})+\beta g(T-T_\infty) \tag{5.3}$$

$$u\frac{\partial T}{\partial x}+v\frac{\partial T}{\partial y}=(\frac{k}{\rho c_p})(\frac{\partial^2 T}{\partial x^2}+\frac{\partial^2 T}{\partial y^2}) \tag{5.4}$$

Due to the very low velocities involved, the dissipation term has been neglected in the energy equation (5.4). T_∞ is the temperature in the undisturbed fluid far from the surface.

The boundary conditions on temperature on window surfaces in the solution are:

$$T=T_H \quad \text{for} \quad x=0 \tag{5.5}$$

$$T=T_C \quad \text{for} \quad x=L \tag{5.6}$$

$$\frac{\partial T}{\partial y}=0 \quad \text{for} \quad y=0, y=H \tag{5.7}$$

One of the difficulties related to the solution of the above equations lies in the presence of the pressure term which can not be obtained directly from the continuity and momentum equations. For this reason, a majority of researchers interested in two dimensional problems prefer to introduce the stream function, ψ, and vorticity, ω, as described by Wan Hassan, 1986. The above equations can be written in terms of stream function, ψ, and the vorticity, ω defined as

$$u=\frac{\partial \psi}{\partial y}, \quad v=-\frac{\partial \psi}{\partial x} \tag{5.8}$$

$$\omega = (\frac{\partial v}{\partial x} - \frac{\partial u}{\partial y}) \tag{5.9}$$

In terms of stream function the momentum equation, continuity equation and energy equation become:

$$\frac{\partial^2 \psi}{\partial x^2} + \frac{\partial^2 \psi}{\partial y^2} = -\omega \tag{5.10}$$

$$\frac{\partial \psi}{\partial y}\frac{\partial \omega}{\partial x} - \frac{\partial \psi}{\partial x}\frac{\partial \omega}{\partial y} = \nu(\frac{\partial^2 \omega}{\partial x^2} + \frac{\partial^2 \omega}{\partial y^2}) - \beta g \frac{\partial T}{\partial x} \tag{5.11}$$

$$\frac{\partial \psi}{\partial y}\frac{\partial T}{\partial x} - \frac{\partial \psi}{\partial x}\frac{\partial T}{\partial y} = \alpha(\frac{\partial^2 T}{\partial x^2} + \frac{\partial^2 T}{\partial y^2}) \tag{5.12}$$

For the boundary conditions, the temperatures of the two vertical walls are assumed to be uniform, and the bottom wall and top wall are adiabatic, as shown in Figure 5.3, so that

$$\frac{\partial \psi}{\partial x} = \frac{\partial \psi}{\partial y} = 0 \tag{5.13}$$

$$\frac{\partial T}{\partial y} = 0 \quad \text{at} \quad y = 0,\ y = H, \tag{5.14}$$

$$T = T_H \ , \ T = T_L \quad \text{at} \ \ x = 0,\ x = L \tag{5.15}$$

The following non-dimensional variables are defined

$$\Psi = \frac{\psi \,\mathrm{Pr}}{\nu}, \quad \Omega = \frac{\omega L^2 \,\mathrm{Pr}}{\nu} \tag{5.16}$$

$$X = \frac{x}{L}, \quad Y = \frac{y}{L} \tag{5.17}$$

$$\Theta = \frac{T - T_C}{T_H - T_C} \tag{5.18}$$

In terms of dimensionless variables, Equations (5.9) to (5.17) become:

$$\frac{\partial^2 \Psi}{\partial X^2} + \frac{\partial^2 \Psi}{\partial Y^2} = -\Omega \tag{5.19}$$

$$\frac{\partial^2 \Omega}{\partial X^2} + \frac{\partial^2 \Omega}{\partial Y^2} = \frac{1}{\mathrm{Pr}}\left(\frac{\partial \Psi}{\partial Y}\frac{\partial \Omega}{\partial X} - \frac{\partial \Psi}{\partial X}\frac{\partial \Omega}{\partial Y}\right) + \mathrm{Ra}\frac{\partial \Theta}{\partial X} \tag{5.20}$$

$$\frac{\partial^2 \Theta}{\partial X^2} + \frac{\partial^2 \Theta}{\partial Y^2} = \frac{\partial \Psi}{\partial Y}\frac{\partial \Theta}{\partial X} - \frac{\partial \Psi}{\partial X}\frac{\partial \Theta}{\partial Y} \tag{5.21}$$

The boundary conditions in terms of dimensionless variables are

$$\Psi = 0 \tag{5.22}$$

$$\frac{\partial \Theta}{\partial Y} = 0 \quad \text{at} \quad Y = 0,\ Y = \mathrm{A}, \tag{5.23}$$

$$\Theta = 1 \ , \ \Theta = 0 \quad \text{at} \quad X = 0,\ X = 1 \tag{5.24}$$

where A = H/L is the aspect ratio of the enclosure.

When radiation heat transfer is considered, the boundary conditions for two horizontal surfaces are as follows according to Ridouane et al. (2004):

$$\frac{\partial T}{\partial x} + N_r Q_r = 0 \tag{5.25}$$

Where Q_r denotes the dimensionless net radiative heat flux at two horizontal adiabatic walls.

The dimensionless radiosity equation for the *i*th element on each wall is determined below

$$G_i = (1-\varepsilon_i)\sum_{S_j} F_{ij} G_j + \varepsilon_i \left(\frac{T_i}{\Theta} + 1\right)^4 \tag{5.26}$$

The dimensionless radiant heat flux is calculated below

$$Q_r = \varepsilon_i \left[\left(1 + \frac{T_i}{\Theta}\right)^4 - \sum_j F_{ij} G_j\right] \tag{5.27}$$

Where F_{ij} represents view factor between segments i and j; G_j represents dimensionless radiosity of segment i; ε_i represents surface emissivity of the ith element.

There are some major disadvantages to the so called stream-function vorticity method. It is a little difficult to specify the value of vorticity ω at the wall. This method is also restricted to 2D problems as the stream function ψ does not exist for 3-D. According to Wan Hassan, (1986), an approach based on vorticity uses six dependent variables-three components of stream function ψ and three components of vorticity ω. The complexity related to this method of 3-D is greater than of treating the 3 velocity components and pressure directly. Another difficulty of using stream-function-vorticity method involves variables, which are harder to visualize and physically to interpret than in the primitive variable approach. As indicated by Tannehill et al. (1997), a stream function does not exist for a truly three dimensional flow.

5.2.3. Thermal transmission of double pane window

The thermal transmittance, U-value, for double pane window could be obtained by using the procedure described in BS 6993 (British Standards Institution, 1989). The thermal transmittance of the glazing is obtained by the following equation:

$$U = \frac{1}{\left[\frac{1}{h_{out}} + \frac{1}{h_t} + \frac{1}{h_{in}}\right]} \tag{5.28}$$

where h_{out} and h_{in} are exterior and interior heat transfer coefficients, which can be obtained from ASHRAE (2001). h_t is the conductance of double pane window unit.

$$\frac{1}{h_t} = (\sum^{N} \frac{1}{h_s} + L_g r_g + L_{PV} r_{PV}) \tag{5.29}$$

where h_s is the air cavity heat transfer coefficient, N is number of window cavities, L_g and L_{PV} are total thickness of glass panes and PV cells, r_g and r_{PV} are thermal resistivity of glass and PV cells.

Air cavity heat transfer coefficient

$$h_s = h_c + h_r \tag{5.30}$$

where h_c is infill air convective heat transfer coefficient, h_r is radiation heat transfer coefficient, which can be determined by

$$h_r = 4\sigma \left[\frac{1}{\varepsilon_o} + \frac{1}{\varepsilon_i} - 1 \right]^{-1} T_m^{\ 3} \tag{5.31}$$

where σ is the Stefan-Boltzmann constant, ε_o is the emittance of outer glass pane, ε_i is emittance of the inner glass pane, T_m is absolute temperature corresponding to the average of the mean pane temperature.

The convective heat transfer coefficient due to natural ventilation of the air in the gap is determined by

$$Nu_Y = -\frac{\partial \Theta}{\partial X}\bigg|_{X=0} \tag{5.32}$$

$$Nu = \frac{1}{A}\int_0^A \mathrm{Nu}_Y dY \tag{5.33}$$

$$h_c = \frac{Nuk_{air}}{L_{air}} \tag{5.34}$$

The major dimensionless parameters that determine the structure of the air flow in the differentially heated air cavity are the Prandtl number and Rayleigh number,

$$Ra = \frac{g\beta\Delta TH^3}{\nu\alpha} \tag{5.35}$$

The parameters used in this chapter are summarized in Table 5.1

5.2.4 Finite-difference approximation

The numerical method of solution is employed extensively in various practical applications to determine the temperature and velocity distribution when computational domain having complicated geometries and boundary conditions. A commonly used numerical method is the finite-difference method. In this method, the partial differential equations (PDE) governing the heat transfer and fluid flow is approximated by a set of algebraic equations fro temperature and velocity at a number of nodal points over the computational domain considered. Before the calculation, the first step is the finite-difference representation or the transformation into a set of algebraic equations of the PDE governing the process.

The following section will introduce the procedure of the finite-difference representation. The finite-difference form of the equation relating the dimensionless vorticity to stream function equation, i.e. Eq (5.19), becomes:

$$\frac{\Psi_{i+1,j}-2\Psi_{i,j}+\Psi_{i-1,j}}{\Delta X^2}+\frac{\Psi_{i,j+1}-2\Psi_{i,j}+\Psi_{i,j-1}}{\Delta Y^2}=-\Omega_{i,j} \tag{5.36}$$

The dimensionless vorticity transport equation, i.e. Eq (5.20), becomes:

$$\begin{aligned}&(\frac{\Omega_{i+1,j}-2\Omega_{i,j}+\Omega_{i-1,j}}{\Delta X^2})+(\frac{\Omega_{i,j+1}-2\Omega_{i,j}+\Omega_{i,j-1}}{\Delta Y^2})\\&=(\frac{1}{\mathrm{Pr}})[(\frac{\Psi_{i,j+1}-\Psi_{i,j-1}}{2\Delta Y})(\frac{\Omega_{i+1,j}-\Omega_{i-1,j}}{2\Delta X})-(\frac{\Psi_{i+1,j}-\Psi_{i-1,j}}{2\Delta X})(\frac{\Psi_{i+1,j}-\Psi_{i-1,j}}{2\Delta Y})]\\&+Ra(\frac{\Theta_{i+1,j}-\Theta_{i-1,j}}{2\Delta X})\end{aligned} \tag{5.37}$$

As the same procedure, the dimensionless energy equation becomes:

$$\begin{aligned}&(\frac{\Theta_{i+1.j}-2\Theta_{i,j}+\Theta_{i-1,j}}{\Delta X^2})+(\frac{\Theta_{i,j+1}-2\Theta_{i,j}+\Theta_{i,j-1}}{\Delta Y^2})\\&=(\frac{\Psi_{i.j+1}-\Psi_{i,j-1}}{2\Delta Y})(\frac{\Theta_{i+1,j}-\Theta_{i-1,j}}{2\Delta Y})-(\frac{\Psi_{i+1,j}-\Psi_{i-1,j}}{2\Delta X})(\frac{\Psi_{i,j+1}-\Psi_{i,j-1}}{2\Delta Y})\end{aligned} \tag{5.38}$$

Followed the same procedure, the boundary conditions could be expressed in terms of finite-difference representations.

Table 5.1 Technical data of the a-Si module used in the glazing system

Items	Description
Panel Dimension (H × W)	0.95 × 0.98 m
PV area (m^2)	0.466 m^2
Solar cell type	Amorphous silicon
PV efficiency	6%
Max power voltage (V)	69 V
Max power current (A)	0.28 A
Open circuit voltage (V)	89 V
Short circuit current (A)	0.38 A

The present investigation deals with numerical predictions of air flow and temperature distribution in a two-dimensional air cavity, which is isothermally heated from one side and cooled on the other side. The Navier-Stokes equations and energy equation in terms of stream function and vorticity formulation are solved numerically by iterative finite difference technique. The governing equations are substituted by a set of difference equations, used to all grid points in the calculation domain being considered. To obtain a grid-independent solution, various grid dimensions were employed. Figure 5.4 shows the variation of the vertical velocity profile at mid-height for various grid sizes. It was found that a 36 × 36 grid size ensured the independence of the grid solution, with reasonable

computation time. The computations are performed on Pentium(R) D CPU 3.40 GHz 3.39 GHz, 1.99 GB of RAM PC using a FORTRAN compiler.

The set of resulting algebraic equations were solved iteratively and were performed by Successive Under-Relaxation (SUR) described by Patankar (1980). SUR is often employed to avoid divergence in the iterative solution of algebraic equations and accelerate the convergence. Convergence of iteration for the solution is obtained until the values of the variables cease to change from the previous iteration to the next by less than the prescribed value. To examine whether the solution is converged, the following criterion is employed:

$$\left| \frac{\phi^{n+1} - \phi^{n}}{\phi^{n+1}} \right| \leq \varepsilon \tag{5.36}$$

where ϕ stands for Ψ, Ω and Θ respectively, and *n* stands for the number of iteration. The value of ε is chosen as 10^{-4}.

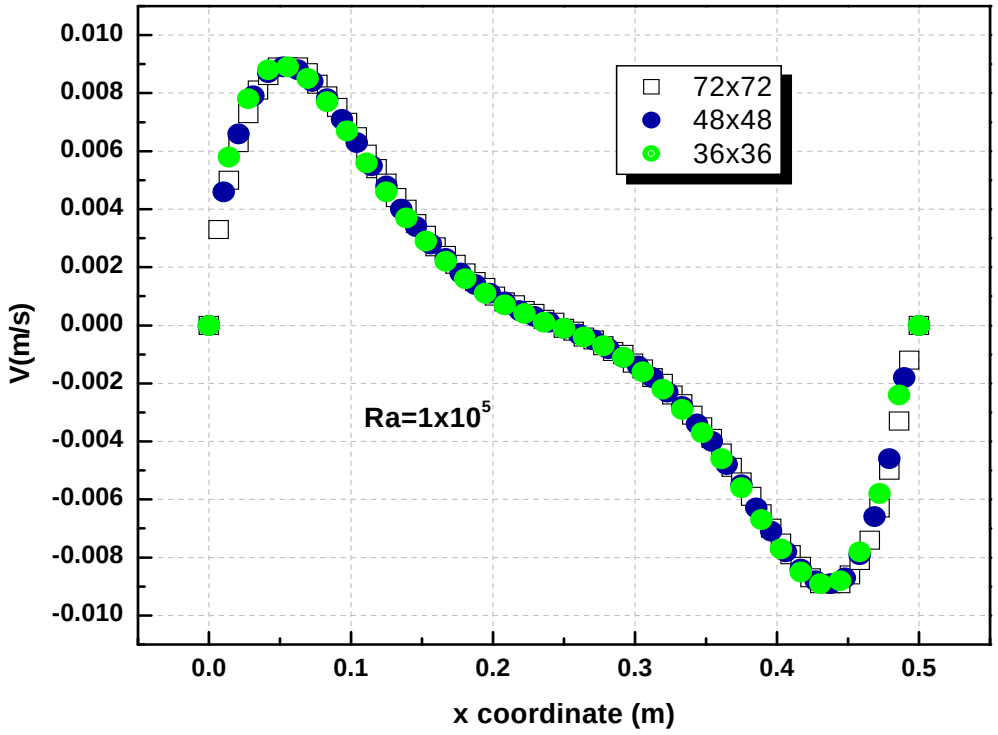

Figure 5.4 Variation of the vertical velocity profile at mid-height for various grid sizes

5.3 Air flow in the closed cavity behind the PV module

The temperature distribution and flow field of the buoyancy forces induced natural convective airflow in the rectangular cavity have been analyzed numerically for different Rayleigh numbers. The flow and temperature fields and heat transfer results were obtained for Pr = 0.7 and Ra ranging from 10^3 to 10^5. Numerical results in terms of stream lines and isotherms are presented at various Rayleigh numbers. The numerical results, including the streamlines and temperatures, are discussed in what follows.

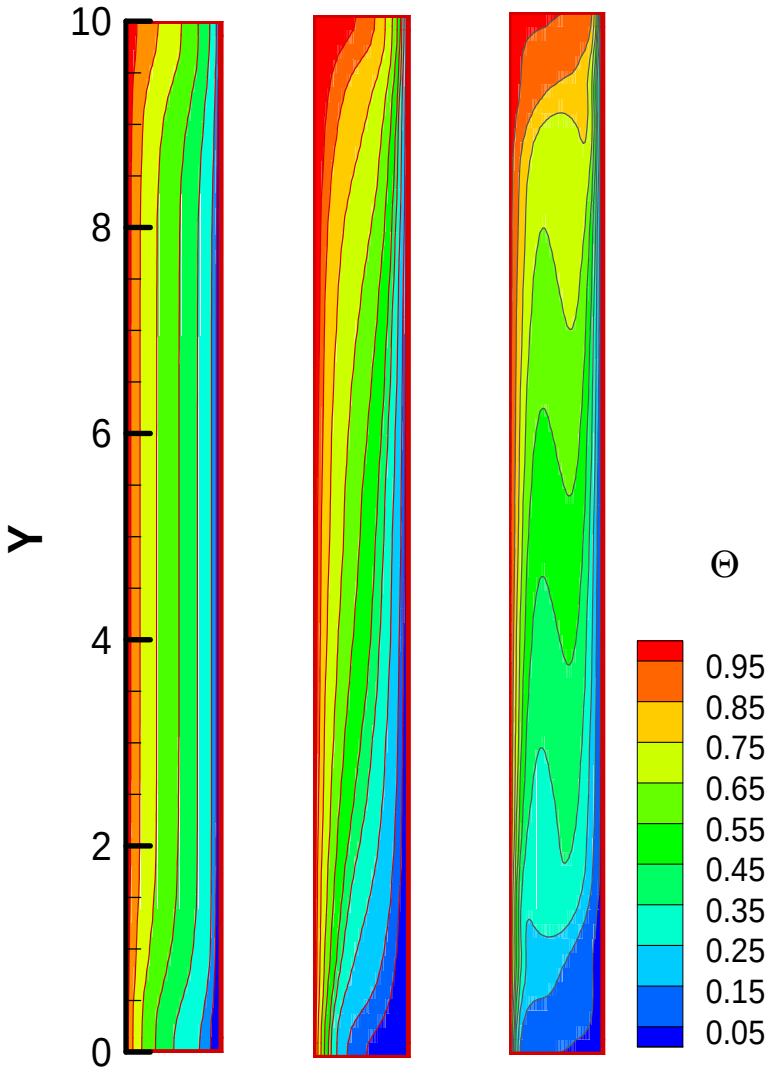

Figure 5.5 Isotherms for values for various Rayleigh numbers Ra = 10^3, 7×10^3, 10^5 (from left to right) for aspect ratio A = 10

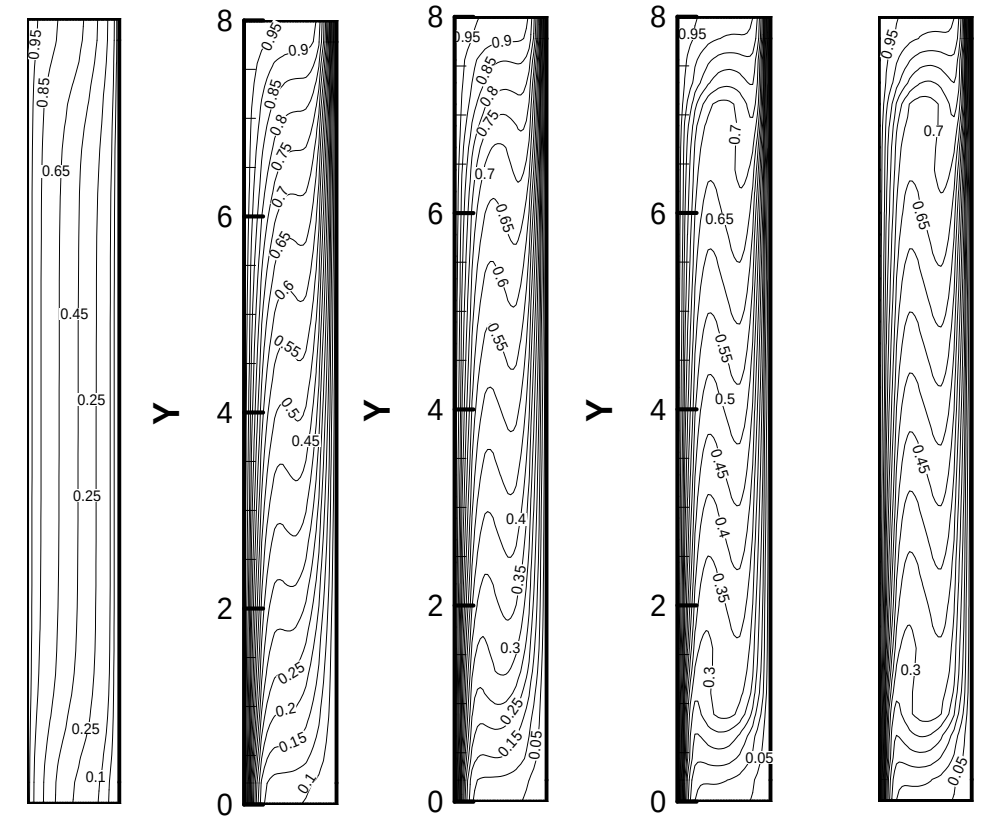

Figure 5.6 Isotherms are shown for Ra = 1×10^3, 3×10^4, 5×10^4, 9×10^4, 10^5, Pr = 0.7 (end walls are adiabatic) for aspect ratio A = 8

Figure 5.5 shows the corresponding isotherm contours for different Rayleigh numbers in the range of $10^3 \leq Ra \leq 10^5$ for aspect ratio A = 10. The results are illustrated for the aspect ratio of 10 and the end walls are assumed adiabatic. In the case of lower Rayleigh number, i.e. Ra = 10^3, the dominant mode of heat transfer is observed by conduction, as shown in Figure 5.5. The isotherms present nearly pure conduction characteristics, almost parallel to the both heated and cooled vertical surfaces. The isotherms are compressed to the two vertical walls with the

increase of the Rayleigh numbers. It can also be seen that warmer fluid becomes dominating the rectangular cavity with increase of the Rayleigh numbers when two thermal boundaries are established gradually. The temperature gradients in the x-direction at bottom left and top right areas of the rectangular cavity are relatively large in comparison with the gradients near the top left and bottom right ends of the glass pane surfaces.

Figure 5.6 shows the corresponding isotherm contours for different Rayleigh numbers in the range of $10^3 \leq Ra \leq 10^5$. The results are illustrated for the aspect ratio of 8 and the end walls are assumed adiabatic.

Streamlines for Pr = 0.7 and aspect ratio A = 10, presented in Figure 5.7. It shows the effect of various Rayleigh numbers on the buoyancy induced natural convective flow in the rectangular cavity for the Rayleigh number in the range of $10^3 \leq Ra \leq 10^5$. The streamlines and isothermal for Rayleigh number in the range of $1 \leq Ra \leq 10^3$ are neglected in this study considering the small variation in the flow patterns. Therefore, this paper presents the effect of Ra on flow patterns and heat transfer for $Ra > 10^3$. The flow patterns have a significant effect on the rate of heat transfer. As shown in Figure 5.7, streamline contours exhibit circulation patterns as the motion of fluid is affected by both vertical heated and cooled glass panes. The direction of the flow due to the thermal buoyancy force is clockwise in this geometry and a single cell is observed in the cavity for all Rayleigh numbers.

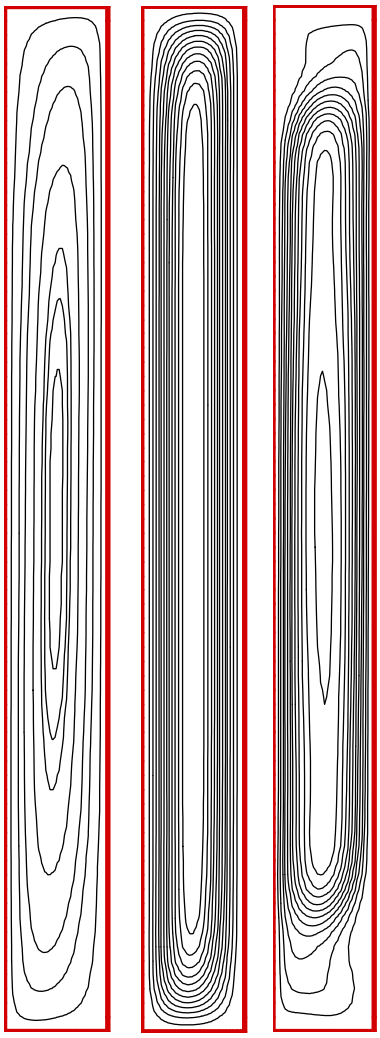

a) **(b)** **(c)**

Figure 5.7 Contours of stream function Ψ for various Rayleigh numbers $Ra = 10^3$; $Ra = 7\times10^3$; $Ra = 10^5$ (from left to right) (a) $\Psi_{min} = -2.61$, $Ra = 10^3$; (b) $\Psi_{min} = -16.1$, $Ra = 7\times10^3$; (c) $\Psi_{min} = -61.5$, $Ra = 10^5$ for aspect ratio A = 10.

Streamlines and vorticity contours for Pr = 0.7 and aspect ratio A = 8, presented in Figures 5.8 and 5.9, show the effect of various Rayleigh numbers on the buoyancy induced natural convective flow in the rectangular cavity for the Rayleigh number in the range of $10^3 \leq Ra \leq 10^5$ for aspect ratio A = 8.

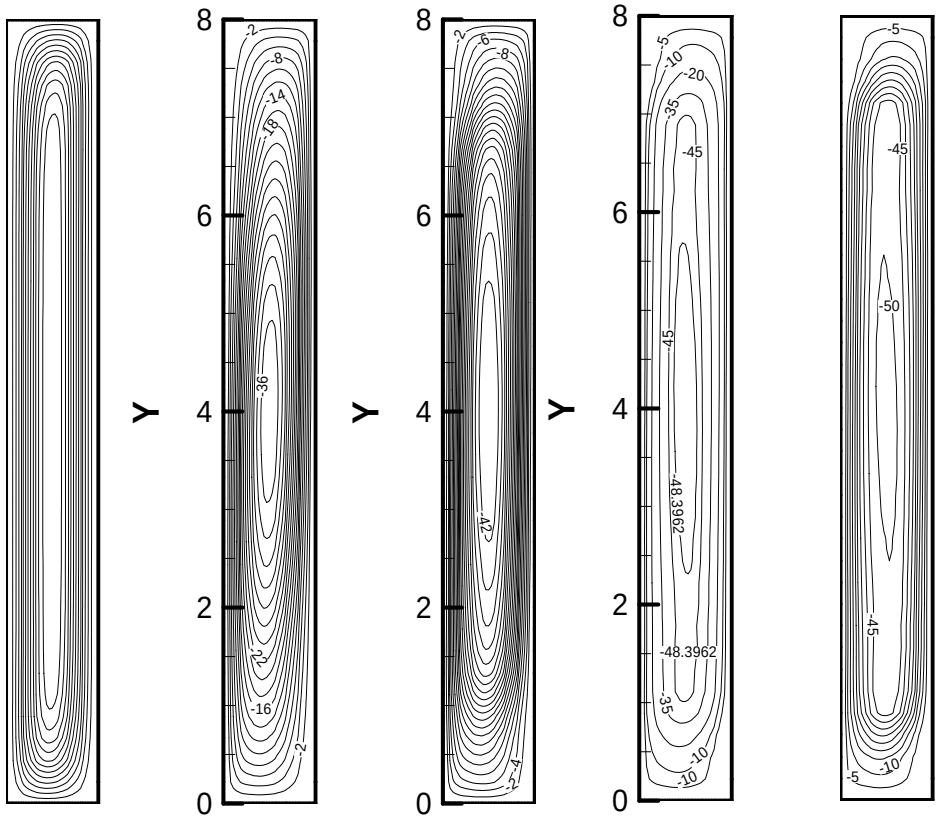

$Ra = 1\times10^3$ $Ra = 3\times10^4$ $Ra = 5\times10^4$ $Ra = 9\times10^4$ $Ra = 1\times10^5$

Figure 5.8 Streamlines for $Ra = 1\times10^3$, 3×10^4, 5×10^4, 9×10^4, 10^5, Pr = 0.7 (end walls are adiabatic) for aspect ratio A = 8

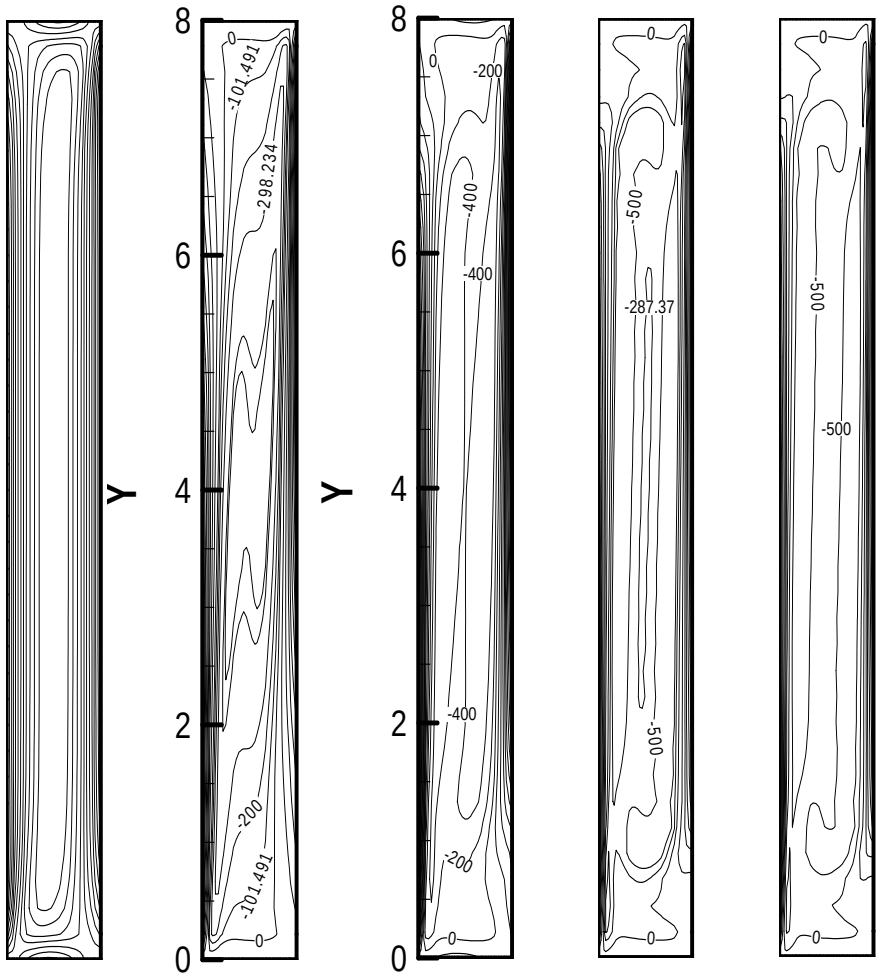

Ra = 1×10^3 Ra = 3×10^4 Ra = 5×10^4 Ra = 9×10^4 Ra = 1×10^5

Figure 5.9 Vorticity for Ra = 1×10^3, 3×10^4, 5×10^4, 9×10^4, 10^5, Pr = 0.7 (end walls are adiabatic) for aspect ratio A = 10

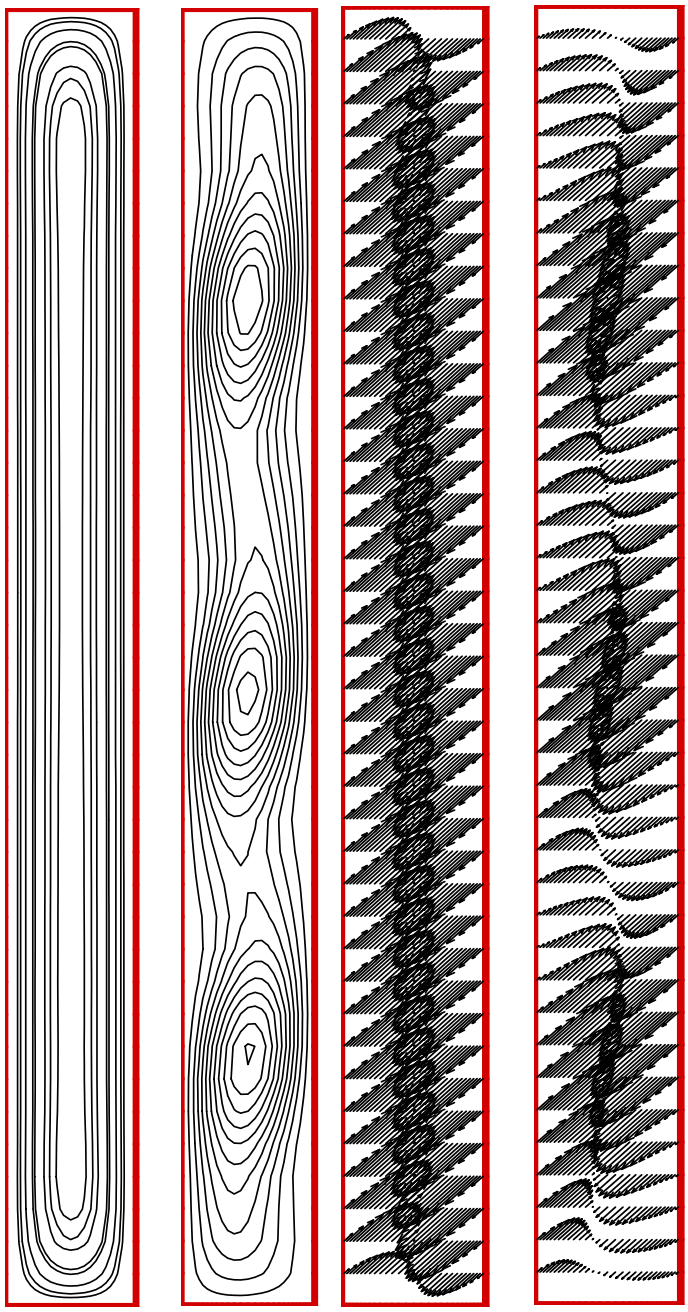

T_{out} **(a)** 42°C **(b)** 38°C **(c)** 42°C **(d)** 38°C

Figure 5.10 Contours of stream function (left a, b) and velocity vectors (right c, d) for radiation and convective heat transfer for outdoor air temperatures $T_{out} = 42^{o}C$ (a, c); $T_{out} = 38^{o}C$ (b, d).

(a) $\psi_{max} = 1.925 \times 10^{-4} m^2/s$; (b) $\psi_{max} = 5.835 \times 10^{-2} m^2/s$.

The solutions for stream function ψ and velocity vectors are shown in Figure 5.10. Combined effect of surface radiation and convection of heat transfer modes are considered simultaneously. Two real climate data used for determination of boundary condition are employed. Convective heat transfer at out pane and heat transfer by conduction at solid part are considered for determining the surface temperatures of the glass pane, and subsequently use the temperature as the boundary condition for the air flow simulation. The maximum stream function ψ, for case I with outdoor air temperature T_{out} = 42°C, is $\psi_{max} = 1.925 \times 10^{-4} m^2/s$, for case II with outdoor air temperature T_{out} = 38°C, is $\psi_{max} = 5.835 \times 10^{-2} m^2/s$. Figure 5.10 (a) shows one single cell structure, and (b) shows three cell structures for the visual examination of the flow field.

5.4 Convective heat transfer coefficients

Figure 5.11 shows the variation of the local Nusselt number with the co-ordinate Y at the Raleigh number of 10^3 for aspect ratio A = 8. In low Rayleigh ranges, the dominant mode of heat transfer is conduction, and small variations in both the airflow pattern and heat transfer are observed especially when the Rayleigh number is less than 10^3. The figure shows that the local Nusselt number decreases with the increase of the height in the cavity. Figure 5.12 shows the variation of the local Nusselt number with co-ordinate X at the mid-height of the cavity for various Rayleigh numbers and A = 8. Figure 5.13 shows the vertical velocity profiles at mid-height for various Rayleigh numbers. It was found that the velocity increases with the increase of the Rayleigh numbers.

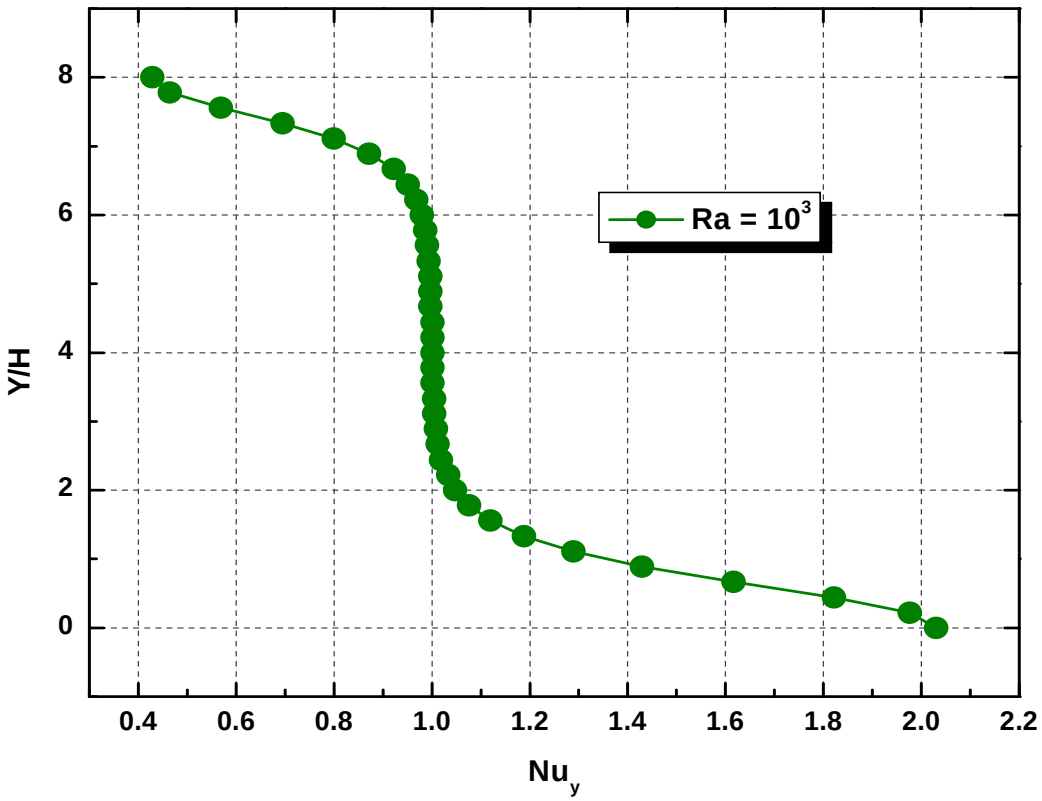

Figure 5.11 Variation of the local Nusselt number with Y for Ra = 10^3 and A = 8

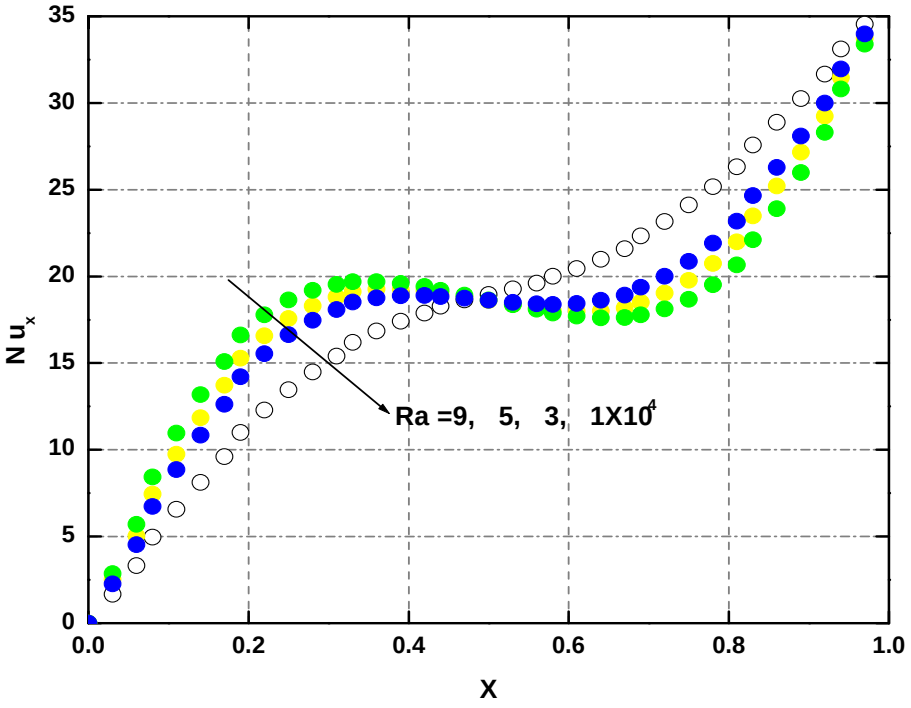

Figure 5.2 Variation of the local Nusselt number with co-ordinate X for various Rayleigh numbers

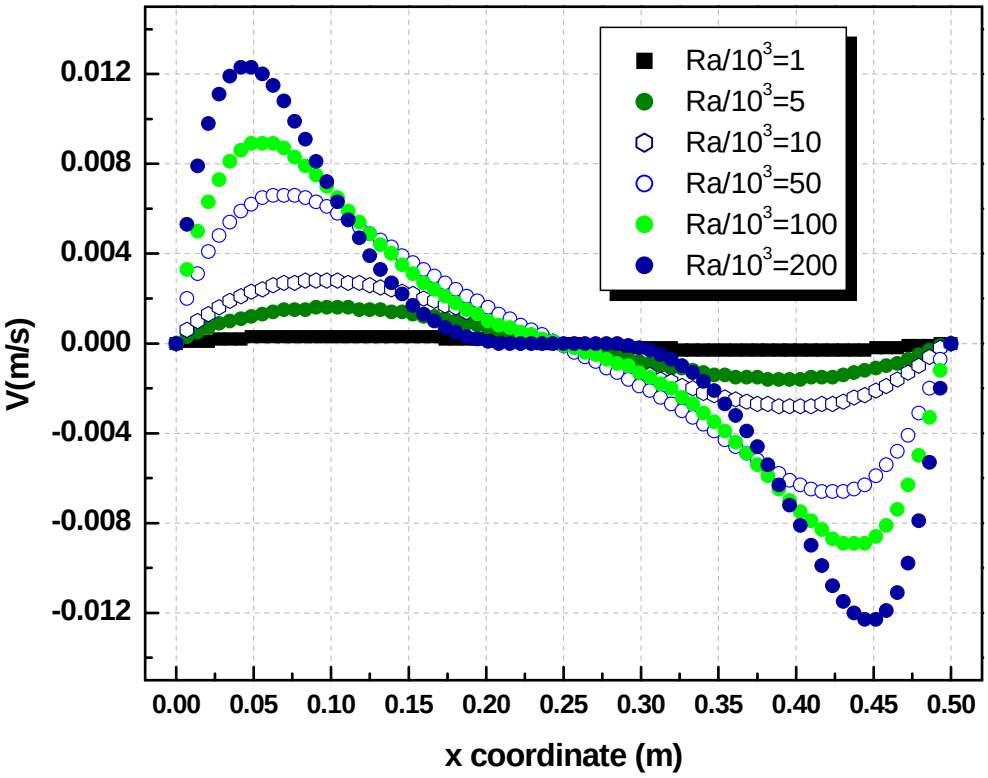

Figure 5.3 The vertical velocity profiles at mid-height for various Rayleigh numbers

5.5 Power generation from the amorphous silicon module

A see-through a-Si solar module was incorporated in the outer pane of the window for possible application in the office room façade an in Hong Kong. The novel type glazing system allows day lighting transmission and without sacrificing vision contact between the occupants and the outdoor environment simultaneously. This design has also been reported by various authors in the literature by Miyazaki, et al. (2005), Sato (1998). Over the past few years, a see-through a-Si solar module has been used in windows and skylights by many Japanese architects according to Takeoka et al. (1993) and Fukai (2000). In Hong Kong, a ventilated solar window system was developed and analyzed by Chow et al. (2006) for possible application in warm climates. They claimed that in the warm climatic regions, the reversible mechanism is not required for the ventilated window. In their recent work (Chow, 2009), a PV module is integrated in the window for cogeneration of electrical power and day lighting utilization.

The I-V characteristics of the see-through a-Si solar cell module have been measured in the Solar Simulation Laboratory of The Hong Kong Polytechnic University. Figure 5.14 shows the characteristic curves of the transparent PV module under specified conditions (solar radiation intensity = 815 W/m^2, measured temperature = 21^{o}C). Table 5.1 shows the technical data of the a-Si cell used in the glazing system. About half of the PV panel area is filled with thin film solar cells. The efficiency of the a-Si module is approximately 6%, which is lower, compared with other types of solar cells, i.e. mono-silicon cell. However, it has a lower

manufacturing cost and has little reliance on the Si as well as little affect on the environment.

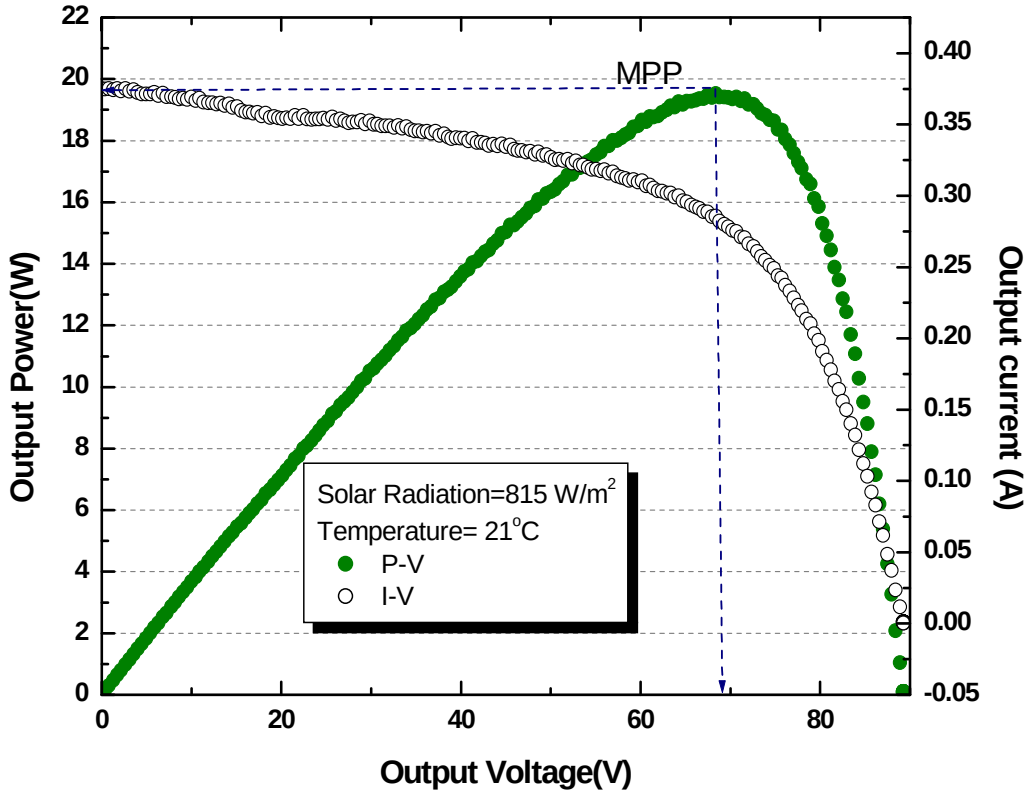

Figure 5.44 Characteristic curves of the Transparent PV module at specified conditions

5.6 Summary

In this chapter, the present investigation deals with numerical predictions of air flow and temperature distribution in a two-dimensional air cavity, which is isothermally heated from one side and cooled on the other side. Steady natural convective airflow in a novel type glazing system with integrated transparent photovoltaic (PV) has been analyzed numerically using a stream function vorticity formulation. Based on the resulting numerical predictions, the effects of Rayleigh numbers on airflow patterns and local heat transfer coefficients on vertical glazing surfaces were investigated for Rayleigh numbers in the range of $10^3 \leq Ra \leq 2\times10^5$. The I-V characteristics of the see-through a-Si solar cell module have been measured and analyzed.

CHAPTER 6: VALIDATION OF THE MATHEMATICAL METHODS USED

6.1 Introduction

Validation of the mathematical methods used is the key for the numerical investigation as predicted numerical results are approximation of the solution of the partial differential equations. Only validated numerical models can be employed for further parametric studies and optimization of the system parameters. Experimental studies, although time consuming and more costly than numerical investigations, could be used for validation of numerical results.

For the validation of the present computational method, the predicted results were compared with the experimental results both from well measured data described in chapter 3 and data available in the literatures. The experimental results employed in this section are these from Yin et al. (1978), Elsherbiny et al. (1982).

6.2 Comparison with the numerical results with experimental data

The present numerical results are evaluated for accuracy against numerical results published in previous works and experimental results reported by various authors. The comparisons of the average Nusselt numbers for laminar natural convective flow in an enclosure between the results from the present computer code and the

published results are shown in Figure 6.1. Significant agreement, which demonstrates the validity of the formulation and the computer code, is observed. The correlations between the average Nusselt numbers with other parameters, proposed by Yin et al. (1978), are listed below:

$$Nu = 0.23A^{-0.131}Ra_L^{0.269} \quad \text{for} \quad 10^3 \le Ra_L \le 5\times10^6 \quad \text{and} \quad 4.9 \le A \le 79.7 \qquad (6.1)$$

The correlations from Elsherbiny et al. (1982) are listed below:

$$Nu_1 = 0.0605 \times Ra_L^{1/3} \qquad (6.2)$$

$$Nu_2 = \left[1 + \left\{\frac{0.104Ra_L^{0.293}}{1+(6310/Ra_L)^{1.36}}\right\}^3\right]^{1/3} \qquad (6.3)$$

$$Nu_3 = 0.242\left(\frac{Ra_L}{A}\right)^{0.272} \qquad (6.4)$$

$$Nu = \max(Nu_1, Nu_2, Nu_3) \qquad (6\text{-}5)$$

for $5 \le A \le 110$, $A = 20 : Ra_L < 2\times10^6$,

$A = 40 : Ra_L < 2\times10^5, A = 80 : Ra_L < 3\times10^4$

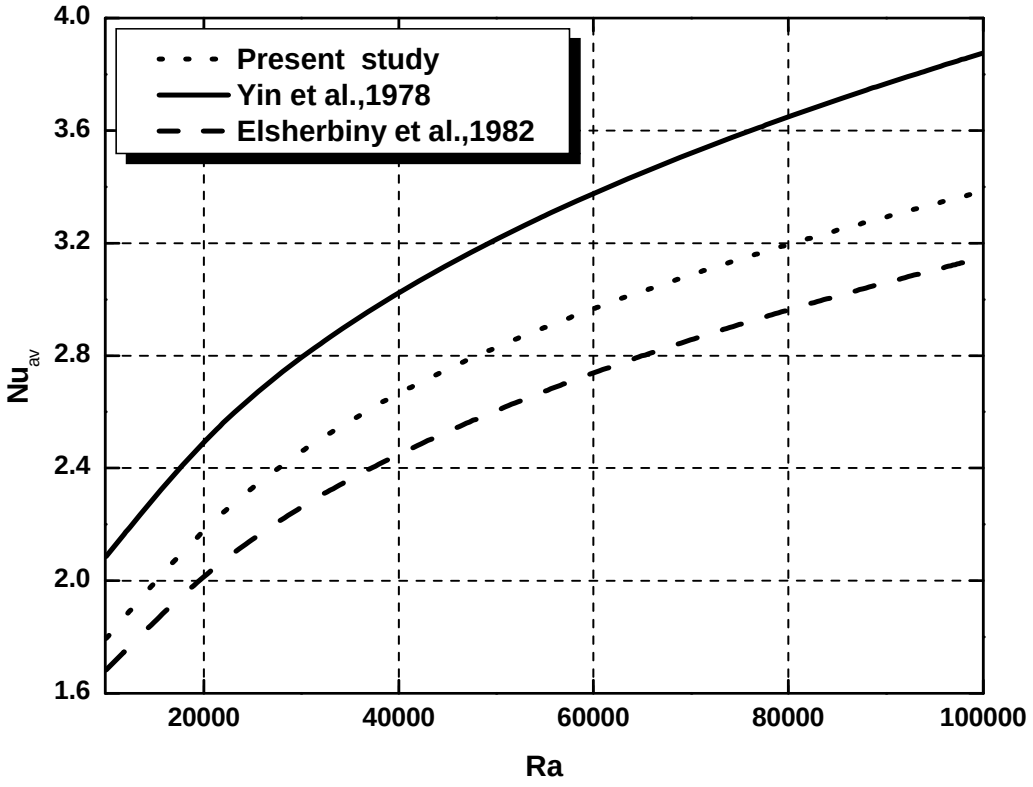

Figure 6.1 Comparisons of Nusselt numbers with literature

6.3 Comparison with measured data

A comparison of the measured and predicted temperature distributions along the air channel is shown in Figure 6.2. It can be found that the measured data (dot) are in good agreement with the predicted results (line). These may validate the validity of the mathematical methods used.

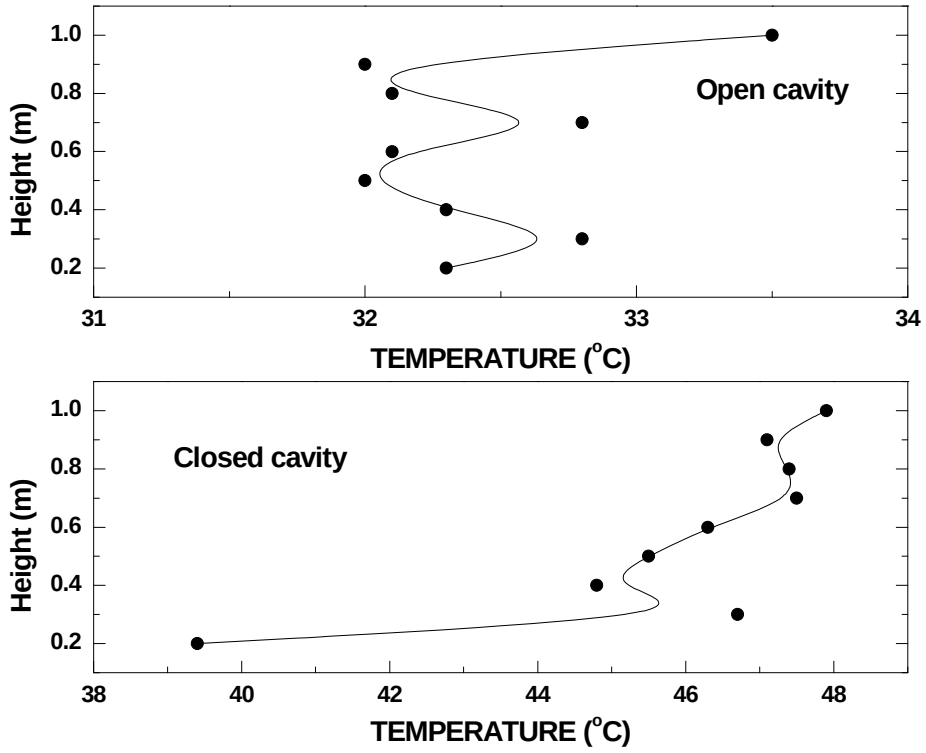

Figure 6.2 Temperature profile along the channel height for different operational models

6.4 Summary

In this chapter, the predicted results from the numerical methods are validated with experimental results available in the existing literature and collected data from experimental measurements of a well developed test rig in Solar Simulation Lab. Experimental measurements taken in the full scale indoor test facility are in good agreement with predicted results.

CHAPTER 7: PARAMETER STUDY

7.1 Effect of the air thickness on the total energy performance

The effect of the thickness of the air layer between two glass panes on the heat flux through the PV window was investigated for different temperature differences ($T_{out} - T_{in}$). In Hong Kong, the outdoor design temperatures for A/C systems are 32^{o}C for summer and 10^{o}C for winter. The indoor air temperature in a typical office in Hong Kong is supposed to be maintained, for energy savings, at 25^{o}C in summer and 22^{o}C in winter.

Figure7.1 shows the effect of the thickness of the air layer in relation to two temperature differences, i.e. 12^{o}C and 7^{o}C. It is indicated in the figure that heat transfer through the window can be considerably reduced by optimizing the thickness of the air layer. Heat flux through the window decreases considerably with the increase of the thickness of the air layer when L is less than 10mm where heat transfer by conduction of the air gap is the dominant mode. The air layer in the window also served as additional thermal insulation. Heat transfer by convection of the air layer becomes pronounced with the increase of the thickness. In this circumstance, the change of heat transfer through the window will be balanced by the increase of conduction heat transfer and the decrease convection heat transfer due to natural convection of the air in the cavity. The overall heat transfer is decreasing slightly when the thickness of the air layer is up to 60mm.

Therefore, the optimum thickness of the air layer could be chosen as 60mm-80mm when energy saving due to less energy transport through the window is considered.

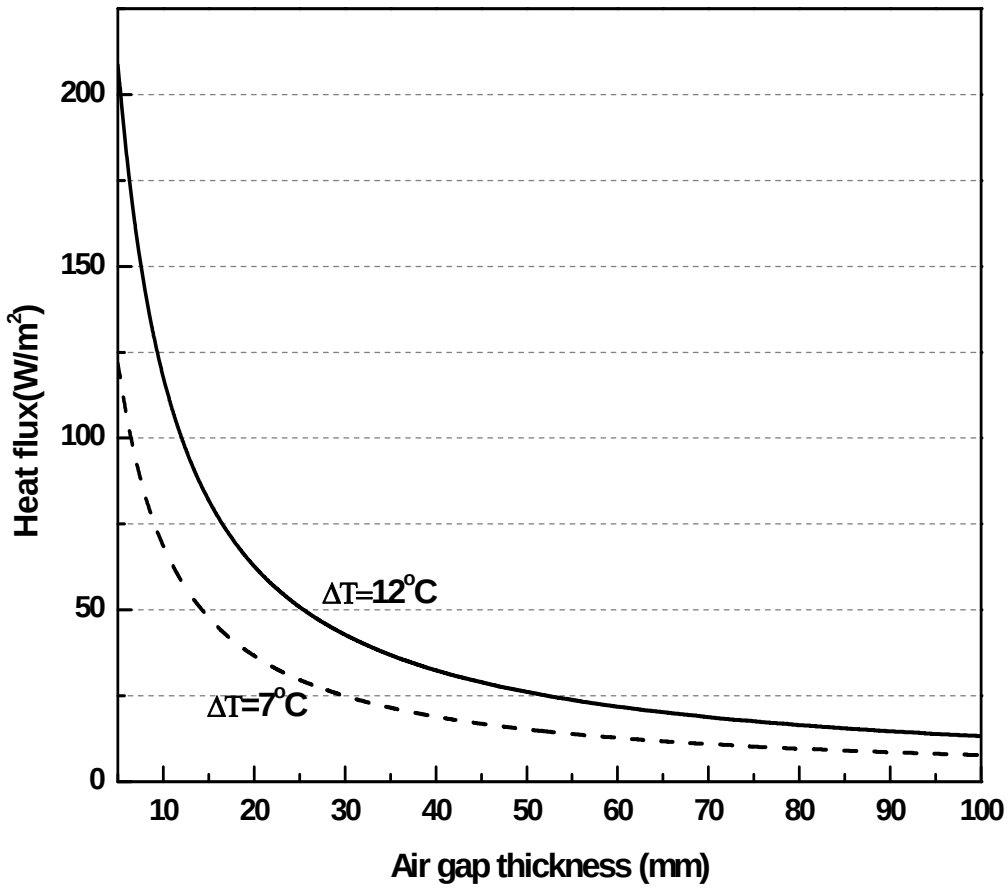

Figure 7.1 Variation of the heat flux (W/m^2) through the PV double-glazed window with different thicknesses of the air cavity

7.2 Effect of the inlet air velocity

The effect of inlet conditions, i.e. inlet air velocity was explored in this section. Many previous studies have indicated that inlet condition is of vital importance in the simulation of the flow in the double skin façade system. In these previous studies, the ambient temperature is often used as the inlet temperature.

Figure 7.2 presents the velocity profiles along the centre line of the cavity height for various inlet velocities. Figure 7.3 presents the velocity profiles for different cavity heights at air inlet velocity 0.9m/s.

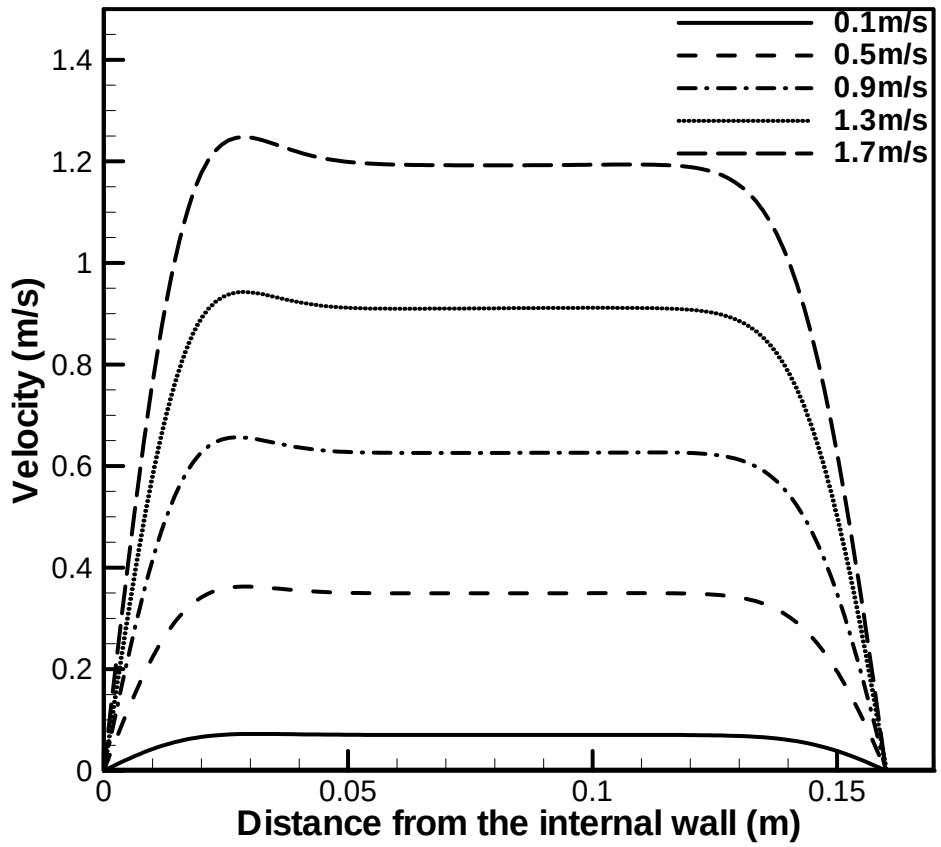

Figure 7.2 Velocity profiles along the centre line of the cavity height for various inlet velocities

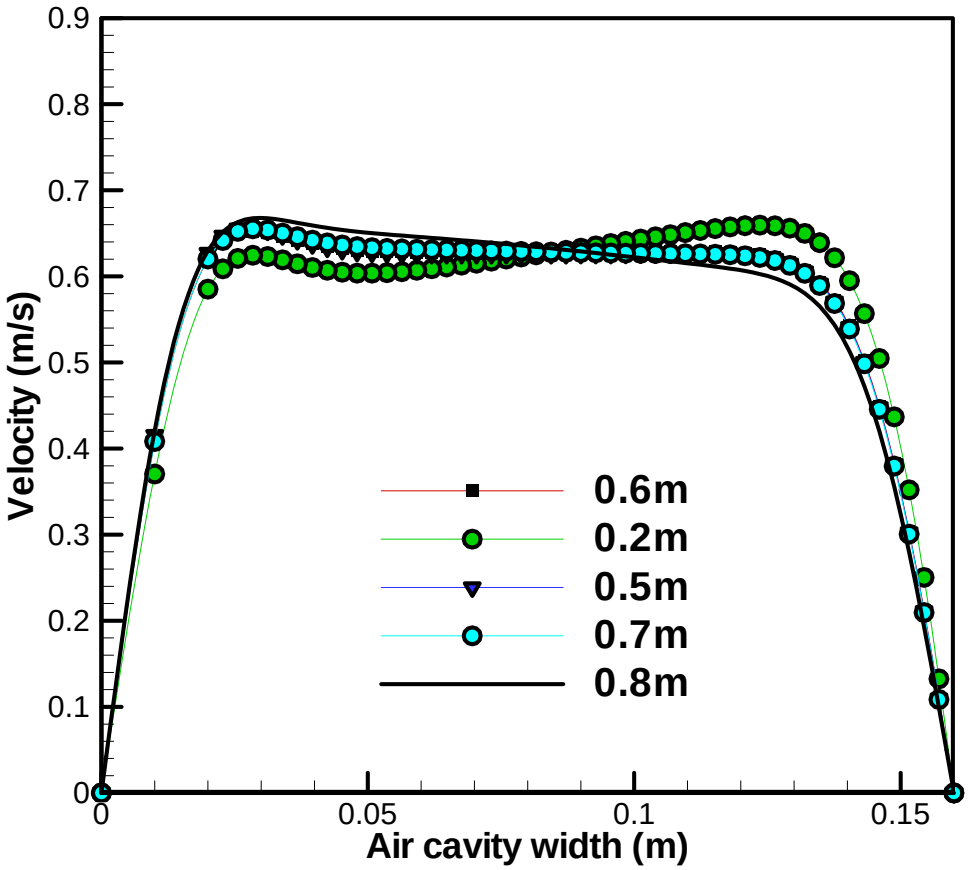

Figure 7.3 Velocity profile for different cavity height at air inlet velocity 0.9m/s

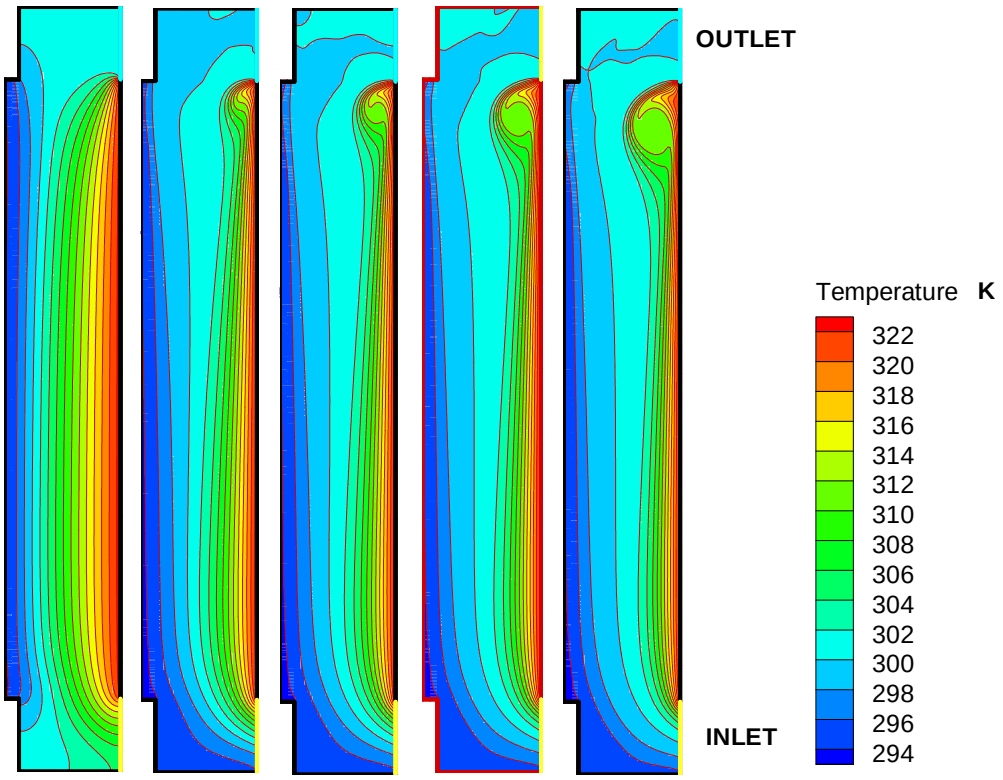

a) 0.1m/s b) 0.9m/s c) 1.3m/s d) 1.7m/s e) 2.1m/s

Figure 7.4 The effect of various inlet conditions on temperature field of the glazing cavity.

Figure 7.4 gives a side view of the temperature field. Various inlet conditions have been examined. It is found that the temperature of air in the channel at the top is obviously lower with increase of the inlet velocities. The inlet velocity condition has an important effect on the thermal field. Previous studies show that complexity of inlet region often gives trouble to the computational fluid dynamic modeling and heat transfer analysis in the system. Some improper assumption of the inlet region can even cause the final modeling results to deviate from the physical reality. It is thus critically important to model accurately the inlet condition to get reasonable results, especially when the flow is in the developing region.

7.3 Effect of the Rayleigh number

The stream function in the mid-height has been plotted in Figure 7.5 for various Rayleigh numbers. Computations are carried out for air as the working fluid with a Prandtl number of 0.75. The influence of Rayleigh number is considered for seven different values: 10^3, 5×10^3, 9×10^3, 10^4, 4×10^4, 8×10^4,10^5.

Figure 7.6 shows the variation of the dimensionless vorticity profiles Ω across the channel for different Rayleigh numbers. As can be seen voticity increase as the Rayleigh number increases and the vorticity profile is symmetric.

The air temperature in the cavity along the window height as a function of Y is shown in Figure 7.7 for various Rayleigh numbers. The non-dimensional

temperature, Θ, is linear. Higher value of Θ indicate higher air temperature according to the definition of the non-dimensional temperature in equation (5-18).

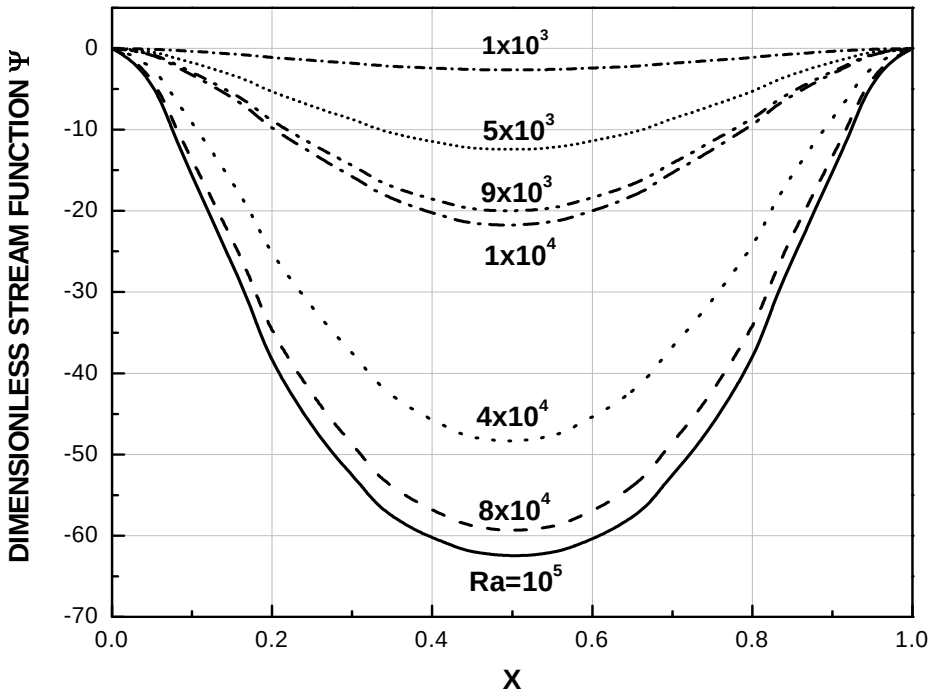

Figure 7.5 Variation of the dimensionless stream function profiles at window mid height with distance (x/W)

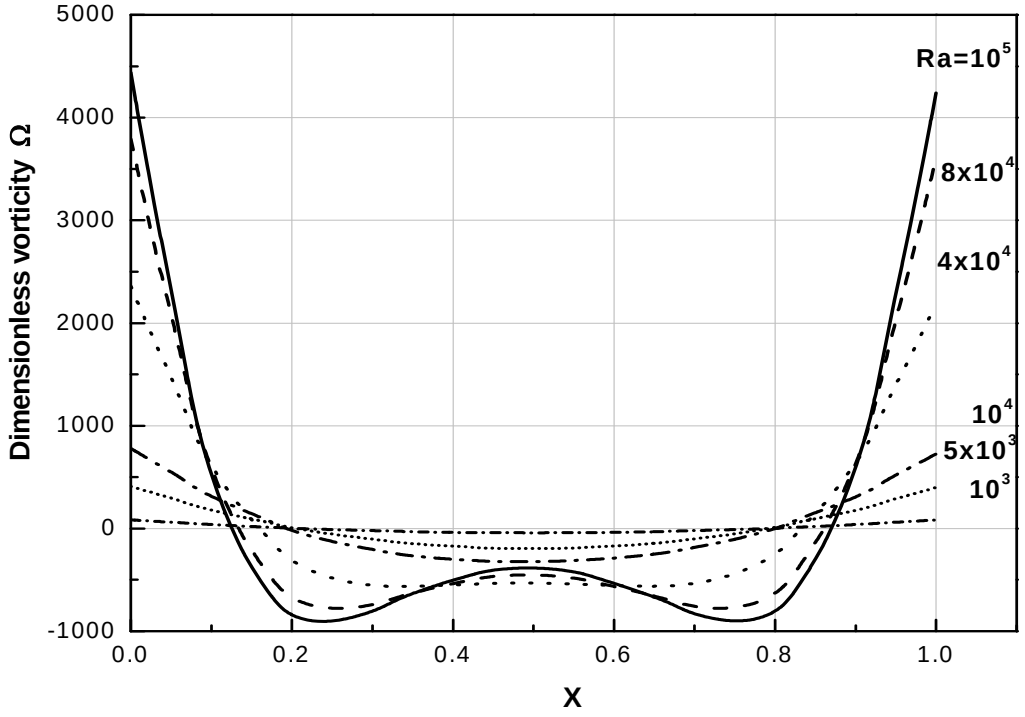

Figure 7.6 Variation of the dimensionless vorticity profiles at window mid height with distance (x/W)

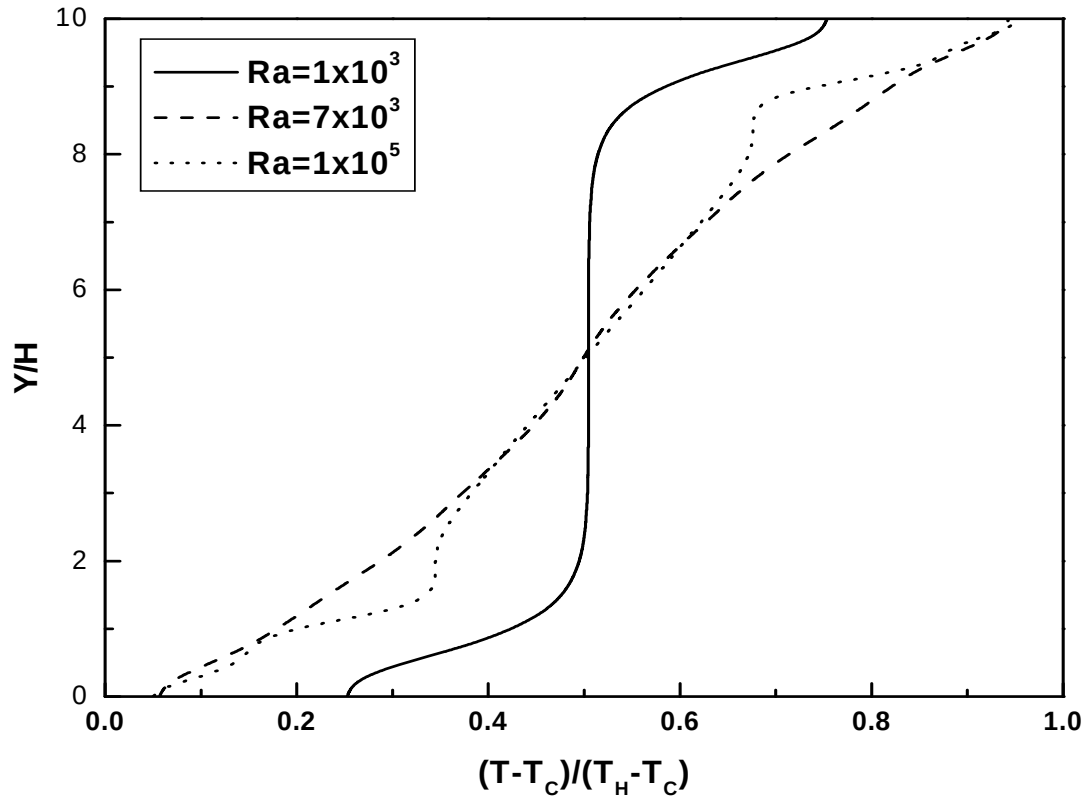

Figure 7.7 Non-dimensional temperature profiles along the height at the mid-wide of the air layer for various Rayleigh numbers.

Other parameters are A = 10, Pr = 0.7.

7.4 Effect of low-e coating on the U-value of glazing units

Low-e coating has significant influence on glazing U-value. Substantial amount of the long wave radiation could be reflected by employing a low-e coating either on one glass surface or both surfaces bounding the air gap of window units.

Figure 7.8 shows the effect of the increase in the emissivity of two surfaces bounding the air gap on the glazing U-value. In the figure, one low-e coating refers to PV glass with low-e coating and its opposite glass surface is uncoated. Two low-e coating refers to two surfaces bounding the air gap are both low-e coated. In general the effective emissivity ranges from 0.05-0.12 for low-e coatings, and for uncoated float glass the emissivity ε is 0.88 in this study.

In air cavity of a double pane window with uncoated surfaces, the longwave radiation exchange between glass surfaces is larger than the case with low-e coatings, thus the glazing U-value could be substantially reduced.

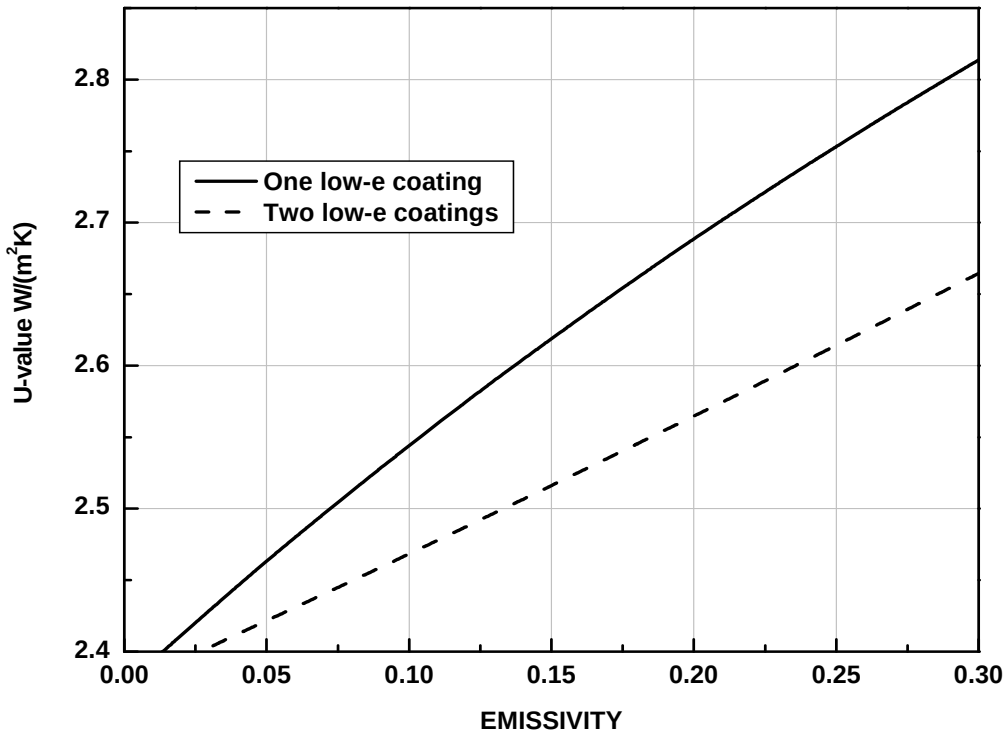

Figure 7.8 Variation of U-value with emissivity of two surfaces bounding the air gap

7.5 Summary

In this chapter, various factors affecting the performance of the double skin photovoltaic façade system has indentified and analyzed in detail. These factors include: the effect of the air thickness on total energy performance, effect of the inlet conditions, i.e. the inlet air velocity, effect of the Rayleigh number, effect of the Low-e coating on the U-value of the glazing units.

It is found that heat flux through the window decreases considerably with the increase of the thickness of the air layer when L is less than 10mm where heat transfer by conduction of the air gap is the dominant mode. The air layer in the window also served as additional thermal insulation. Heat transfer by convection of the air layer becomes pronounced with the increase of the thickness. In this circumstance, the change of heat transfer through the window will be balanced by the increase of conduction heat transfer and the decrease convection heat transfer due to natural convection of the air in the cavity. The overall heat transfer is decreasing slightly when the thickness of the air layer is up to 60 mm. Therefore, the optimum thickness of the air layer could be chosen as 60 mm - 80 mm when energy saving due to less energy transport through the window is considered. Low-e coating has significant influence on glazing U-value. A substantial amount of the long wave radiation could be reflected by employing a low-e coating either on one glass surface or both surfaces bounding the air gap of window units.

CHAPTER 8: CONCLUSIONS AND FUTURE RESEARCH

8.1 Overall conclusions

This thesis presents a numerical and experimental analysis of heat transfer and airflow in double skin facades (DSF) with integrated a-Si PV cells at the Hong Kong Polytechnic University, which generate both electricity and providing day lighting. A 2D numerical model is developed to explore the thermal behaviour and fluid dynamics in the air cavity of the DSF system for both open and closed inlet and outlet operational modes. The combined radiation and convection heat transfer in the air cavity were analyzed in detail in this thesis.

Steady natural convective airflow in a novel type glazing system with integrated semi-transparent photovoltaic (PV) cells has been analyzed numerically using a stream function vorticity formulation. Based on the resulting numerical predictions, the effects of Rayleigh numbers on airflow patterns and local heat transfer coefficients on vertical glazing surfaces were investigated for Rayleigh numbers in the range of $10^3 \leq \mathrm{Ra} \leq 2 \times 10^5$. Good agreement for the Nusselt numbers was observed between numerical simulation results in this study and those of earlier experimental and theoretical results available from the literature.

In addition, the effect of air gap thickness in the cavity on the heat transfer through

the cavity was evaluated. The effect of the thickness of the air layer between two glass panes on the heat flux through the PV window was investigated for different temperature differences ($T_{out} - T_{in}$). In Hong Kong, the outdoor design temperatures for A/C systems are 32°C for summer and 10°C for winter. The indoor air temperature in a typical office in Hong Kong is supposed to be maintained, for energy savings, at 25°C in summer and 22°C in winter. The effect of the thickness of the air layer in relation to two temperature differences, i.e. 12°C and 7°C has been evaluated. It is found that heat transfer through the window can be considerably reduced by optimizing the thickness of the air layer. Heat flux through the window decreases considerably with the increase of the thickness of the air layer when L is less than 10mm where heat transfer by conduction of the air gap is the dominant mode. The air layer in the window also served as additional thermal insulation. Heat transfer by convection of the air layer becomes pronounced with the increase of the thickness. In this circumstance, the change of heat transfer through the window will be balanced by the increase of conduction heat transfer and the decrease convection heat transfer due to natural convection of the air in the cavity. The overall heat transfer is decreasing slightly when the thickness of the air layer is up to 60mm. Therefore, the optimum thickness of the air layer could be chosen as 60mm-80mm when energy saving due to less energy transport through the window is considered.

Various turbulence models (RNG $\kappa - \varepsilon$ model, Standard $\kappa - \varepsilon$ model, Realizable $\kappa - \varepsilon$ model) were employed and velocity and temperature profiles

predicted were compared, discussed and reported in Chapter 4. A test rig were developed and calibrated for this study. Experimental studies were carried out in the lab of the Department of the Building Services Engineering. Predicted results were then compared with experimental data to evaluate the numerical simulation accuracy.

The I-V characteristics of the see-through a-Si PV module have been measured in the Solar Simulation Laboratory of The Hong Kong Polytechnic University and reported in Chapter 5. About half of the PV panel area is filled with thin film solar cells. The efficiency of the a-Si module is approximately 6%, which is lower, compared with other types of solar cells, i.e. mono-silicon cell. However, it has a lower manufacturing cost and has little reliance on the Si as well as little affect on the environment.

In addition to the theoretical aspect, experimental studies have been conducted to show reliability of the theoretical model. The simulation results are reasonably close to the experimental results. Experimental measurements taken in the full scale indoor test facility are in good agreement with predicted results. An outdoor measurement also has been conducted at the campus of The Hong Kong Polytechnic University in order to explore the thermal performance of the double sided PV (DSPV) façade when working under the real subtropical whether conditions. The experimental results indicated that the inside air temperature for DSPV façade is quite lower than temperature in conventional façade with internal curtain for shading purposes. It is found that the temperature in the DSPV façade

system is more stable. The temperature variation in conventional façade system with internal curtain is larger. There are 4 temperature peak have been observed during the measurement. The maximum temperature for conventional facade is close to 34^{o}C at 13:10 PM, 29^{o}C for DSPV facade. This indicated that the effectiveness of the solar screening through the use of the naturally ventilation of air beneath the PV module. The temperature deviation between the two systems becomes smaller late in the afternoon.

8.2 Recommendations for future research

Due to time limitation, this study can not cover all aspect of the factors which need to be considered both in the numerical investigation and the experimental study. This may be the basis of further studies.

The current theoretical studies only consider the steady state 2D flow in the flow domain. Future study could expand to transit 2D analysis to explore the transit effect and dynamic characteristics of the double skin photovoltaic façade system. A possible development of the model could be the inclusion of the conduction part of the solid glass. On the other hand, the effect of the double skin photovoltaic façade system on the space cooling load could be explored in the future study to further examine the energy performance of the current novel glazing system.

The further study could evaluate the energy performance and thermal behaviors of the double pane windows integrated with semi-transparent solar cells operating

under the subtropical climatic conditions. A numerical simulation model may be developed for analyzing their heat transfer mechanism and energy performance based on the typical-meteorological year (TMY) weather data of Hong Kong. Heat gains in summer could be substantially reduced and considerable annual electrical power could also be generated from such windows on an annual basis.

REFERENCES

Anwar, S., 2005. Natural convection flow in parallel-plate vertical channels. Master degree thesis, King Fahd University of Petroleum and Minerals, Saudi Arabia.

ASHRAE. 2001. Handbook of Fundamentals. Atlanta: American Society of Heating, Refrigerating and Air-Conditioning Engineers, Inc.

Belgian Building Research Institute (BBRI), 2002. Source book for a better understanding of conceptual and operational aspects of active facades, Version No.: 1.

Brandle, K. and Boehm, R.F., 1982. Airflow windows: Performance and applications, Proceedings of the ASHRAE/DOE Conference on Thermal performance of the Exterior Envelopes of Buildings II.

Brinkworth, B.J., Cross, B.M., Marshall, R.H., Yang, H., 1997. Thermal regulation of photovoltaic cladding. *Solar Energy* 61, 169~178.

Brinkworth B.J., Marshall, R.H., Ibrahim, Z., 2000. A validated model of naturally ventilated PV cladding. *Solar Energy* 69, 67~81.

Brinkworth B.J., 2005. Coupling of convective and radiative heat transfer in PV cooling ducts. *ASME Journal of Solar Energy Engineering* 124, 250~55.

Brinkworth B.J., Sandberg, M., 2006. Design procedure for cooling ducts to minimize efficiency loss due to temperature rise in PV arrays. *Solar Energy* 80, 89~103.

British Standards Institution, 1989 BS 3993, Part I, London.

Cho, S.H., Shin, K.S., and Zaheer-Uddin, M. 1995. The effect of slat angle of windows with venetian blinds on heating and cooling loads of buildings in south Korea. *Energy* 20, 1225~1236.

Chow, T.T., Fong K. F., He W., Lin Z., Chan A. L. S., 2007. Performance evaluation of a PV ventilated window applying to office building of Hong Kong. *Energy and Buildings* 39, 643~650.

Chow, T.T., Lin, Z., He, W., Chan, L.S., Fong, K.F., 2006. Use of ventilated solar screen window in warm climate. *Applied Thermal Engineering* 26, 1910~1918.

Chow, T.T., Pei, G., Chan, L.S., Lin, Z., Fong, K.F., 2009. A comparative study of PV glazing performance in warm climate. *Indoor and Built Environment* 18, 32~40.

Chow, T.T., Qiu, Z.Z., Li, C.Y., 2009. Potential application of "see‐through" solar cells in ventilated glazing in Hong Kong. *Solar Energy Materials and Solar Cells* 93, 230~238.

Crawley, D.W., Lawrie L.K., Pedersen C.O., 2000. Winkelmann F.C., EnergyPlus: energy simulation program. *ASHRAE Journal* 42, 49~56.

Double–skin façade, From Wikipedia, The free encyclopedia. http://en.wikipedia.org/wiki/Double–skin_facade

Elenbaas, W., 1942. Heat dissipation of plates by free convection. *Physica* 9, 1~28.

ElSherbiny, S.M., Raithby, G.D., Hollands, K.G., 1982. Heat transfer by natural convection across vertical and inclined air layers. *Journal of Heat Transfer*

Transactions of the ASME 104, 96~102.

Faist, A.P., 1998. La Façade double‐peau, Report of the Ecole Polytechnique Federal (EPF) de Lausanne, Lausanne, CH.

Fedorov AG, Viskanta R, 1997. Turbulent natural convection heat transfer in an asymmetrically heated, vertical parallel-plate channel. *International Journal of Heat and Mass Transfer* 40, 3849~3860.

Fossa, M., Menezo, C., Leonardi, E., 2008. Experimental natural convection on vertical surfaces for building integrated photovoltaic (BIPV) applications. *Experimental Thermal and Fluid Science* 32, 980~990.

Fedorov, A.G., Viskanta, R., 1997. Turbulent natural convection heat transfer in an asymmetrically heated vertical parallel plate channel. *International Journal of Heat and Mass Transfer* 40, 3849~3860.

Fung, Y.Y., Yang, H., 2006. Study on thermal performance of semi-transparent building-integrated photovoltaic glazing. *Energy and Buildings* 40, 341~350.

Fung, Y.Y., 2006. Energy performance of semi-transparent PV modules for applications in buildings. PhD thesis, The Hong Kong Polytechnic University.

Grabe, J. V., 2002. A prediction tool for the temperature field of double facades. *Energy and Buildings* 34, 891~899.

Fukai, K., 2000. Solar power generation system in Ota city hall, development of a seethrough-type amorphous module in laminated glasses. *Journal of the Institute of Electrical Installation Engineers of Japan* 20, 427~429.

Poirazis, H., 2004. Double skin facades for office buildings. Division of energy

and building design, Department of Construction and Architecture, Lund University, Report EBD-R-04/3.

Tannehill, J. C., Anderson, D. A. and Pletcher, R. H., 1997. Computational fluid mechanics and heat transfer (Taylor & Francis) 657.

Tonui, J. K. and Tripanagnostopoulos, Y., 2005. Ventilation benefit accrued from PV module installed in building. International Conference, Passive and low energy cooling for the built environment, Santorini, Greece 861~866.

Haddad, K.H., and Elmahdy, A.H., 1998. Comparison of the monthly thermal performance of a conventional window and a supply-air window. *ASHRAE Transactions* 104, 1261~1270.

Haddad, K.H., and Elmahdy, A.H., 1999.Comparison of the thermal performance of an exhaust-air window and a supply-air window. *ASHRAE Transactions* 105, 918~926.

Hamza, N. and Underwood, C., 2005. CFD supported modeling of double skin facades in hot arid climates. Ninth International IBPSA Conference Montreal, Canada Auguest 15~18.

Hayashi, T., Katayama, T., Sugai, T. and Watanabe, T. 1989. Time-variable numerical model of heat transfer around solar shading device on windows, Proceedings of the ASHRAE/DOE Conference on thermal performance of the exterior envelopes of buildings, 405~413.

Hsieh, S.S. and Yang, S.S., 1997. Flow structure and temperature measurements in a 3-D vertical free convective enclosure at high Rayleigh numbers. *International Journal of Heat and Mass Transfer* 40, 1467~1480.

Ibrahim, Z., Marshall, R., Spratt, M. Simplified loop analysis for a naturally ventilated channel heated from one side by PV elements, Proceedings of Second World Conference and Exhibition on Photovoltaic, Solar Energy Conversion, 6~9 July, Vienna, Austria, 2605~2608.

Ismail, K.A.R., Salinas, C.T., Henriquez, J. R., 2009. A comparative study of naturally ventilated and gas filled windows for hot climates. *Energy Conversion and Management* 50, 1691~1703.

Ismail, K.A.R., Henriquez, J.R., 1998. U-values optical and thermal coefficients of composite glass systems. *Solar Energy Material and Solar Cells*, 52 155~182.

King, D.L., Kratochvil, J.A., Boyson, W.E., 1997. Temperature Coefficients for PV modules and arrays: measurement methods, difficulties and results, in: 26th IEEE Photovoltaics Specialists Conference, Anaheim, CA, USA.

Lasnier, F. Ang, T. G., 1990. Photovoltaic engineering handbook. Adam Hilger Ltd, Bristol, UK.

Leal, V., Maldonado, E., Erell, E., Etzion, Y., 2003. Modelling a reversible ventilated window for simulation within ESP-r - the SOLVENT case. Eighth International IBPSA Conference, Eindhoven, Netherlands, 713~720.

Lee, E., Selkowitz, S., Bazjanac, V., Inkarojrit, V., Kohler, C., 2002. High-Performance Commercial Building Façades. Building Technologies Program, Environmental Energy Technologies Division, Ernest Orlando Lawrence Berkeley National Laboratory (LBNL), University of California, Berkeley, USA (LBNL~50502)

Liao, L., 2005. Investigation of building integrated photovoltaic – thermal systems. Master thesis Concordia University Montreal, Quebec, Canada.

Luecke, G.R. and Slaughter, J., 1995. Design, Development, and testing of an automated window shade controller. *Transactions of the ASME* 117, 326~332.

Markvart,T. (Eds.), 2000. Solar electricity, John Wiley & Sons.

Martin, S., Seitz, C., and Saman, W., 2003. Techniques for reducing the operating, temperature of solar cell modules. International Solar Energy Society Conference, Goteborg, Sweden, 43.

Mei, L., Infield, D., Eicker, U., Loveday, D., Fux, V., 2006. Cooling potential of ventilated PV façade and solar air heaters combined with a desiccant cooling machine. *Renewable Energy* 31, 1265~1278.

Mittelan, G., Alshar, A., Davison, J. H., 2009. A model and heat transfer correlation for rooftop integrated photovoltaic with a passive air cooling channel. *Solar Energy* 83, 1150~1160.

Miyazaki, T. Akisawa, A., Kashiwagi, T., 2005. Energy saving of office buildings by the use of semi-transparent solar cells for window. *Renewable Energy* 30, 281~304.

Miyamoto, M., Katoh, Y., Kurima, J. and Sasaki, H., 1986. Turbulent free convection heat transfer from vertical parallel plates. Heat Transfer, Proceeding of the International Heat Transfer, conference 8th 4, 1593~1598.

Moshfegh, B. and Sandberg, M., 1998. Flow and heat transfer in the air gap behind photovoltaic panels. *Renewable & Sustainable Energy Reviews* 2,

287~301.

Moshfegh, B., Sandberg, M., 1996. Investigating of fluid flow and heat transfer in vertical channel heated from one side by PV elements Part I-numerical study. World Renewable Energy Congress, 248~253.

Mueller, H.F.O., 1984. Exhaust air ventilated windows in office buildings. *ASHRAE Transactions*, 932~947.

Onur, N., Sivrioğlu, M., Turgut, O., 1996. An experimental study on air window collector having a vertical blind for active solar heating. *Solar Energy* 57, 375~380.

Oosthuizen, P.H, Naylor D., 1999. Introduction to convective heat transfer analysis. McGraw-Hill Series in Mechanical Engineering.

Ozisik, M.N., 1987. Interaction of radiation with convection, in: Handbook of Single-Phase Convective Heat Transfer, Wiley, New York.

Ridouane, E.H., Hasnaoui, M., Amahmid, A., Raji, A., 2004. Interaction between natural convection and radiation in square cavity heated from below. *Numerical Heat Transfer A* 45, 289~311.

Ripatti, H., 1984. Airflow window system - Making fenestration the solution rather than the problem in energy use. *ASHRAE Transactions* 90, 917~931.

Robbins, C.L., 1986. *Daylighting: Design and Analysis*, Van Nostrand Reinhold Company.

Park, C., 2003. Occupant responsive optimal control of smart façade systems. PhD thesis, Georgia Institute of Technology.

Park, C.S., Augenbroe, G., Messadi, T., Thitisawat, M., Sadegh, N., 2004. Calibration of a lumped simulation model for double-skin façade systems. *Energy and Buildings* 36, 1117~1130.

Park, K.E., Kang, G.H., Kim, H.I., Yu, G.J., Kim, J.T., 2010. Analysis of thermal and electrical performance of semi-transparent photovoltaic (PV) module. *Energy* 35, 2681~2687.

Patankar, S.V. 1980. Numerical Heat Transfer and Fluid Flow Hemisphere Publishing Corporation.

Saelens, D., Hens, H., 2001. Experimental evaluation of airflow in naturally ventilated active envelopes. *Journal of Building Physics* 25, 101~127.

Saelens, D., 2002. Energy performance assessment of single storey multiple–skin facades, PhD thesis, Katholieke Universiteit Leuven ISBN: 90 – 5682 – 370 – 1.

Saelens, D., Roels, S., Hens, H., 2004. The inlet temperature as a boundary condition for multiple-skin façade modeling. *Energy and Buildings* 36, 825~835.

Saelens, D., Roels, S., Hens, H., 2008. Strategies to improve the energy performance of multiple-skin facades. *Building and Environment* 43, 638~650.

Sandberg, M., Moshfegh, B., 2002. Buoyancy-induced air flow in photovoltaic facades-effect of geometry of the air gap and location of solar cell modules. *Building and Environment* 37, 211~218.

Sato A. 1998. Semitransparent solar battery system at Tammatukuri-onsen ‘yuyu’.

Journal of Illuminating Engineering Institute of Japan 82, 756~8.

Seki, N., Fukusako, S., Youan, G.W., 1989. The formation of phenomena of water flow between two cooled parallel plates. *Transactions of the ASME* 106, 498~505.

Silva, F.M., Gomes, M.G., 2008. Gap inner pressures in multi-storey double skin facades. *Energy and Buildings* 40, 1553~1559.

Sparrow, E.M. and Azevedo, L. F., 1985. Vertical channel natural convection spanning between the fully-developed limit and the single-plate boundary-layer limit. *International Journal of Heat Mass Transfer* 28, 1847~1857.

Takeoka, A., Kouzunma, S., Tanaka, H., Inoue, H., Murata, K., Morizane, M., et al. 1993. Development and application of see-through a-Si solar cells. *Solar Energy Materials and Solar Cells* 29, 234~52.

Tonui, J.K., Tripanagnostopoulos, Y., 2008. Performance improvement of PV/T solar collectors with natural air flow operation. *Solar Energy* 82, 1~12.

Trony Solar Holdings Company Limited. http://www.trony.com

Tsuji, T., Nagano, Y., 1988. Characteristics of a turbulent natural convection boundary layer along a vertical flat plate. *International Journal of Heat Mass Transfer* 31, 1723~1734.

van Paassen, D. and van der Voorden, M. 2000. Development of simplified tools for evaluation energy performance of double façade, Proceedings of International Building Physics Conference, Eindhoven, the Netherlands, 347~355.

Vliet, G., Liu, C.K., 1969. An experimental study of turbulent natural convection boundary layers. *Journal of Heat Transfer* 91, 517~531.

Wan Hassan, M. N., 1986. The natural convection in a cavity at high Rayleigh numbers, PhD thesis, University of Washington.

Yang, H.X., Burnett, J., Ji, J., 2000. Simple approach to cooling load component calculation through PV walls. *Energy and Buildings* 31, 285~290.

Yang, H.X., Zheng, G., Lou, C.Z., An, D.W., Burnett, J., 2004. Grid-connected building‐integrated photovoltaics: a Hong Kong case study. *Solar Energy* 76, 55~59.

Yin, S.H, Wung, T.Y, Chen, K., 1978. Natural convection in an air layer enclosed within rectangular cavities. *International Journal of Heat and Mass Transfer* 21, 307~315.

Yun, G. Y., McEvoy, M., Steemers, K., 2007. Design and overall energy performance of a ventilated photovoltaic façade. *Solar Energy* 81, 383~394.

Zhai, Z., Chen, Q., Haves, P., Klems, J. H., 2002. On approaches to couple energy simulation and computational fluid dynamics programs. *Building and Environment* 37, 857~864.

Zhai, Z., Chen, Q., 2003. Solution characters of iterative coupling between energy simulation and CFD programs. *Energy and Buildings* 35, 493~505.

Zhai, Z. J., Chen, Q. Y., 2005. Performance of coupled building energy and CFD simulations. *Energy and Buildings* 37, 333~344.

Zollner, A., Winter, E.R.F., Viskanta, R., 2002. Experimental studies of combined heat transfer in turbulent mixed convection fluid flows in double-skin-facades. *International Journal of Heat and Mass Transfer* 45, 4401~4408.